Elucidating the Unknown Role of Cyclin Dependent Kinase 5 in Cardiac Pathophysiological Conditions

Danielle Aina-Badejo

Submitted in partial fulfillment of the
requirements for the degree of
Doctor of Philosophy
under the Executive Committee
of the Graduate School of Arts and Sciences

COLUMBIA UNIVERSITY

2021

Abstract

Elucidating the Unknown Role of Cyclin Dependent Kinase 5 in Cardiac Pathophysiological Conditions

Danielle Aina-Badejo

Until now, the role of cyclin dependent kinase 5 (CDK5) in cardiac pathophysiology has not been explored. While CDK5 has been well studied in the neuroscience/Alzheimer's field as a cyclin-independent kinase, there is currently no investigation into the cardiac-specific role of CDK5. Recently, it was established that inhibition of *CDK5* in stem cell derived cardiomyocytes from individuals with Timothy Syndrome (TS) rescued the delayed inactivation phenotype; TS is a fatal genetic long QT syndrome (LQTS) caused by delayed inactivation of the L-type voltage gated Ca^{2+}channel $Ca_V1.2$. While it is evident that CDK5 plays an important role in regulating $Ca_V1.2$ function, its role in cardiac tissue remains to be elucidated.

To determine whether CDK5 is essential for cardiac function, two separate mouse models were established—a cardiac-deficient Cdk5 mouse model (*Cdk5 flox* x αMHC-MerCreMer$^+$) and a Cdk5 activation mouse model via overexpression of Cdk5's known activator, p35 (*Cdk5r1/*p35 OE *x* αMHC-MerCreMer$^+$). Immediately after spatiotemporal induction of deficiency/activation of Cdk5 in adult mice, echocardiography, histology and proteomic analysis were performed to examine effects on cardiac structure and function. Analysis of cardiac function and morphology in Cdk5 deficient mice revealed severe systolic dysfunction and a dilated cardiomyopathy-like phenotype. These results were further validated by a pathway analysis of quantified global proteome changes. Conversely, mice with an activation of Cdk5 displayed only minor changes in

cardiac function with a modest reduction in fractional shortening and ejection fraction. Notably, these mice did not have any significant changes in cardiac chamber morphology, nor any significant changes to their global proteome. Interestingly, however, phosphoproteomic analysis revealed over 3,000 differentially phosphorylated proteins.

Pathway and gene ontology analysis of proteome changes revealed significant hits related to cell adhesion. Evidence for the extensively studied role of CDK5 in the brain has demonstrated a critical role for CDK5 kinase activity in the regulation of cell adhesion. Alterations in cell adhesion are observed in a number of cardiac pathologies including heart failure and dilated cardiomyopathy; it is therefore plausible that CDK5 potentially regulates cardiac function via cell adhesion mechanisms. A comparison of the phospho-proteome acutely after Cdk5 depletion vs the phospho-proteome acutely after Cdk5 activation, allowed for the identification of a novel cardiac-specific Cdk5 substrate, beta taxilin (Txlnb). Validation of this potential phospho-substrate with an *in situ* proximity ligation assay demonstrated the co-localization of Cdk5-Txlnb in wildtype mouse cardiac tissue sections. When looking at co-localization in Cdk5 deficient tissue sections, no signals were observed.

Lastly, our lab obtained donor cardiac tissue samples from individuals who passed away due to either heart failure or non-cardiac causes (serving as control cardiac tissue). Analysis of cardiac tissue samples revealed a significant increase in both CDK5 and p35 expression in heart failure samples. Dysregulation of phosphorylation has been implicated in cardiac dysfunction, with known contribution to contractile failure and a number of cardiac pathologies including cardiomyopathies. These findings further support a role for CDK5 in cardiac function.

In conclusion, it appears that CDK5 is imperative for the maintenance of healthy cardiac function. Cardiac-specific homozygous and heterozygous Cdk5 deficiency revealed severe

systolic dysfunction along with a dilated cardiomyopathy-like phenotype. While the effects of Cdk5 activation in the heart need to be further investigated, initial findings report significant downstream effects on the phosphorylation of a number of proteins, including Txlnb. Moreover, Txlnb was identified as a potential novel cardiac-specific substrate of Cdk5.

The importance of identifying a role for CDK5 in the heart extends beyond this study. CDK inhibitors have been at the forefront of drug development for cancer therapeutics and immunotherapy. While modulation of CDK5 activity may be beneficial in one physiological system, it may prove deleterious in another. It is therefore imperative that the full range of molecular and physiological roles of each CDK be fully elucidated prior to therapeutic application. Furthermore, outcomes from this study have the potential to be translational for drug discovery and the development of new therapeutic avenues for heart disease.

Table of Contents

List of Figures

List of Tables

Abbreviations

CDK	Cyclin dependent kinase
CDK5	Cyclin dependent kinase 5
ADP	Adenosine diphosphate
Thr160	Threonine 160
ALS	Amyotrophic Lateral Sclerosis
LQTS	Long QT syndrome
LQTS8	Long QT syndrome type 8
CACNA1C	Calcium Voltage-Gated Channel Subunit Alpha 1 C
TS	Timothy syndrome
RyR	Ryanodine receptors
hiPSCs	Human induced pluripotent stem cells
CM's	Cardiomyocytes
DN	Dominant negative
Myh6	Myosin heavy chain 6
αMHC	Alpha myosin heavy chain
LBD	Ligand binding domains
HSP90	Heat shock protein 90
TMT	Tandem mass tag
WT	Wild type
WT^{MCM}	WT*:* αMHC-$MerCreMer^{+}$
I.P.	Intraperitoneal

Tam	Tamoxifen
Echo	Echocardiography
DCM	Dilated cardiomyopathy
qRT-PCR	Quantitative real time polymerase chain reaction
EF	Ejection Fraction
FS	Fractional Shortening
LV	Left ventricle
LVEDD	Left ventricular end diastolic diameter
LVEDV	Left ventricular end diastolic volume
MT	Mason's Trichrome
H&E	Hematoxylin and eosin
LC-MS/MS	Liquid chromatography coupled with mass spectrometry
Nmrk2	Nicotinamide riboside kinase 2
Mpo	Myeloperoxidase
Chil3	Chitinase-like protein 3
ROS	Reactive oxygen species
Pdelc	Calcium/calmodulin-dependent 3',5'-cyclic nucleotide phosphodiesterase 1C
Fbxo40	F-box only protein 40
Fhod3	FH1/FH2 domain-containing protein 3
Slc29a1	Equilibrative nucleoside transporter 1
Serpina1e	Serpin family A member 1
Cdca2	Cell division cycle-associated protein 2

Rplp1	60S acidic ribosomal protein P1
IPA	Ingenuity Pathway Analysis
IC	Intercalated discs
IACUC	Institutional Animal Care and Use Committee
SPS	Synchronous precursor selection
HCD	Higher energy collision-induced dissociation
mESC	Mouse embryonic stem cells
LSL	LoxP-STOP-LoxP cassette
PKA	Protein Kinase A
Txlnb	Beta-taxilin
Cx43/Gja1	Connexin 43/gap junction a1
Fhod3	Formin homology 2 domain containing 3
C4orf54	Chromosome 4 open reading frame 54
Plec	Plectin
Tnc	Tenascin C
Asph	Aspartate beta-hydroxylase
Sorbs1	Sorbin and SH3 domain containing 1
Htatsf1	HIV-1 Tat specific factor 1
Cap2	Cyclase associated actin cytoskeleton regulatory protein 2
Tln2	Talin 2
Cavin4	Caveolae associated protein 4
ECM	Extracellular matrix
Denr	Density regulated re-initiation and release factor

PLA	Proximity ligation assay
PVFD	Polyvinylidene difluoride
Cam-PK	Ca^{2+}-calmodulin protein kinase
PKC	Protein kinase C
MAPK's	Mitogen-activated protein kinases
AAV	Adeno-associated virus
pAAV	Plasmid adeno-associated virus
cTNT	cardiac troponin T

Acknowledgments

There are many people I would like to acknowledge whose help has been invaluable to the completion of my thesis. First, of course, my mentor, Dr. Masayuki Yazawa. Dr. Yazawa accepted me into his lab with minimal knowledge of the cardiovascular system. Prior to joining his lab, I had only worked in the field of diabetes. It was a very big learning curve, but Dr. Yazawa did not have any doubts in my accomplishments, even when I may have. He is not only a brilliant scientist, both technically and theoretically (a master of patch-clamping), but he is also an example of someone who does it all—an incredible dad and husband for his wonderful family. I truly admire him on so many levels and his dedication to his work, his students, his lab members, his colleagues and of course, his family. I am very grateful for the opportunity to work in his lab.

I would also like to thank the members of the Yazawa lab who were helpful in more ways than one during my pregnancy/breastfeeding journey. I would also like to extend my thank you to the wonderful friends I've made in the program, especially Virginia Aimiuwu who was not only there for scientific encouragement, but also personal support, checking in on Remi and I every week. It meant the world to me to feel so much love and support from a fellow PhD student. I must also acknowledge our collaboration with the CUMC proteomics and macromolecular crystallography core directed by Dr. Rajesh Soni and the molecular pathology core directed by Dr. Hanina Hibshoosh. Additionally, I would like to thank Dr. Kazato Ito whose extensive commitment to helping us perform echocardiography was greatly appreciated.

I would like to acknowledge my incredible thesis/thesis defense committee that has been invaluable to my training as a translational research scientist: Dr. Rudy Leibel, Dr. Angela Christiano, Dr. Kimara Targoff and Dr. Henry Ginsberg. I've been fortunate enough to have been guided by Dr. Leibel throughout my scientific career and personal growth. He has been an integral

part of my experience at Columbia and I hope to be just a little of the scientist, thought leader and human that he is. Dr. Christiano has been one of the kindest and strongest forces behind women and student advocacy, on top of being one of the most well-accomplished scientists at Columbia. My knowledge of genetics and introduction to bioinformatic approaches to scientific questions stems from her lab, and I am very grateful for all of the instrumental input and advice she has given me throughout the years. I have been very fortunate to have Dr. Targoff as part of my thesis committee with expertise not only in cardiac research but also clinical cardiology. Her translational skillset in the cardiac field was extremely helpful for the progression of my thesis project. She is also a highly respected physician-scientist by her peers, having been highly recommended as an asset to my thesis committee by Dr. Teresa Lee. Lastly, I would like to thank Dr. Ginsberg for not only his scientific acumen, but also his guidance in the field of precision medicine. Dr. Ginsberg was the director of one of the fellowships I was awarded (CTSA TL1 Precision Medicine Fellowship) during my last two years at Columbia. I can speak for everyone in saying that we truly looked forward to seminar when Dr. Ginsberg was there to give opening remarks—whether it be about new research, updates on the pandemic, or just general discussion about life. I am very grateful to have my PhD experience shaped by each of these individuals.

Lastly, I would like to acknowledge the IHN and all of their efforts in helping our program run so smoothly (Zachary Corter, Alexander Sosa, Sara Sternglass, Leslie De Pena, Yonette Beaton). A special thank you to Dr. Wolgemuth whose been one of my biggest faculty supporters while at Columbia. She takes a special interest into everyone's personal well-being in the program and was more than just a program director to each of her students. I'd also like to thank Dr. Richard Deckelbaum, the former director of the IHN, who not only asked important questions at each

student seminar, but also ensured that students of the IHN and families were all taken care of during the pandemic.

Dedication

I would like to dedicate this thesis to the three most important people in my life: My husband Ore—I could not imagine a better life partner than you. We are raising THE most incredible/brilliant/loving children. We literally built our lives together from the ground up and you are truly one of the best humans that I have ever met. It takes a lot for me to be happy with something I've done, but I can say with ease is that I am so proud of us. I love you. To my 4-legged daughter Mikka: THE MOST incredible pup you will ever meet. I know everyone says that about their dog but Mikka is truly a legend. If you know, you know. My two-legged son Remi (aka Remilah, aka Sir, aka Remo, aka Big Man, aka Remchunks) Where to begin… Remilah, I'm not sure how we made you so amazing. I am the world's most annoying mom because of how much I can't help but boast about every little thing you do. Even when you sleep I just :3 We knew you were the most incredible person from the time you were born. You are SO sweet, hilarious, happy, loving, insanely smart and such a handsome papa. I love how much you love your sister Mikka and how generous you are with cuddles and kisses (and a little too generous with your food, especially to Mikka). You amaze your daddy and I everyday with everything you do. We love you forever. P.S. no matter what daddy says I'm a cool mom.

I'd also like to dedicate this thesis to my Saba, the person who raised me and unfortunately passed away during my PhD. He was one of the most selfless, kind, supportive and loving people in my life and I hope to be as special to Remi as you were to me.

Chapter 1: Introduction

1.1 Cyclin Dependent Kinases

Cyclin dependent kinases (CDK's) are a family of heterodimeric proline directed serine/threonine kinases that were first discovered for their indispensable role in eukaryotic cell cycle regulation.[1,2] Traditionally, ubiquitously expressed CDK's are activated upon binding with the regulatory protein subunit cyclin, having no enzymatic activity on their own.[3,4] Once activated, CDK's can integrate extracellular and intracellular signals for the modulation of gene transcription and cell cycle progression.[2,5] Cyclin-CDK complexes can recognize and phosphorylate hundreds of protein substrates. They do so by transferring a phosphate group from adenosine triphosphate (ATP) to specific amino acid sequences on their protein substrate target.[6,7] This mechanism yields two final products—a phosphorylated substrate and an adenosine diphosphate (ADP) (**Fig 1**). Because cyclin-CDK complexes can act on numerous substrates, CDK's are central regulators in the coordination of simultaneous molecular events that occur during each phase of the cell cycle.[3]

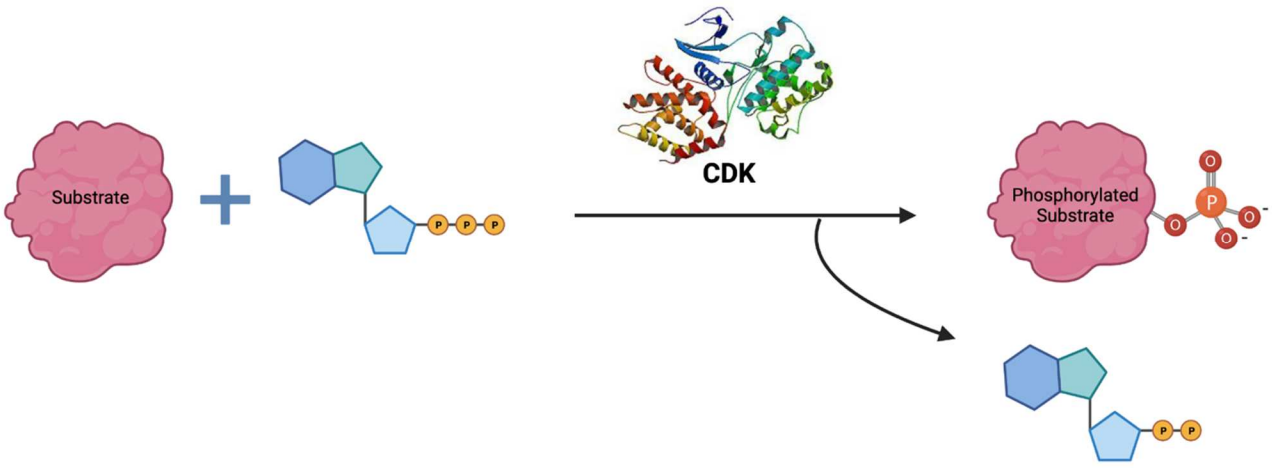

Figure 1.1: Schematic of cyclin dependent kinase phosphorylation | Cyclin dependent kinases selectively modify their substrates by removing a phosphate group from ATP and covalently bonding the group to a free hydroxyl group on a serine or threonine of the substrate target.

CDK's are two lobed proteins that range from about 250 to 1,500 amino acid residues in length.[2,8] The conserved active site, a central protein kinase domain, is flanked by a small N-terminal and larger C-terminal lobe that contain ß-sheets and α-helices (referred to as PSAALRE), respectfully. The activation segment of CDK is contained within the C-terminal lobe and is referred to as the T-loop/activation loop. In the unbound state, CDK's have two characteristics that make them inactive: (1) the T-loop is positioned in a way at the C-terminal that closes the catalytic cleft, preventing the binding of a protein substrate at the active-site cleft and (2) essential amino-acid side chains in the active site are partially disordered, preventing enzymatic activity prior to conformational changes in the active site.[8-11]

While CDK's were traditionally thought to play a role in cell cycle regulation and gene expression, evolutionary divergence has resulted in an expansion in type and function of many of these kinases.[12] CDK's were initially discovered in yeast and frogs through both genetic and biochemical studies.[13] There are currently 20 known CDK's in the human genome that are subcategorized based on evolutionary relationship (**Fig 2**).[13] Currently, CDK's 1-11 have been most extensively studied, having mainly cell-cycle dependent roles. In summary, CDK's 1, 2, 3, 4, 6 and 11 play a major role in the maintenance of cell division, with known functions including regulation of DNA replication mitotic, progression, and regulation of growth signaling pathways.[14,15] CDK's 7-9 play a major role in RNA polymerase II transcription, a DNA-dependent RNA polymerase that functions in the transcription of genes that code for mRNA and small nuclear RNA's.[16] Lastly, CDK10's main role is in cell proliferation, maintaining G2-M phase transition.[2] As previously mentioned, functional roles of certain CDK's have evolved beyond cell cycle regulation, behaving as a "non-conventional" CDK. CDK5, the most unconventional and

diversified CDK, has known roles in cell cycle arrest and differentiation, promotion of T cell survival and motility, the control of β-cell insulin secretion, regulation of pain sensory pathways as well as neuronal migration—the known molecular and physiological roles of CDK5 will be addressed in the next sub section.[12]

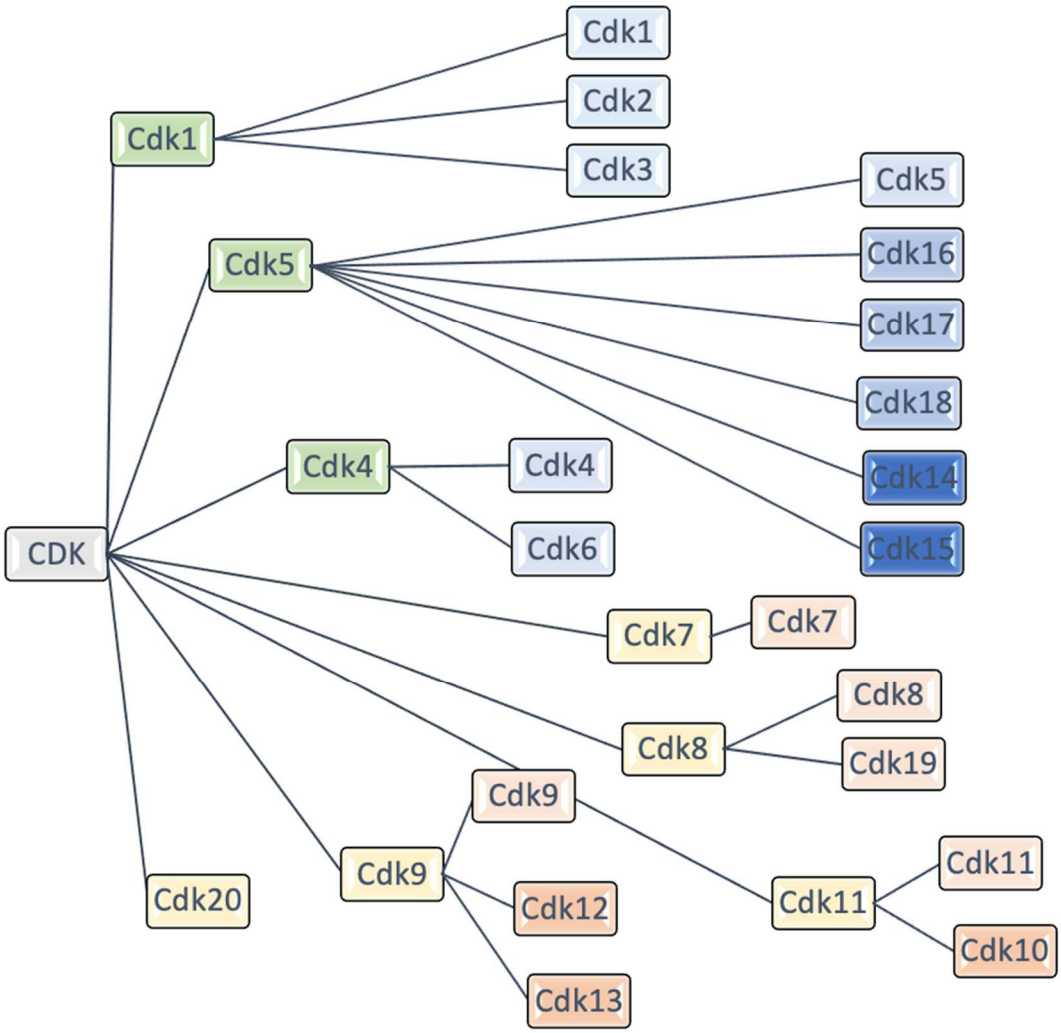

Figure 1.2: Mammalian CDK subfamilies based on evolutionary similarities| Categorization of CDK subfamilies is based on traditionally known functions—cell cycle (green) or gene transcription (yellow). Further sub-branching based on evolutionary relationships are shown via color gradient.

1.2 Structure of Cyclin Dependent Kinase 5

One such non-conventional CDK is cyclin dependent kinase 5 (CDK5), a unique CDK in both activity as well as function. *CDK5* is a 3.95kb stretch of DNA that has been mapped to chromosome 7q36.[11] CDK5 is a 33 kDa proline directed serine/threonine kinase that phosphorylates a serine or threonine residue immediately upstream of a proline. It most commonly phosphorylates its substrates following the "(S/T)PX(K/H/R)" consensus motif ("S" represents serine, "T" represents threonine, "P" represents the requisite proline, "X" represents any amino acid, "K" represents glycine, "H" represents histidine and "R" represents arginine).[11,17,18] CDK5 was initially identified as a CDK in 1992 due to its high nucleotide sequence homology to CDC2 (61%), the human homolog of Cdk1.[8,12,19-21] It also shares significant homology (50-60%) with CDK2, CDK4 and CDK6.[22] Structurally, CDK5 is quite similar to other CDK's—it contains a catalytic domain (ePK) with N and C terminal lobes sharing an ATP binding site and a 20 residue activation T-loop (**Fig 1.3)**.[8]

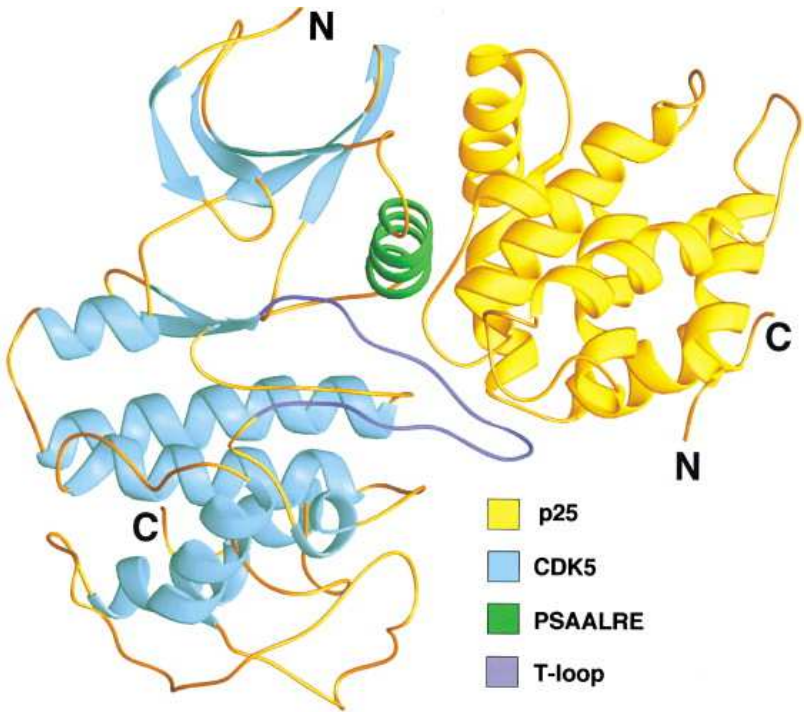

Figure 1.3: Ribbon/Richardson diagram of CDK5-p25 complex| Ribbon/Richardson diagram of CDK5 (light blue) in complex with its cleaved activator, p25 (yellow). The p25 moiety is comprised of an NT helix, 2 C-terminal helices and a cyclin box-fold domain. The αC-helix, PSAALRE, the binding site of p25 to CDK5, is shown in green. The 20-residue T- loop is shown in purple. Phosphorylation of the T-loop is not required for CDK5 activity (*This figure is reproduced from Tarricone, et al.*)[10]

1.2 Regulation of Cyclin Dependent Kinase 5

Despite significant homology with other CDK's, CDK5s primary method of activation is independent of the regulatory protein cyclin. Instead, its activation is dependent upon binding with membrane localized p35 or p39 (as well as its cleaved counterparts p25/p29) encoded by *CDK5R1/CDK5R2*.[8,11,18,21,23,24] Both CDK5-p35 and CDK5-p39 complexes localize to the cell membrane and can sometimes localize to the cytoskeleton.[25] Unlike other CDK's, CDK5 does not require phosphorylation of its T-loop at the threonine160 (Thr160) residue for activation; the binding of CDK5 to p35/p39 alone is sufficient for full activation. Maximum activation, however, can be achieved when binding of p35/p39 is joined by phosphorylation of Thr160 on the T-loop.[21]

*CDK5R1/*p35 is the primary and most effective activator of *CDK5* both *in vitro* and *in vivo*.[24] p39 is the isoform of p35, with a 72% sequence homology in CDK5-activation domain, and 57% homology in overall amino acid sequence.[25] Prior research has shown *CDK5R1/*p35 to be essential for full physiological function of CDK5, as p39 WT/p35 null mutant mice display deficits in full CDK5 function resulting in cortical lamination defects, inversion of neuronal layering, defects in neuronal migration, seizures and sporadic adult lethality.[11,12,26,27] p39 knockout mice, on the other hand, do not display any obvious phenotypical differences.[5,26,28] Both p35 and p39 contain an N-terminal myristoylation motif that localizes it to phospholipid cell membranes.[25] Additionally, while p35/p39 has little amino acid sequence homology to cyclins, it adopts a cyclin-

box tertiary structure when in complex with CDK5 that is similar to the CDK-cyclin complexes' cyclin box fold domain.[29] p35 is reported to have highest expression in post-mitotic neurons of the central nervous system.[8,28] It is degraded rapidly by proteosomes, with an *in vivo* half-life of approximately 20 minutes.[21,30] p35 degradation is ubiquitin-dependent, although a recent study has reported degradation via a ubiquitin-independent pathway in physiological conditions (**Fig 1.4**).[31]

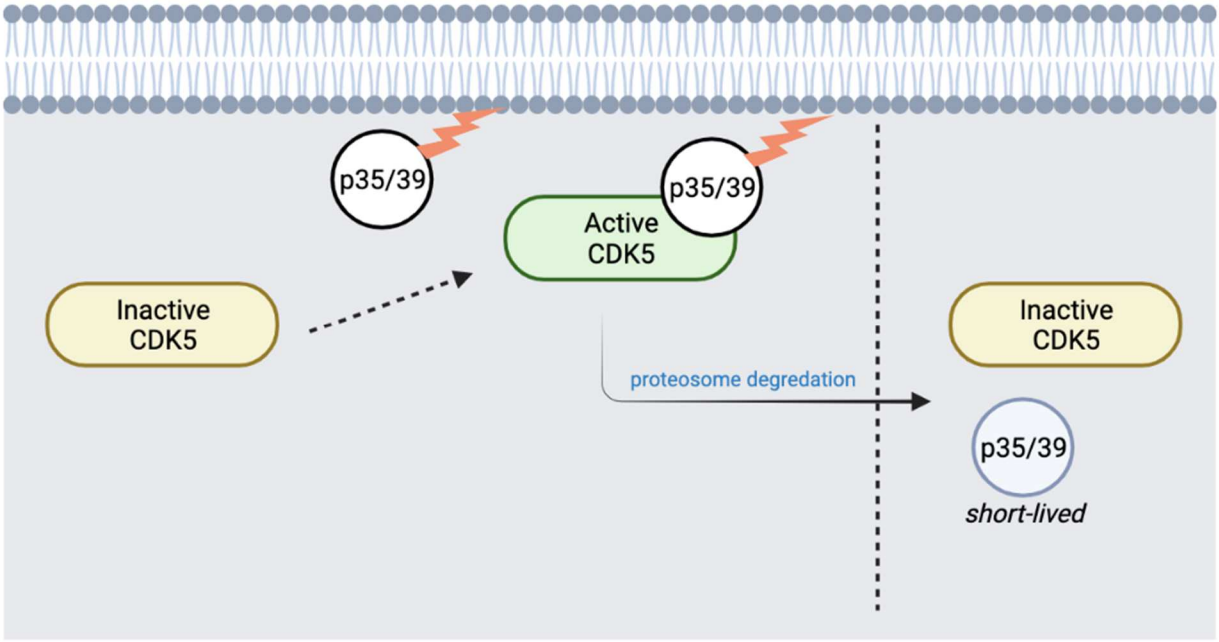

Figure 1.4: Mechanism of CDK5 activation by p35/p39 | While CDK5 is inert on its own, it becomes activated by translocating to the membrane and interacting with the myristoylated regulatory subunit p35 or p39. p35/p39 is short lived in the cell and is subsequently degraded by the proteosome. p35 degradation is hypothesized to occur post-phosphorylation.

In certain stressful pathophysiological conditions, p35 is cleaved into p25 by calpain, a calcium-dependent protease.[19] This truncated form of p25 contains residues 99-307 of p35, a stretch of amino acids that include the CDK5 activation domain.[10,23] When complexed with CDK5, p25 is known to hyperactivate CDK5 activity and increase its stability.[23] Unlike p35, p25 does not get degraded easily and therefore accumulates in target tissue. Such lack of degradation causes dysregulation of CDK5 activity resulting in both mis-localization and abnormal phosphorylation

of substrates—this includes hyperphosphorylation of known substrates and phosphorylation of non-physiological substrates.[10,11,22,23,32] Currently, CDK5 has only been biochemically purified in complex with p25, with the structure/complex of CDK5-p35/p39 based off of the CDK5-p25 complex (**Fig 1.3**).[22] While p25 presence is normally low in tissue, significant tissue accumulation has been reported in neurodegenerative disease states such as Alzheimer's Disease, Amyotrophic Lateral Sclerosis (ALS) and Parkinson's Disease.[22,32]

1.3 Cyclin Dependent Kinase 5 in the Brain

CDK5 was first purified from bovine brain microtubule fractions due to its sequence homology with CDK2.[8,12] Initially, CDK5 was solely thought to have a role in the central nervous system, as p35/p39 is most abundantly expressed in post-mitotic neurons and astrocytes.[11] Through phosphorylation of a slew of neuronal proteins, CDK5 is critical for brain development during embryogenesis and has essential roles in all aspects of neuronal physiology, a majority of which have been extensively studied.[12] Some of these critical neuronal functions include regulation of cell-to-cell adhesion, neuronal survival, neuronal migration and differentiation, membrane trafficking, synaptic function/plasticity, neurite outgrowth, cytoskeletal remodeling, memory formation and pain signaling.[11,12,21,30,32,33] *Cdk5*$^{-/-}$ mutant mice experience perinatal mortality, with 60% reportedly dying in utero. This lack of survival has been primarily attributed to deficits in cortical laminar structure and cerebellar foliation. Such deficits were a result of defects in neuronal migration, with a lack of neuronal layering in the cerebral cortex, cerebellum and hippocampus.[34]

CDK5 deficiency and hyperactivity has also been linked to several neuro-pathological conditions including Alzheimer's disease, ALS, Huntington's disease and Parkinson's disease.[33]

Since CDK5 function has been primarily elucidated in the brain, the majority of known human CDK5 substrates are neuronal specific (**Table 1.1**).

CDK5 substrate	Putative function of phosphorylation
p35	Promotes ubiquitin-mediated proteolysis
p39	
PAK1	Inhibits PAK1 activity, regulation of actin dynamics
Src	Regulation of cell adhesion, actin dynamics, integrin signalling
Cables	Regulation of interaction with *c-Abl*
β–catenin	Regulation of cell adhesion, decreases association with Presenilin1
Tau	Decreases binding to microtubules, and inhibits microtubule nucleation
MAP1B	Regulation of microtubule stability
Nudel	Regulation of dynein-mediated axonal transport
NFH/NFM	Regulation of intermediate filament structure and transport
Synapsin 1	Regulation of synaptic transmission
MUNC18	Disrupts the MUNC18/Syntaxin 1A complex, regulation of neurosecretion
Amphyphysin 1	Regulation of synaptic vesicle endocytosis
β-APP	Regulation of APP localization, membrane transport
DARPP32	Regulation of dopaminergic signalling
PP1-inhibitor	Modulation of amplitude of cAMP-dependent signalling
Pgamma (PDE regulator)	Regulation of retinal phototransduction
ERBB	Regulation of signalling at the neuromuscular junction
pRb	Neuronal differentiation and apoptosis

Table 1.1*:* Previously identified substrates of CDK5 | List of reported CDK5 substrates in the literature (*this figure is reproduced from Dhavan and Tsai*[21]).

1.4 Non-Neuronal Functions of Cyclin Dependent Kinase 5

While the role of CDK5 has been extensively studied in the brain, current literature, demonstrates the critical roles of CDK5 in other non-neuronal biological systems and processes. Some of these known functions include roles in insulin secretion, metabolism, myogenesis, the immune system, the lymphatic system, cell motility, apoptosis, cell cycle regulation, angiogenesis, cell migration and cancer progression (**Table 1.2).**[26]

Biological system/ process	CDK5 function	Mechanism
Central nervous system	Support growth cones	CDK5 phosphorylates CRMP2A at Ser27 during semaphorin3A stimulation. CDK5 also phosphorylates neurofilament heavy chain to promote neurofilament assembly [33-35]
	Growth cone collapse	CDK5 associates with alpha2-chimerin and phosphorylates CRMP2 at Ser522. CRMP2 further phosphorylated and inactivated by GSK3beta [37]
Immune system	Increased IFNγ-induced PD-L1 expression	CDK5 expression decreases the expression of PD-L1 transcriptional repressors (IRF2 and IRF2BP) [55]
Insulin secretion	Reduction of insulin secretion	CDK5 phosphorylates L-VDCC and prevents exocytosis of insulin [13]
Vascular	Promotes angiogenesis	CDK5 expression increases abundance of HIF-1α [53]
Lymphatic	Lymphatic valve formation	CDK5 phosphorylates Foxc2, which regulates the expression of connexin 37 [59]
Cell Cycle	Increased expression of cyclins and other CDK's	Rb is a downstream target of CDK5's activity [50]
	Reduction of CDK5 activity	Cyclin D1 and cyclin E can bind CDK5 to prevent CDK5's activation [39, 40]
Cancer Progression	Cell proliferation	Reduction of p25 expression or CDK5 expression can prevent proliferation [50]
	Cell migration/ metastasis	CDK5 activity leads to caldesmon phosphorylation and actin polymerization. CDK5 enhances pro-migratory P13K/AKT signaling [61, 62]

Table 1.2*:* Known physiological functions of CDK5 | List of the known functions/mechanisms of CDK5 in various biological and cellular processes (*this figure is reproduced from Shupp, et al*).[26]

1.5 Discovery of Cyclin Dependent Kinase 5 as a New Player in Cardiac Function

Sudden death due to cardiac arrhythmia is the most common clinical manifestation of cardiovascular disease, accounting for nearly 50 percent of all cardiovascular-related mortality. [35] Several cardiac disorders are known to contribute to the development of cardiac arrhythmia, with the primary contributor being ischemic heart disease. Arrhythmogenic disorders with genetic

origin accounts for a much small subset of all cardiac arrhythmia, around 2%. One relatively common congenital disorder is long QT syndrome (LQTS), estimated to occur in about 1 in 2,500 individuals. [36,37] Inherited LQTS, the most prevalent inherited cardiac channelopathy, results from mutations in genes encoding ion channels/regulatory molecules implicated in the regulation of ventricular repolarization.[38] Despite the identification of 14 disease causing genes, the underlying mechanisms of LQTS remain to be fully elucidated. Individuals with LQTS often develop ventricular tachycardia, which can lead to fainting, heart failure, as well as sudden death. [39,40] One such fatal LQTS, long QT syndrome type 8 (LQTS8), also termed Timothy Syndrome (TS), is caused by a de-novo gain-of-function mutation in the gene, Calcium Voltage-Gated Channel Subunit Alpha 1 C (*CACNA1C)*. *CACNA1C* encodes the L-type cardiac voltage gated calcium channel $Ca_V1.2$. This L-type channel plays an essential role in both cardiac function and development, contributing to excitation-contraction (EC) coupling of the heart in synchronization with ryanodine receptors (RyR) in the membranes of the sarcoplasmic/endoplasmic reticulum.[41] Individuals with TS experience delayed inactivation of $Ca_V1.2$, causing an abnormally prolonged flow of Ca^{2+} ions into the cardiac muscle.[37]

1.5 Timothy Syndrome and Cyclin Dependent Kinase 5

Human cellular models of TS have been developed by our lab in the past by reprogramming patient specific skin fibroblasts to human induced pluripotent stem cells (hiPSCs). These hiPSC's are subsequently differentiated into cardiomyocytes (CM's), displaying an abnormal cardiac phenotype associated with TS.[42,43] In prior studies, our lab found that roscovitine, a CDK inhibitor that can bind to and increase the voltage-dependent inactivation of $Ca_V1.2$, rescued the abnormal action potential and cardiac $Ca_V1.2$ channel function phenotypes. [43] When testing several different roscovitine analogs/classes of CDK inhibitors, our lab found that four out of five compounds

capable of rescuing the TS phenotype specifically inhibited CDK5; this suggested a potential role for CDK5 in this LQTS (**Fig 1.5**). Additionally, our lab found that CDK5 activator, p35, along with its transcription factor, early growth response-1 (EGR1), and phosphorylated MAPK1/ERK, were all significantly increased in the TS-hiPSC-CM model (**Fig. 1.6**).[44]

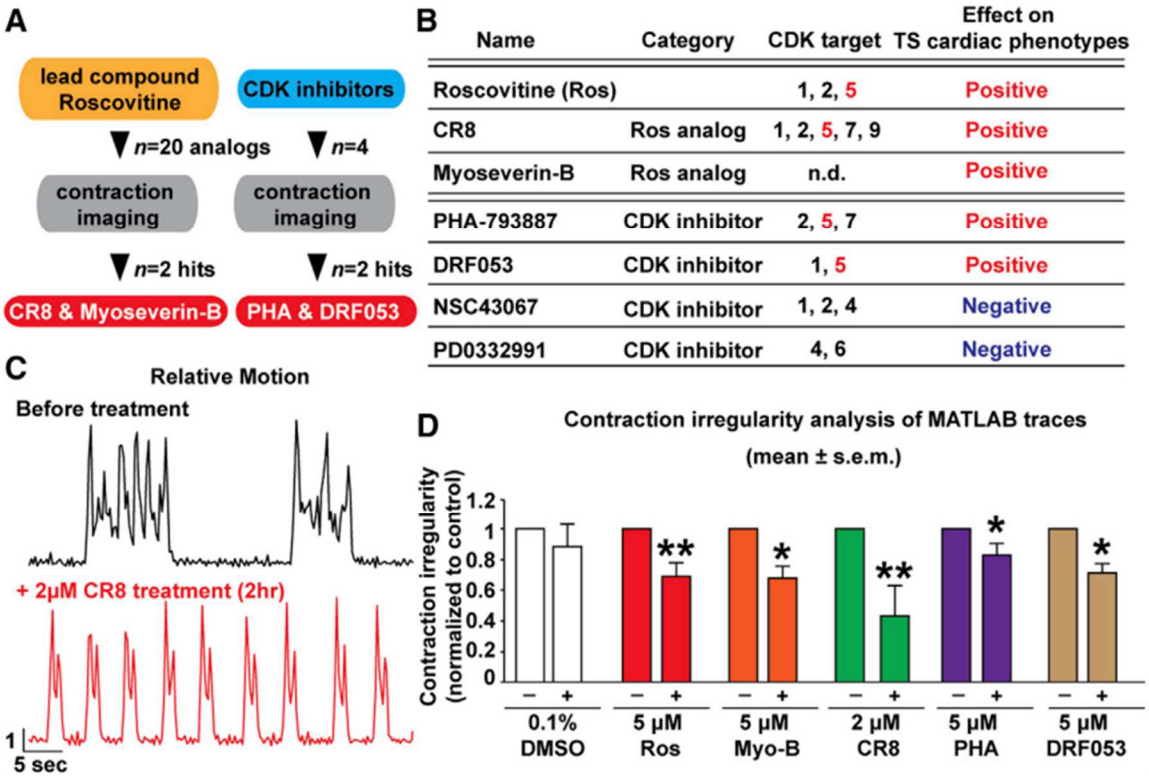

Figure 1.5*:* Summary of Roscovitine analog and CDK inhibitor tests|
A) Schematic illustration of roscovitine analog and CDK inhibitor tests.
(B) A summary of the CDK targets of the positive roscovitine analogs and CDK inhibitors. Eighteen other roscovitine analogs did not show positive effects.
(C) Representative traces from the MATLABbased analysis of TS CM contractions before treatment and 2 hr after the treatment of 2 mM CR8.
(D) The analysis of contraction irregularity of TS CMs before treatment and 2 hr after the treatment of each positive compound (n = 10 for the chemical compounds and n = 5 for DMSO control from one TS iPSC line; the irregularity value after treatment was normalized to the corresponding irregularity value before treatment for each sample in each group). *p < 0.05, **p < 0.01; Student's t test, paired. Ros, roscovitine; Myo-B, myoseverin-B; PHA, PHA-793887. The replicates (n) are independent biological replicates from multiple rounds of experiments. (*This figure is reproduced from Song, et* al).[44]

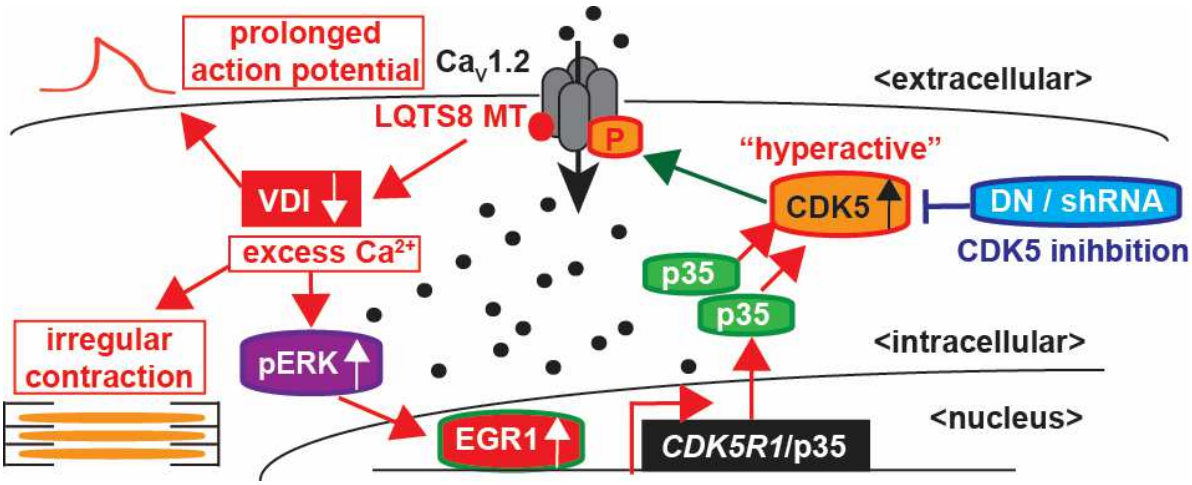

Figure 1.6*:* Proposed mechanism of aberrant signaling pathways in Timothy Syndrome cardiomyocytes | Schematic representation of the proposed signaling pathway in Timothy syndrome cardiomyocytes (*this figure is reproduced from Song, et. al).*[44]

Whole exome sequencing in TS patients revealed no mutations in *CDK5*, *CDK5R1/2*, *EGR1* or *CAPN* genes. This led our lab to hypothesize that increased CDK5 activity could result from altered Ca^{2+} handling due to mutations in $Ca_V1.2$. Lastly, our lab found that CDK5 reduction/inhibition using a dominant negative (DN) mutant and shRNA alleviated cardiac phenotypes in the TS models associated with aberrant Cdk5 hyperactivation (**Fig. 1.7**).[44] While it is evident that aberrant CDK5 activity in TS has lethal consequences, it is unclear as to what the role of CDK5 is at baseline, in the healthy human heart. The aforementioned studies as well as this current study enable us to identify CDK5 as a novel player in cardiac function and cardiac pathophysiological conditions.

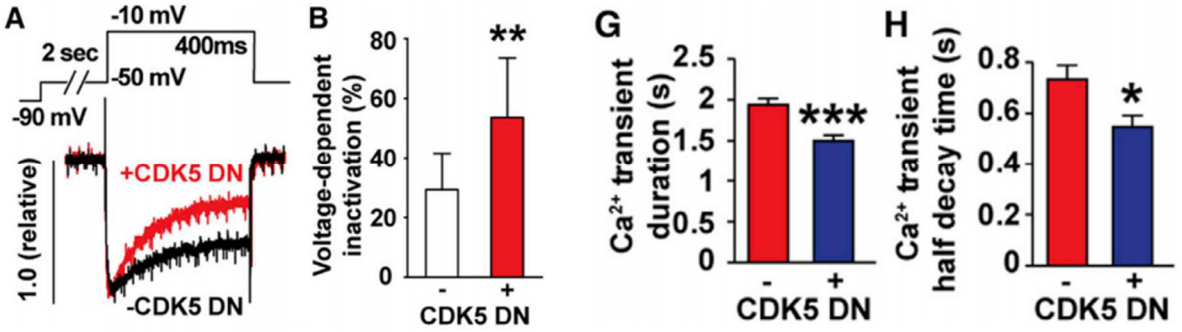

Figure 1.7: CDK5 inhibition alleviated the phenotypes in TS-hiPSC-CM's | (A) Representative voltage-clamp recordings of Ba^{2+} currents in the TS CM with (+CDK5 DN) and without (CDK5 DN) CDK5 DN expression. ''1.0 (relative)'' means that the data points were normalized to the corresponding peak current value to make the traces. (B) Voltage-dependent inactivation percentage quantification in TS CMs with (n = 19) and without (n = 7) CDK5 DN expression. (G & H) The analysis of Ca^{2+} transient duration, half decay time, amplitude, and integrated calcium transients (area under curve) in the paced TS CMs with and without CDK5 DN expression (n = 7 for the group without CDK5 DN, n = 17 for the group with CDK5 DN). (*This figure is reproduced from Song, et. al*)[44]

1.6 Cyclin Dependent Kinase 5 Inhibitors in the Clinic

The importance of identifying a role for CDK5 in the heart extends beyond this study. CDK inhibitors have been at the forefront of drug development for cancer therapeutics and immunotherapy.[4,45] Abnormal increases in CDK activity have been shown to result in unrestricted cell cycle phase transition and promote incessant proliferation, giving rise to tumorigenesis and malignant progression.[46,47] In neu-induced breast cancer, for example, CDK4 is essential for tumorigenesis, with inhibition of the CDK4-cyclin D1 complex shown to suppress tumor formation/progression.[48] *CDK11* expression has shown to be significantly upregulated in biopsy samples from primary multiple myeloma.[49] Non-cell cycle CDK's have also been the focus of cancer treatment targets, including *CDK58*, *CDK9*. In colon cancer, *CDK8* copy number gains of >60% have been observed in colorectal tumors.[50] A search for active clinical trials testing CDK

inhibitors as of June 2021 (ClinicalTrials.gov search criteria includes: recruiting, not yet recruiting, active not recruiting and enrolling by invitation) returns 141 results. While the cell-cycle related roles of CDK's have been extensively studied, the majority of human CDK's have unknown roles in cell physiology, particularly the more "unconventional" CDK's including CDK5, CDK5-10-11, CDK14-18, and CDK-20.[51] While modulation of CDK activity may serve beneficial in one physiological system, it may prove deleterious in another. It is therefore imperative that the full range of molecular and physiological roles of each CDK be fully elucidated prior to therapeutic application.

Recent studies implicate a role for hyperactive activity and expression of *CDK5* in a variety of cancer types including colon, melanoma, thyroid, breast, lung, brain, colon, leukemia and lymphoma (Table 1.4).[52] Previously, the development of cancer therapeutics was mainly focused on targeting tumor-associated mutations, however, the multifaceted role of *CDK5* expression/activity in cancer targets mechanisms including tumor proliferation via the DNA damage response, growth, migration into secondary organs, metastatic invasion, anti-tumor immunity and predictions of cancer severity.[21,52-56] Alternatively, other groups have suggested *CDK5*'s role as a tumor suppressor via the facilitation of apoptosis and inhibition of proliferation. Some of the previously studied functions of CDK5 in different human cancer have been outlined in **Table 1.3**.[52]

Expression of Cdk5 in human cancers

Cancer	Cdk5 function
Breast	Proliferation, survival, EMT, metastasis
Colorectal	Proliferation
Gastric	Cell cycle suppressor
Glioma, glioblastoma	Invasion
Hepatocellular carcinoma	Migration, angiogenesis, inflammation, lymphatic development
Head and Neck -	Not known
Leukemia	Survival
Lung - Small cell lung cancer (SCLC), carcinoids	Proliferation, migration
Lung – Non small cell lung cancer (NSCLC)	Proliferation, migration, invasion
Mantle cell lymphoma	Proliferation
Medulloblastoma	Immune evasion
Melanoma	Proliferation, invasion
Multiple myeloma	Not known
Ovary	Migration
Pancreatic	Proliferation, migration, invasion, metastasis
Pituitary Adenoma	Migration, invasion
Prostate	Proliferation, migration, invasion, metastasis, apoptosis
Thyroid - Medullary thyroid carcinoma	Proliferation

Table 1.3*:* Known roles of CDK5 in various types of cancer | (*Reproduced from Pozo and Bibb*).[52]

Current efforts to pinpoint CDK5 and their downstream targets include small molecule inhibitors that occupy the ATP binding/catalytic pocket in order to impede kinase activity, termed CDKi's.[51] Such pharmaceutical agents, however, inhibit more than one CDK since catalytic pockets are highly conserved across CDK family members (**Table 1.4**).[52] One such non-specific inhibitor is Flavopiridol (L86-8275), which was initially developed for the treatment of multiple myeloid leukemia. Flavopiridol has also been studied for treatment of autoimmune rheumatoid arthritis as well as atherosclerosis [57-61] Drug discovery efforts have also led to the development of CDK5-substrate or activator specific peptides to block CDK5 binding, with one such example

being AT519.[62-64] Such peptide blockers are still non-specific, with AT519 known to target CDK2, CDK4 and CDK9 in addition to CDK5.[52]

List of Compounds that Inhibit CDK5 in Clinical Trials (Past and Present)

Compound	Disease	CDK Targets
R-roscovitine (CYC202)	Advanced solid tumors, non-small cell lung cancer, breast cancer, Cushing's disease, rheumatoid arthritis, cystic fibrosis	1, 2, 4, **5***, 6, 7, 8, 9
Dinaciclib (SCH727965)	Advanced malignancies, relapsed multiple myeloma, cholangiocarcinoma	1, 2, **5***, 9
Flavopiridol (L86-8275)	Leukemia, multiple myeloma, lymphoma, sarcoma, solid tumors	1, 2, **5***, 9
AT7519	Advanced/metastatic solid tumors, lymphoma	2, 4, **5***, 9
CYC065	Relapsed or refractory chronic lymphocytic leukemia, relapsed or refractory myelodysplastic syndromes, relapsed or refractory acute myeloid leukemia	2, 3, **5***, 9
Olomoucine	Advanced solid tumors	1, 2, **5***, 6
Purvalanol A	Advanced solid tumors, follicular lymphoma, diffuse large B-cell non-Hodgkin's lymphoma	1, **5***
SNS-032	Advanced Chronic Lymphocytic Leukemia and Multiple Myeloma	2, **5***, 7, 9
AT7519	Solid tumors	1, 2, 3, 4, **5***, 6, 9

Table 1.4: List of CDK5 inhibitors previously/currently in clinical trials | The above table represents a partial list according to a literature search of compounds/drugs known to inhibit CDK5 (in addition to other CDK's) that were used for cancer treatment.

With the widespread use of CDK inhibitors, it's essential to elucidate the unknown physiological role these CDK's play in each cell type/tissue type/organ system. Prior to findings from the Yazawa Lab, a role for CDK5 in the cardiovascular system had not been discussed in the literature. If CDK5 is to be used as a target for drug discovery, a cardiac-specific role of CDK5 at baseline must be known. Furthermore, modulation of CDK5 activity may provide further insight

into heart disease pathology and help with drug discovery for conditions lacking effective treatment options.

Chapter 2: Effects of Cdk5 Depletion on the Adult Mouse Myocardium

2.1 Introduction

Published findings from the Yazawa lab utilizing hiPSC-CM's from TS patients carrying a mutation in *CACNA1C* have demonstrated a critical role for CDK5 in the underlying cardiac pathophysiology of TS.[43,44] The disease causing *de novo* gain of function mutation, G1216A in *CACNA1C,* the gene that encodes the L-type voltage gated Ca^{2+} channel $Ca_V1.2$, resulted in a G406R mutation in $Ca_V1.2$. Due to this mutation TS-hiPSC-CM's displayed an irregularity in contraction/electrical activity, excess intracellular calcium influx, abnormal calcium transients and prolonged action potentials. TS-hiPSC-CM's also showed a significant increase in CDK5 activity along with an overexpression of *CDK5R1*/p35, CDK5's known activator. Based on these findings, a role for CDK5 in cardiac Ca^{2+} channel regulation via phosphorylation in the II-III loop of $Ca_V1.2$ was proposed. In individuals with TS, the hyper-activation of CDK5 causes cardiac Ca^{2+} channel irregularity. At baseline, however, in an individual with a healthy heart, the role of CDK5 has yet to be established. It is therefore the overarching goal of this study to determine whether CDK5 is essential for adult cardiac function. To answer this question, a novel transgenic mouse line with a cardiac specific temporospatial depletion of Cdk5 was established.

Cardiac-specific Cdk5 deficiency in the adult mouse heart was achieved by generation of a temporal Cre-mediated knockout of *Cdk5* driven by the cardiomyocyte specific *Myh6* promoter. Murine *Myh6* (located on chromosome 14:54,941,921-54,966,641) codes for the protein αMHC, an alpha heavy chain subunit of cardiac myosin, which is expressed exclusively in juvenile and adult cardiomyocytes. [65-68] It functions directly in cardiomyocyte contraction, serving as a fast

ATPase myosin.[69,70] Using Cre-LoxP technology, commercially available *Cdk5* flox mice (*Cdk5* flanked by LoxP recombinase recognition sequences) were crossed with commercially available αMHC-MerCreMer^{+} transgenic mice.

MerCreMer consists of Cre recombinase fused to two mutated ligand binding domains (LBD) termed "Mer" (modified estrogen receptor).[71,72] Each LBD Mer no longer has the ability to bind to estrogen/progesterone, however, it does have the ability to bind to a synthetic estrogen receptor ligand such as tamoxifen (Tam).[72-76] In the absence of Tam, MerCreMer is sequestered to the cytoplasm by heat shock protein 90 (HSP90). Once Tam is administered, MerCreMer becomes unbound from HSP90 and translocates from the cytoplasm to the nucleus.[71,77] This translocation allows for recombination of tissue/cell type-specific floxed genes, in this case, cardiac specific depletion of *Cdk5* (**Fig 2.1**).[78]

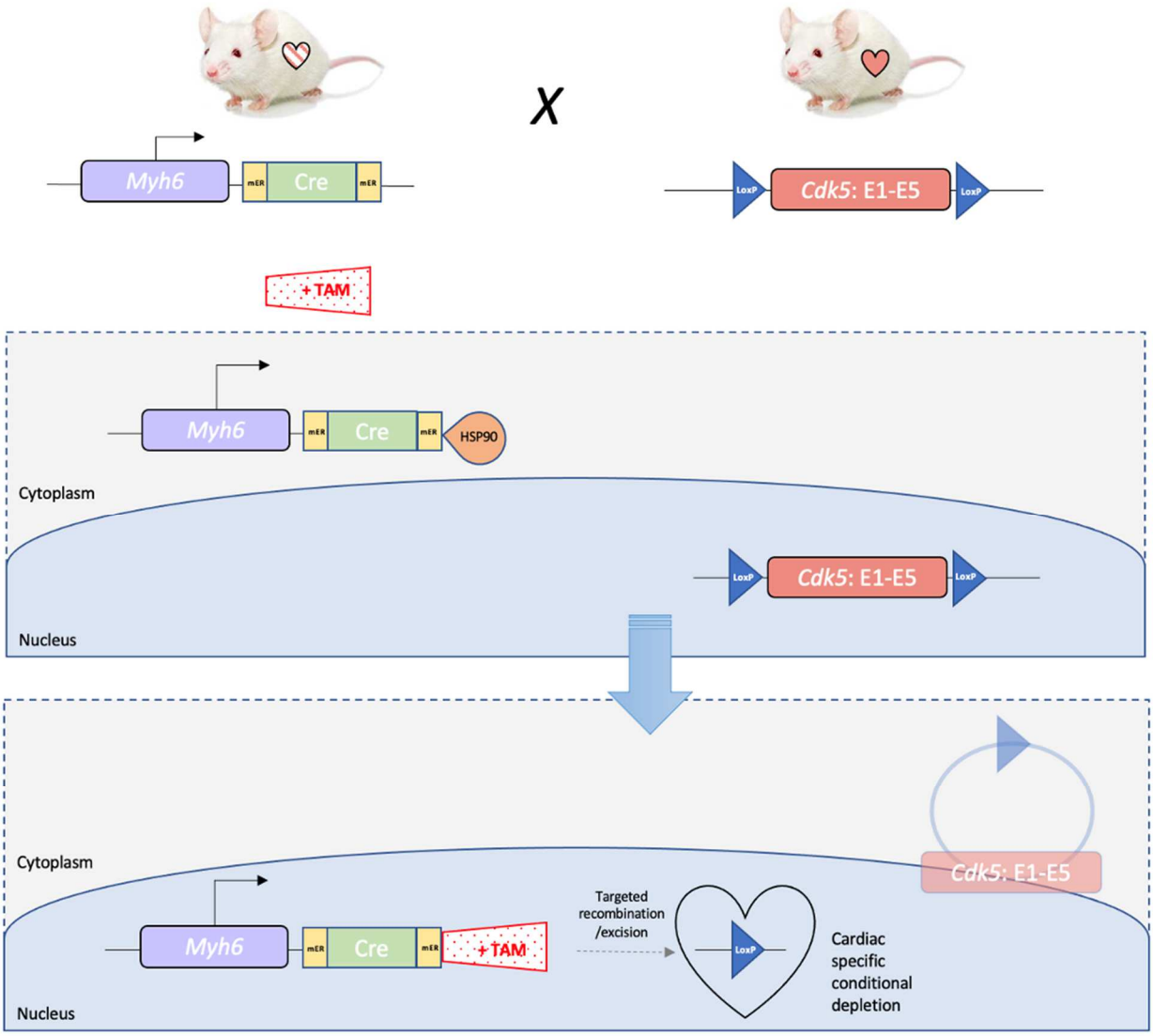

Figure 2.1: Mechanism for cardiac-specific depletion of Cdk5 using the MerCreMer Cre-LoxP recombinase system

To characterize the phenotype of these Cdk5 deficient mice, heart histology, echocardiography (echo) and bottom-up tandem mass tag (TMT)-based quantitative proteomic studies were conducted. Results from the studies discussed in this chapter indicated severe systolic dysfunction in both heterozygous and homozygous depletion models, alongside development of an acute dilated cardiomyopathy (DCM)-like phenotype.

2.2 Results

To determine the non-developmental, cardiac-specific role of CDK5, a cardiac-specific inducible Cdk5 deficient mouse model was developed (*Cdk5*$^{fl/fl}$ or *Cdk5*$^{fl/fl}$; αMHC-MerCreMer^{+}). The Cdk5 deficient mouse was established by crossing a *Cdk5*$^{fl/fl}$ mouse (B6.129S4(Cg)-*Cdk5*$^{tm1.1Lht}$/J, JAX #:014156) with an αMHC-MerCreMer^{+} transgenic mouse (*Myh6-cre/Esr1**, JAX #5657) (**Fig 2.2**). A total of four groups with four distinctive phenotypes were used for this study: (1) *Cdk5*$^{fl/fl}$: αMHC-MerCreMer^{+}, (2) *Cdk5*$^{fl/+}$: αMHC-MerCreMer^{+}, (3) *Cdk5*$^{fl/fl}$ or *Cdk5*$^{fl/fl}$ x WT and (4) WT*:* αMHC-MerCreMer^{+}. Going forward, cohort/genotype short-hand will read: (1) *Cdk5*$^{fl/fl}$, (2) *Cdk5*$^{fl/+}$ (3) WT and (4) WT^{MCM} , respectfully. The latter two cohorts, WT and WT^{MCM}, are two distinct control groups—"WT" serving as a control for *Cdk5,* and "WT^{MCM}" serving as a control for spatiotemporal Cre recombination. For breeding efficiency purposes, WT mice served as the control littermate cohort in this chapter.

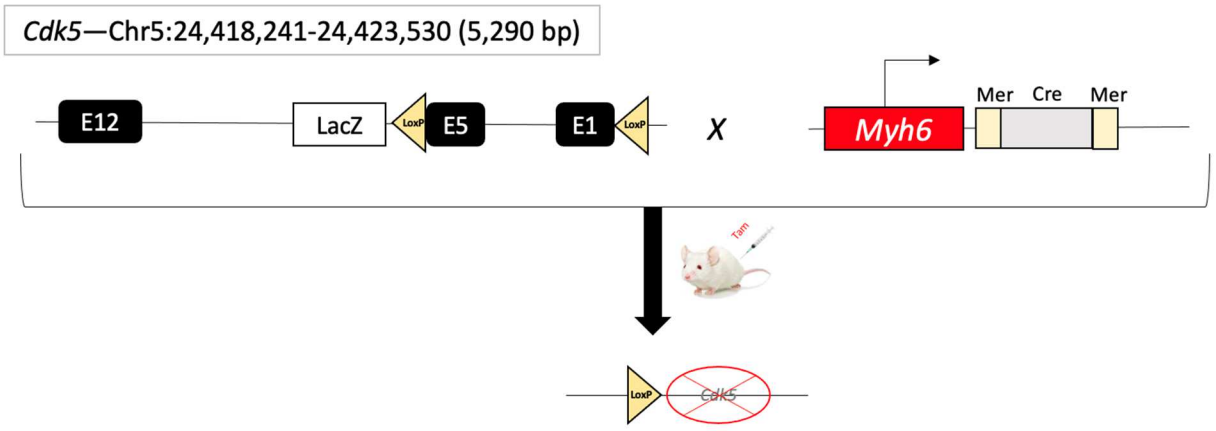

Figure 2.2*:* Generation of inducible cardiac-specific Cdk5 depletion mouse model | *Cdk5 flox* line was crossed with αMHC-MerCreMer (*Myh6-cre/Esr1**, JAX #5657) line. Recombination was inducible upon administration of Tamoxifen.

At 12 weeks of age, Tam was administered via intraperitoneal (I.P.) injection to induce cardiomyocyte-specific Cdk5 depletion (**Fig. 2.2**). A high concentration of Tam is known to have

adverse effects on normal heart function, more so significant in male mice.[79] Our lab has previously optimized the dosing schedule of our current lot of Tam (Sigma-Aldrich, Lot #WXBC1801V) to accomplish the Cdk5 deficiency in both adult male and female flox mice with minimal cardiotoxicity. Female mice received 50 mg/kg (~3mg/mouse total) of Tam for three sequential days and male mice received 37.5 mg/kg (~3.75 mg/mouse total) over five sequential days.

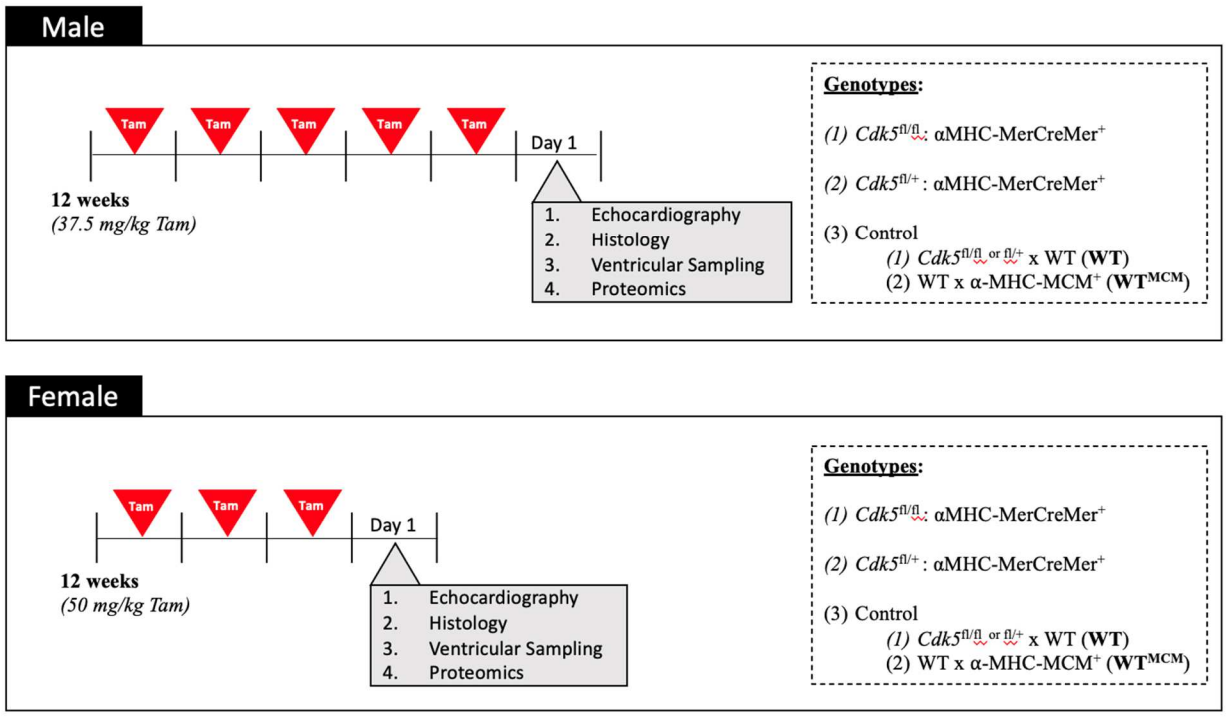

Figure 2.3: Experimental outline | Inducing cardiac-specific Cdk5 deficiency using a previously optimized gender specific protocol. Male mice received 37.5 mg/kg of Tam over 5 days; female mice received 50mg/kg Tam over 3 days. Assay's conducted post-Cdk5 depletion include echocardiography, histology, ventricular sampling and proteomic analysis.

Echo measurements were taken one day post final Tam injection. An echo is a non-invasive ultrasound of the heart that captures real-time images to observe cardiac structure and function.[80] This technique allows for the detection of any structural or hemodynamic abnormalities that may

be present. [81,82] In both *Cdk5*$^{fl/fl}$ and *Cdk5*$^{fl/+}$ mice, echo measurements indicated severe systolic dysfunction defined by impaired ventricular contraction (i.e. the loss of inotropy), while both WT and WT^{MCM} mice were within normal limits for a standard C57B/6J mouse (**Fig 2.4—A, B**),.[83,84] *Cdk5*$^{fl/+}$ and *Cdk5*$^{fl/fl}$ mice displayed a significant decrease in ejection fraction (EF) ($p<0.0001$): *Cdk5*$^{fl/+}$: 20.81 ± 7.539, *Cdk5*$^{fl/fl}$: 17.96 ± 7.216 vs WT: 66.49 ± 2.625 and WT^{MCM}: 61.88 ± 7.207. EF represents the percentage of pooled blood the left ventricle (LV) can pump out with each contraction. Fractional shortening (FS), the percent change in the diameter of the LV during systole, was also significantly decreased in Cdk5 deficient mice vs control mice ($p<0.0001$): *Cdk5*$^{fl/+}$: 9.483 ± 3.559, *Cdk5*$^{fl/fl}$: 8.155 ± 3.491 vs WT: 35.92 ± 1.905 and WT^{MCM}: 32.72 ± 4.674 (**Fig 2.4—B**).

Furthermore, echo features of a DCM-like phenotype were observed. This included LV chamber dilation, thinning of the LV muscle walls, systolic dysfunction and decreased contractility (**Fig 2.4—A,B**).[85] Measures of left ventricular end diastolic diameter (LVEDD) were as follows: *Cdk5*$^{fl/+}$: 4.453 ± 0.4904, *Cdk5*$^{fl/fl}$: 4.612 ± 0.3882 vs WT: 3.436 ± 0.7930 and WT^{MCM}: 3.627 ± 0.4394. Measures of left ventricular end diastolic volume (LVEDV) were as follows: *Cdk5*$^{fl/+}$: 91.63 ± 22.37, *Cdk5*$^{fl/fl}$: 98.87 ± 18.37 vs WT: 49.02 ± 8.374 and WT^{MCM}: 55.90 ± 18.49. WT and WT^{MCM} were statistically similar in nearly all echo read-out values, with only a slight reduction in FS ($p<0.05$), however still within standard measures for a healthy C57B/6J mouse. The slight difference in FS was most likely due to experimental limitations of a cardiac-specific inducible system, with MerCreMer translocation from the cytoplasm to the nucleus thought to have a transient baseline level of cardiotoxicity.[79]

Lastly, there was no statistically significant difference in cardiac function between *Cdk5*$^{fl/+}$ and *Cdk5*$^{fl/fl}$ cohorts. Quantitative real time PCR (qRT-PCR), however, revealed a significant

difference (*p<0.05) in mRNA expression between *Cdk5*$^{fl/+}$ and *Cdk5*$^{fl/fl}$ when normalized to *Gapdh*—0.6726 ± 0.09121 vs 0.3533 ± 0.1455, respectively (**Fig 2.4—C**). One potential explanation is that *Cdk5* is a haploinsufficient gene, where just one functioning copy of *Cdk5* is not adequate to preserve gene function. Haploinsufficiency is commonly observed in a number of genes implicated in congenital cardiac syndromes.[86] Haploinsufficiency in genes encoding kinases, however, are less common, but still found to exist. In mice, a heterozygous loss of function mutation in *Cdk9* resulted in cardiac, skin and epididymis morphological deficiencies.[87] Additional haploinsufficient kinases include liver kinase B1, a serine-threonine kinase responsible for the phosphorylation and activation of AMP-activated protein kinase, as well as CDK12 and CDK13.[88,89] From this point forward, *Cdk5*$^{fl/+}$ and *Cdk5*$^{fl/fl}$ cohorts will be collectively referred to as "Cdk5 deficient" mice.

A

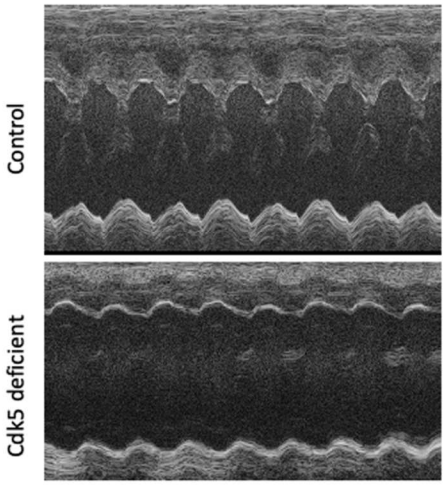
Control
Cdk5 deficient

C

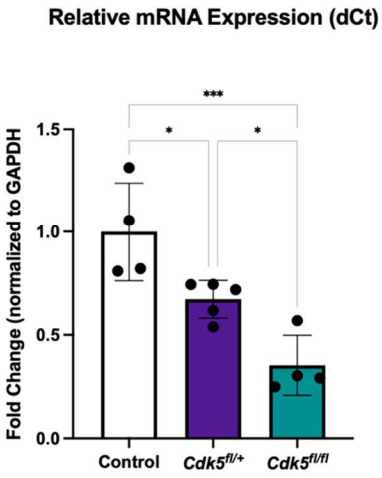
Relative mRNA Expression (dCt)
Fold Change (normalized to GAPDH
1.5
1.0
0.5
0.0
***
*
*
Control
Cdk5fl/+
Cdk5fl/fl

B

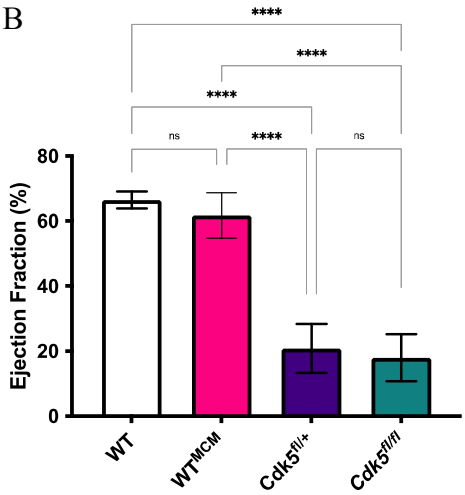
Ejection Fraction (%)
80
60
40
20
0
****
****
****
ns
****
ns
WT
WTMCM
Cdk5fl/+
Cdk5fl/fl

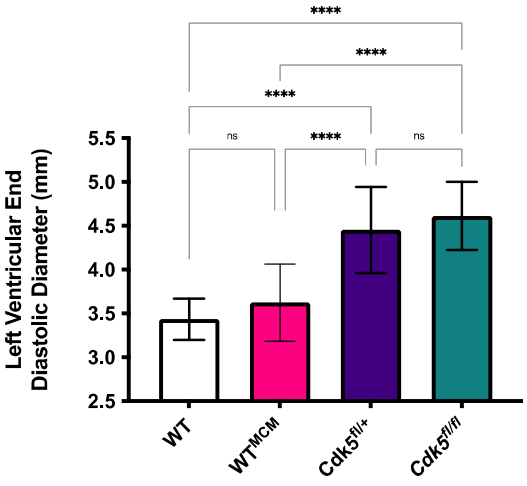
Left Ventricular End Diastolic Diameter (mm)
5.5
5.0
4.5
4.0
3.5
3.0
2.5
****
****
****
ns
****
ns
WT
WTMCM
Cdk5fl/+
Cdk5fl/fl

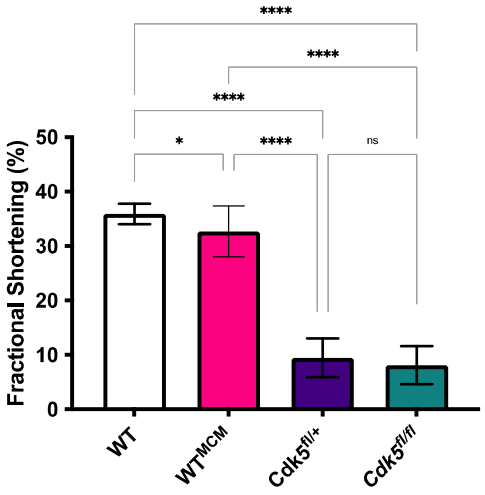
Fractional Shortening (%)
50
40
30
20
10
0
****
****
****
*
****
ns
WT
WTMCM
Cdk5fl/+
Cdk5fl/fl

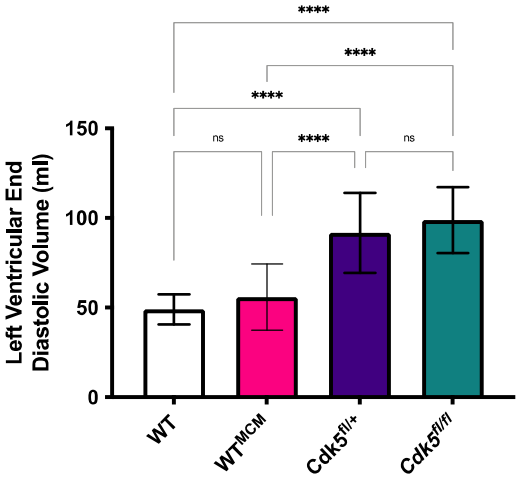
Left Ventricular End Diastolic Volume (ml)
150
100
50
0
****
****
****
ns
****
ns
WT
WTMCM
Cdk5fl/+
Cdk5fl/fl

Figure 2.4*:* Echo analysis of cardiac structure and function in Cdk5 deficient mice|
A) Representative echo images in M-mode from a littermate control (example from female WT mouse) and Cdk5 deficient mouse (example from female *Cdk5*$^{fl/fl}$ mouse).
B) Cardiac function was measured with echocardiography. Four measured values including ejection fraction (EF), fractional shortening (FS) , left ventricular end diastolic diameter (LVEDD) and left ventricular end diastolic volume (LVEDV) are shown. WT n=21 ; WT^{MCM} n=16 ; Cdk5$^{fl/+}$ n=10 ; Cdk5$^{fl/fl}$ n=12. All error bars represent standard deviation. Statistical analysis done with on ordinary one-way ANOVA using Tukey's post-hoc multiple comparison using GraphPad Prism 8/9; P-values <0.05 were considered significant; *p<0.05, **p<0.01, ***p<0.001, ****p<0.0001; mean ± S.D).
C) qRT-PCR of *Cdk5*$^{fl/fl}$ *Cdk5*$^{fl/+}$ and littermate control (WT) mice (*p<0.05 using on ordinary one-way ANOVA with Tukey's post-hoc multiple comparison using GraphPad Prism 8/9, control n=4; *Cdk5*$^{fl/fl}$ n =5 ; *Cdk5*$^{fl/fl}$ n =4; mean ± S.D.).

Histopathological analysis with Mason's trichrome (MTS) and hematoxylin and eosin (H & E) stains of whole heart ventricular tissue revealed a DCM-like phenotype (**Fig. 2.5—A-F)**. It should be noted that no observable histological differences were seen between WT and WT^{MCM} cohorts.

Cdk5 deficient mice had notable thinning of both the left and right ventricle walls. Additionally, the LV was significantly dilated in Cdk5 deficient mice. Staining with MTS revealed some collagen fiber deposition as indicated by the green arrows (**Fig 2.5—I, K, M**). H&E staining revealed enlarged myocytes and nuclei in Cdk5 deficient mice compared with that of WT mice (**Fig 2.5—H, J, L**). Furthermore, H&E staining appeared to show a focal myocarditis-like phenotype with mononuclear cell infiltrate. In summary, histological findings support a LV dilation/DCM-like phenotype, consistent with the readouts observed during echo.

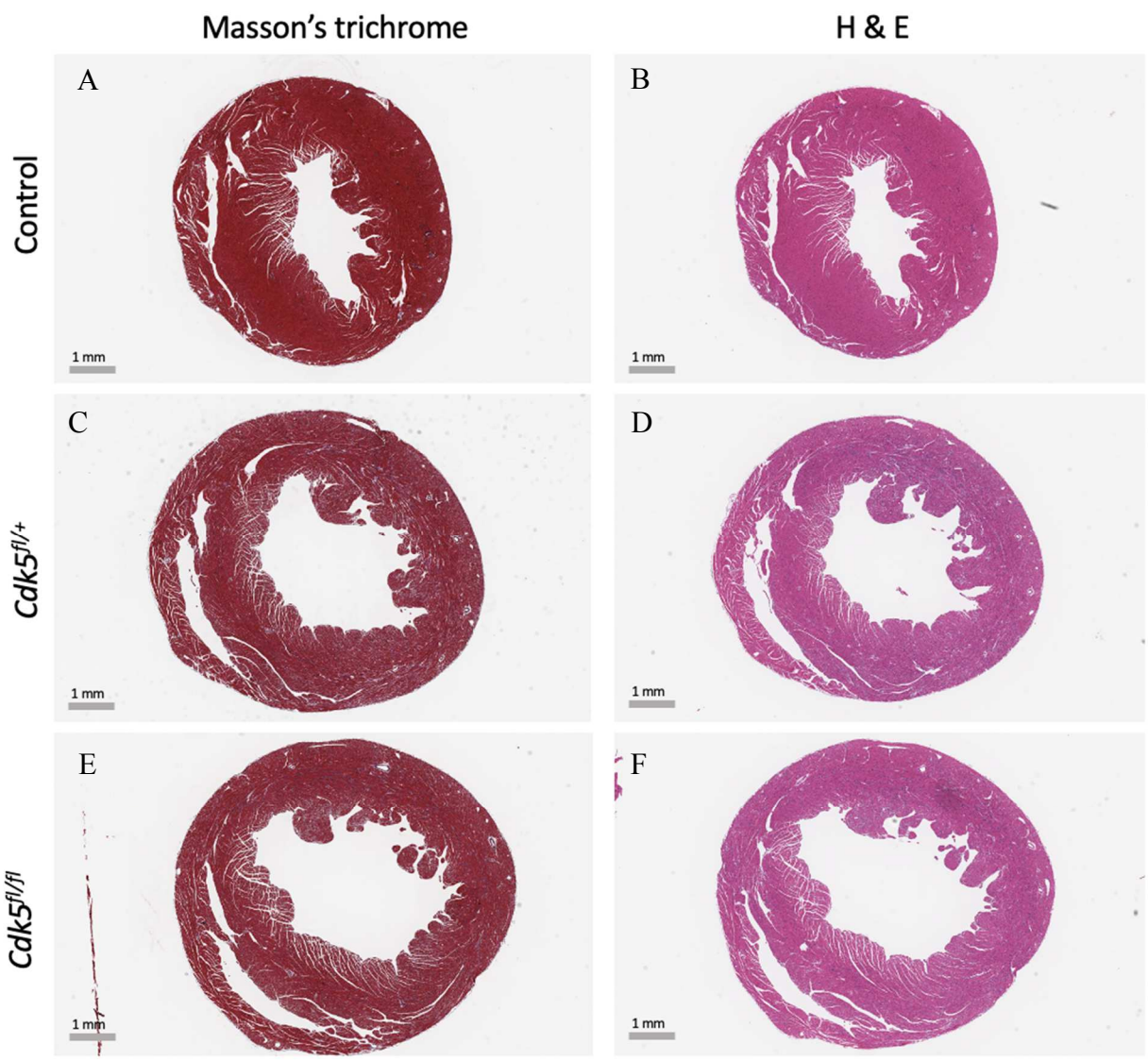
Masson's trichrome
H & E
Control
Cdk5fl/+
Cdk5fl/fl
A
B
C
D
E
F
1 mm
1 mm
1 mm
1 mm
1 mm
1 mm

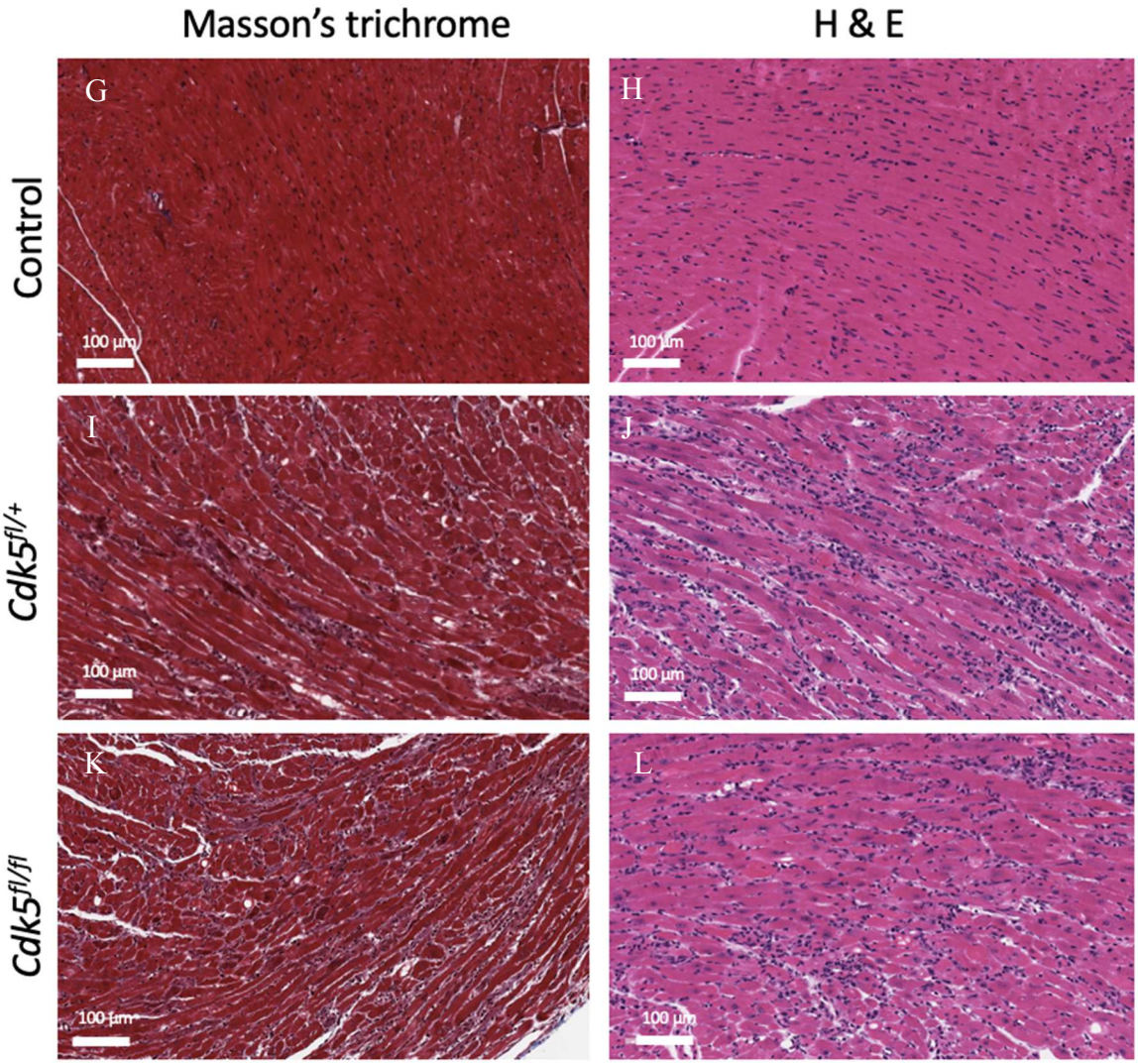
Masson's trichrome
H & E
Control
Cdk5fl/+
Cdk5fl/fl
G
H
I
J
K
L
100 µm

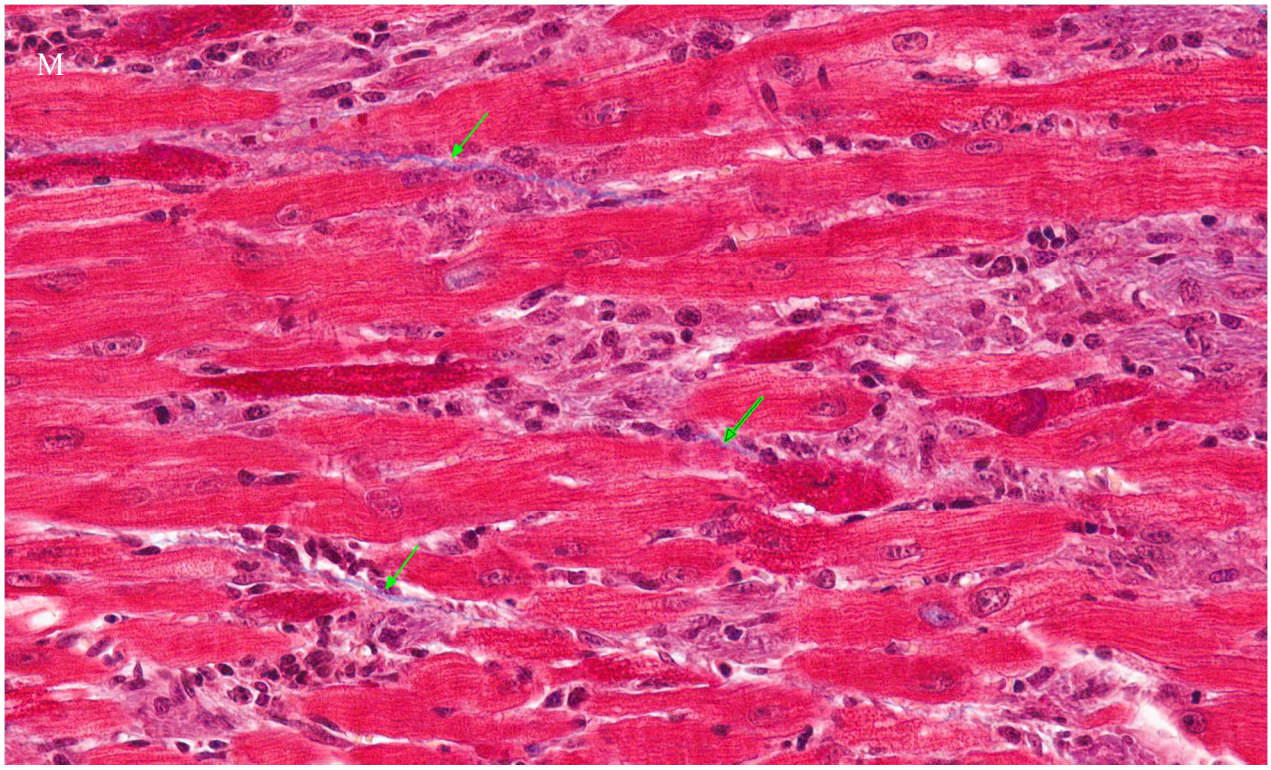

Figure 2.5*:* Histopathology of ventricular cardiac tissue from 12-week old Cdk5 deficient mice| Representative histological images from whole heart ventricular cross-sections of littermate control (WT), $Cdk5^{fl/+}$ and $Cdk5^{fl/fl}$. Staining for morphology assessment is done with Mason's Trichome stain (MTS) and hematoxylin & eosin (H&E). In the MTS slides, nuclei and other basophilic structures are stained purple, while smooth muscle tissue stains bright red and collagen fibers appear in blue. In H&E stained slides, extracellular matrix and cytoplasm stain pink while nuclei appear in dark blue/purple.
A-F) Image of whole heart ventricular cross section with a scaling bar drawn to 1 mm.
G-L) Zoomed in image from left ventricle muscle with scaling bar drawn to 100 µm
M) Magnified and color contrasted image of a representative Cdk5 deficient mouse from TMS stain with signs of fibrosis

Bottom-up global and phosphoproteomic studies were conducted via liquid chromatography coupled with mass spectrometry (LS-MS/MS). Sixteen flash frozen whole heart ventricular tissue samples were lysed with urea and proteins were subsequently converted into peptides by tryptic digestion. The resulting peptide mixture for individual samples were labeled with reporter ions using TMT labeling, and samples were mixed in bulk to ensure homogenous

labeling. Proteins then underwent fractionation, and high throughput LS-MS/MS was used to analyze and quantify intact proteins. Lastly, data was analyzed for statistical significance and biological relevance (**Fig 2.6**). In this chapter, I will focus on results from global proteomic LC-MS/MS; results from phosphoproteomic LC-MS/MS will be discussed in Chapter 4.

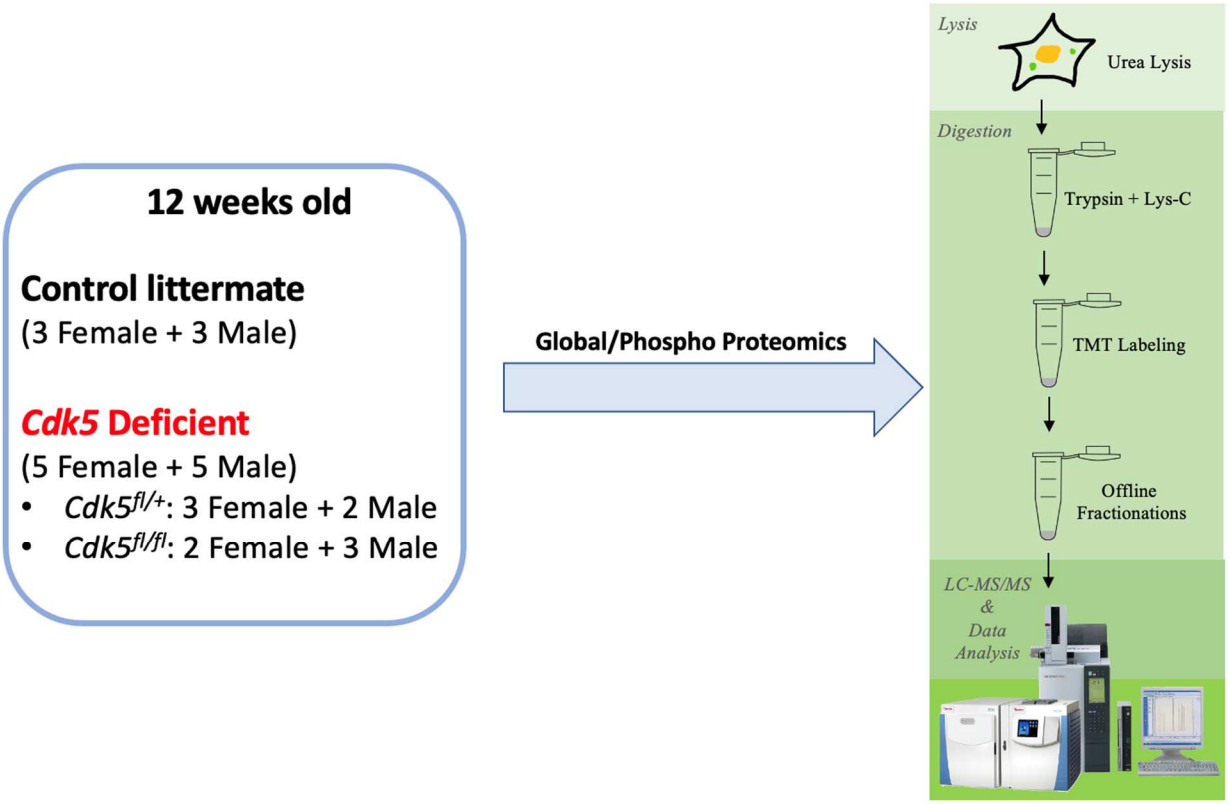

Figure 2.6*:* Experimental setup/ bottom-up proteomic workflow for Cdk5 deficient mice

Differential expression analysis of the global proteome when comparing Cdk5 deficient vs control mice resulted in 2,027 differentially expressed proteins (FDR = 0.05, S0=0.1) (**Fig 2.7—A,B**). The top three proteins with the most significant increase in fold change were nicotinamide riboside kinase 2 (Nmrk2), myeloperoxidase (Mpo) and chitinase-like protein 3 (Chil3), all with

about a 3x fold increase. NMRK2 is a muscle-specific β1 integrin binding protein that is seldom expressed in healthy cardiac tissue. Significant upregulation of Nmrk2 in several different mouse models of DCM has been reported in the literature.[90-92] NMRK2 is required for the maintenance of cardiac structure and function, with upregulation observed during cardiac remodeling efforts related to DCM.[91] MPO is a leukocyte-derived enzyme and is key player in the innate immune response via catalysis of the formation of several reactive oxygen species (ROS) and recruitment of leukocytes.[93,94] Elevated MPO has been implicated in heart failure, cardiac arrhythmia and coronary artery disease. Dysregulation of MPO is also associated with cardiac tissue damage and an increased risk stratification for various cardiovascular diseases. [93,95-97] Lastly, CHIL3 (also termed YKL-40) is an inflammatory glycoprotein that's secreted by activated leukocytes in inflamed tissue. As a biomarker of cell adhesion, CHIL3 is reportedly upregulated in individuals with chronic heart failure, myocardial infarction and coronary artery disease.[98,99]

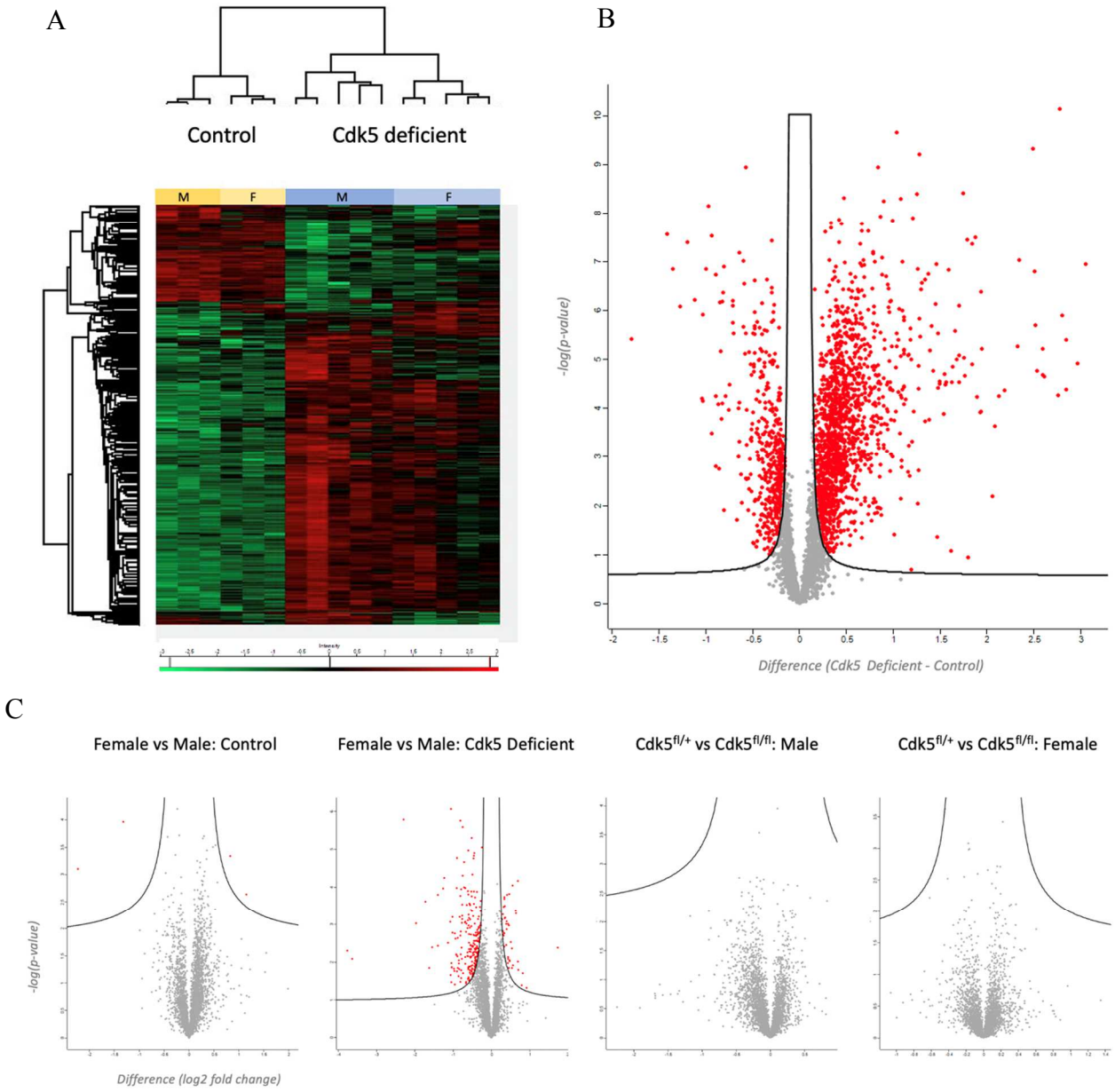

Figure 2.7*:* Comparative analysis of the global proteome

A) Unsupervised hierarchical clustering of 2,027 differentially expressed proteins (Cdk5 deficient n = 10; littermate control WT n = 6).

B) Volcano plot showing proteins with differential abundance when comparing cardiac tissue of Cdk5 deficient mice vs that of littermate control. Red filled circles in the right area of the volcano plot represent proteins more significantly abundant in the Cdk5 deficient cohort; red filled circles in the left area of the volcano plot represent proteins more significantly abundant in the control cohort.

C) Volcano plot representing proteins with differential abundances when comparing: (1) *Cdk5*$^{fl/+}$ female vs *Cdk5*$^{fl/fl}$ female (2) *Cdk5*$^{fl/+}$ male vs *Cdk5*$^{fl/fl}$ male (3) Cdk5 deficient female vs Cdk5 deficient male and (4) Control female vs control male.

*For each protein, significance is expressed as FDR adjusted p-value as a function of difference between samples (log_2 fold change). FDR = 0.05, s0= 0.1. Significantly upregulated/downregulated proteins are shown with red circles. Figures generated with MaxQuant—Perseus software.

Proteins with the most significance decrease in fold change were calcium/calmodulin-dependent 3',5'-cyclic nucleotide phosphodiesterase 1C (Pde1c), F-box only protein 40 (Fbxo40) and FH1/FH2 domain-containing protein 3 (Fhod3). PDE1C is highly expressed in human cardiomyocytes and is known to regulate cardiac function via cyclic AMP and cyclic GMP. Interestingly, the literature reports an upregulation in PDE1C during heart failure, with inhibition of PDE1C thought to have attenuative effects on cardiomyocyte apoptosis. A role for the downregulation of PDE1C at baseline has yet to be elucidated.[100-103] Fbxo40, a ubiquitin ligase, is expressed in skeletal and cardiac muscle. In the literature, *in vivo* knockdown of Fbxo40 has been associated with induction of significant myocardial hypertrophy as well as significant thickening in myotubules as part of uncontrolled cardiac hypertrophy.[104,105] The third most significantly downregulated protein, Fhod3, is a diaphanous related formin known to play a role in cardiomyocyte actin filament polymerization. Reduction in FHOD as well as loss of function mutations in *FHOD3* are directly correlated with development of DCM.[106,107] A list of the top 30 up and down regulated proteins in Cdk5 deficient mice can be found in **Table 2.1**.

Further hierarchical sub-clustering based on gender within each of the two cohorts was observed (**Fig 2.7—A**). Additional analysis between gender in control and Cdk5 deficient cohorts, was conducted to look at gender-specific differentially expressed proteins. In control mice, only four proteins were found to be differentially expressed: decreased expression—(1) equilibrative nucleoside transporter 1(Slc29a1), (2) serpin family A member 1 (Serpina1e) and increased expression—(3) cell division cycle-associated protein 2 (Cdca2) and (4) 60S acidic ribosomal protein P1(Rplp1) (**Fig 2.7—C**). In Cdk5 deficient mice, however, 278 proteins were found to be

differentially expressed—231 proteins with a decrease in quantitative abundance and 46 with an increase in quantitative abundance in female mice.

There was no observed difference in differential protein expression between heterozygous and homozygous *Cdk5 flox* mice in either the male or female cohorts (**Fig. 2.7—C**). This lack of difference between heterozygous and homozygous *Cdk5 flox* mice was in concordance with echo and histology results.

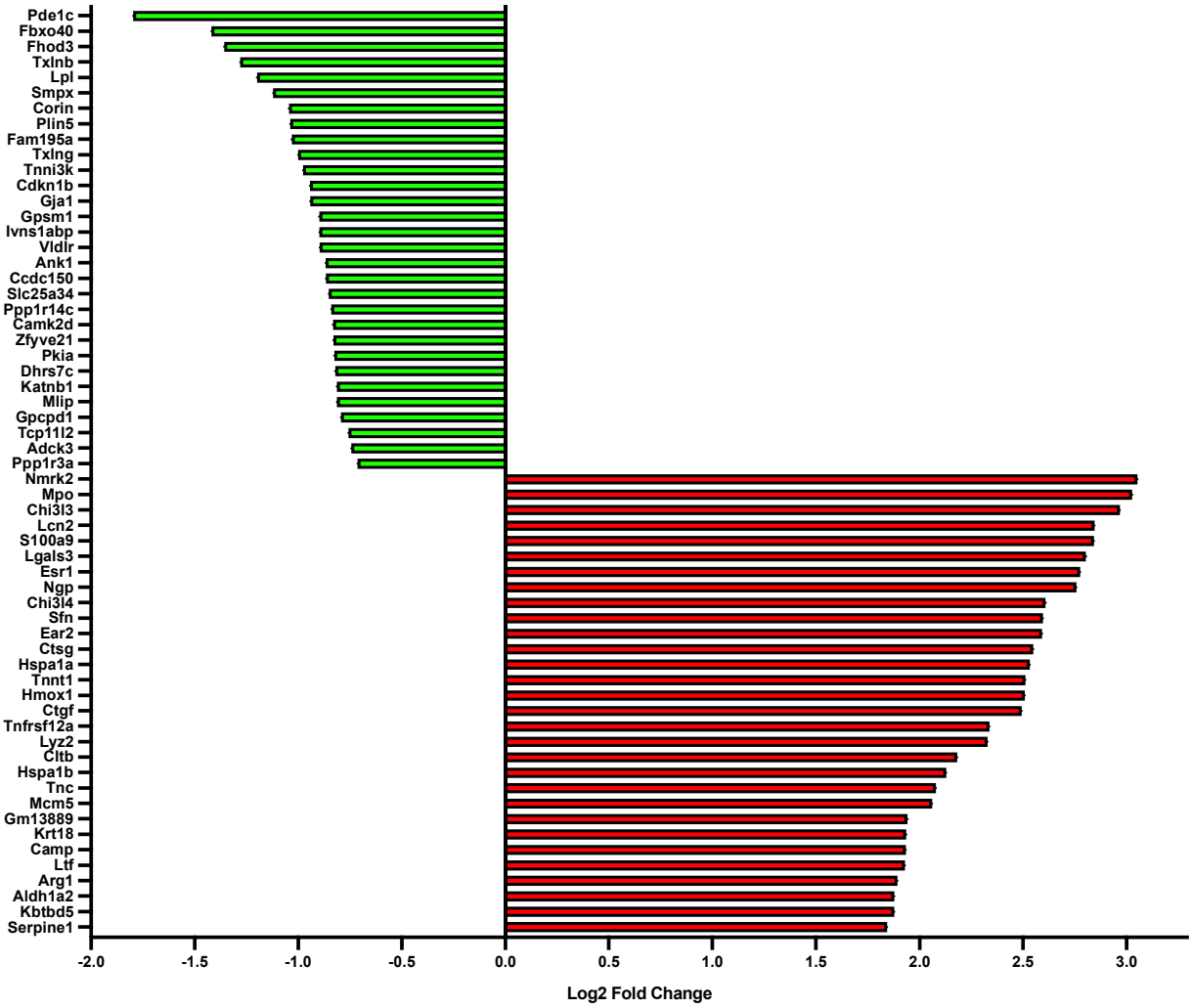

Fold Change	Protein Symbol	Protein Name	-log(p-value)
-1.80	Pde1c	Isoform 1 of Calcium/calmodulin-dependent 3',5'-cyclic nucleotide phosphodiesterase 1C	5.417846911
-1.42	Fbxo40	F-box only protein 40	7.566723921
-1.36	Fhod3	FH1/FH2 domain-containing protein 3	6.85036835
-1.28	Txlnb	Beta-taxilin	6.089037256
-1.20	Lpl	Lipoprotein lipase	7.409877691
-1.12	Smpx	Small muscular protein	6.218618177
-1.04	Corin	Atrial natriuretic peptide-converting enzyme	4.208936341
-1.04	Plin5	Perilipin-5	4.157064994
-1.03	Fam195a	MAPK regulated corepressor interacting protein 2	5.92942765
-1.00	Txlng	Gamma-taxilin	6.855783036
-0.98	Tnni3k	Serine/threonine-protein kinase TNNI3K	8.162305843
-0.94	Cdkn1b	Cyclin-dependent kinase inhibitor 1B	3.487448035
-0.94	Gja1	Gap junction alpha-1 protein	7.537539279
-0.90	Gpsm1	G-protein-signaling modulator 1	2.800521104
-0.90	Ivns1abp	Influenza virus NS1A-binding protein homolog	4.255728159
-0.90	Vldlr	Very low-density lipoprotein receptor	6.74018785
-0.87	Ank1	Isoform Mu7 of Ankyrin-1	4.089605693
-0.87	Ccdc150	Coiled-coil domain-containing protein 150	2.760771103
-0.85	Slc25a34	Solute carrier family 25 member 34	6.170633474
-0.84	Ppp1r14c	Protein phosphatase 1 regulatory subunit 14C	5.181045513
-0.83	Camk2d	Isoform 3 of Calcium/calmodulin-dependent protein kinase type II subunit delta	3.786531337
-0.83	Zfyve21	Zinc finger FYVE domain-containing protein 21	6.187891722
-0.83	Pkia	cAMP-dependent protein kinase inhibitor alpha	4.100326452
-0.82	Dhrs7c	Dehydrogenase/reductase SDR family member 7C	6.377581815
-0.81	Katnb1	Katanin p80 WD40 repeat-containing subunit B1	1.910021404
-0.81	Mlip	Muscular LMNA-interacting protein	6.904763124
-0.79	Gpcpd1	Glycerophosphocholine phosphodiesterase GPCPD1	4.258580865
-0.76	Tcp11l2	T-complex protein 11-like protein 2	3.979998014
-0.74	Adck3	Atypical kinase COQ8A, mitochondrial	4.483254276
-0.71	Ppp1r3a	Protein phosphatase 1 regulatory subunit 3A	6.106345969
3.05	Nmrk2	Nicotinamide riboside kinase 2	6.962376248
3.03	Mpo	Myeloperoxidase	2.735351185
2.97	Chi3l3;Chil3	Chitinase-like protein 3	4.928590881
2.85	Lcn2	Neutrophil gelatinase-associated lipocalin	4.398244158
2.84	S100a9	Protein S100-A9	5.407080067
2.80	Lgals3	Galectin-3	5.905126815
2.78	Esr1	Estrogen receptor	10.16350906
2.76	Ngp	Neutrophilic granule protein	4.278056175

2.61	Chi3l4	Chitinase-like protein 4	4.653325154
2.60	Sfn	14-3-3 protein sigma	4.686944022
2.59	Ear2	Eosinophil cationic protein 2	5.224398378
2.55	Ctsg	Cathepsin G	2.679678427
2.53	Hspa1a	Heat shock 70 kDa protein 1A	4.779394743
2.51	Tnnt1	Troponin T, slow skeletal muscle	5.700575621
2.51	Hmox1	Heme oxygenase 1	6.807515762
2.49	Ctgf	CCN family member 2	9.339136873
2.34	Tnfrsf12a	Tumor necrosis factor receptor superfamily member 12A	7.03984747
2.32	Lyz2	Lysozyme C-2	5.266438035
2.18	Cltb	Clathrin light chain B	4.382265275
2.13	Hspa1b	Heat shock 70 kDa protein 1B	4.264586952
2.08	Tnc	Tenascin	3.647974575
2.06	Mcm5	DNA replication licensing factor MCM5	2.184882083
1.94	Gm13889	Uncharacterized protein C11orf96 homolog	5.229940129
1.94	Krt18	Keratin, type I cytoskeletal 18	6.396581344
1.94	Camp	Cathelicidin antimicrobial peptide	3.942329356
1.93	Ltf	Lactotransferrin	3.929013667
1.89	Arg1	Arginase-1	4.243952584
1.88	Aldh1a2	Retinal dehydrogenase 2	1.694566956
1.88	Kbtbd5	Kelch-like protein 40	7.512997574
1.84	Serpine1	Plasminogen activator inhibitor 1	4.905107551

Table 2.1*:* Graph and corresponding list of the top 30 proteins with a decrease (green) /increase (red) in expression log ratio in Cdk5 deficient cardiac tissue

Analysis of disease-based protein networks based on global proteome changes were mapped using Qiagen's Ingenuity Pathway Analysis (IPA) software. The top 5 cardiovascular disease hits included cardiac enlargement (p-value = 3.69E-25; 170 proteins), cardiac dilation (p-value = 2.37E-16; 90 proteins), cardiac necrosis/cell death (p-value = 1.03E-14; 72 proteins) cardiac fibrosis (p-value = 9.84 E-14; 63 proteins) and cardiac dysfunction (p-value = 1.51E-13; 74 proteins). Corresponding differentially expressed proteins with each disease state can be found in **Table 2.2**.

Top Cardiovascular Disease Functions		
Category	**p-value (maximum from range)**	**Protein List**
Cardiac Enlargement	3.69E-25	ABCC9,ACSL1,ACTC1,ACTN2,ADCY6,ADK,AKT1,ALDH1A2,ANKRD1,APOE,ATP6V1E1,BGN,BNIP3,CACNA1C,CACNA2D1,CACNB2,CAMK2D,CAPNS1,CCN2,CD2AP,CD36,CDH2,CDKN1B,CDS2,CKMT2,CNOT3,COL3A1,CORIN,COX7A1,CPT2,CREB1,CRK,CRYAB,CTNNA3,CTNNB1,CTSB,CTSC,CTSD,CTSV,CYBB,DES,DMD,DNAJC19,DNAJC3,DNM1L,DSP,DTNA,EGLN1,EIF2B5,EIF4EBP1,EMD,ENDOG,ERBIN,FASN,FHL2,FHOD3,FLNC,FN1,GJA1,GLRX5,GNA11,GPX1,GPX7,GSN,HDAC2,HMOX1,Hnrnpa1,HPRT1,Hspa1b,HSPB2,HSPB7,HSPB8,IGF2R,INSR,ITGAV,JPH2,JUP,KCNJ11,LASP1,LDB3,LIMS2,LMCD1,LMNA,MAP2K1,MAP2K3,MAPK1,MB,MLIP,MPC1,MTPN,MYBPC2,MYBPC3,MYH10,MYH6,MYH9,MYL2,MYL3,MYLK3,MYOM1,MYOZ2,MYZAP,NCF1,NDUFS6,NEXN,NPPA,NT5E,PARP1,PDLIM5,PFKM,PFN1,PLIN5,Pln,PNKD,POSTN,PPIA,PRKAA1,PRKAR1A,PRKG1,PRMT5,PROC,PTPN11,RAB1A,RAC1,RBM20,RHEB,RNLS,ROCK2,RRAD,RRM1,RTN4,RYR2,S100A6,SCN5A,SCO2,SDHA,SERPINE1,SGCD,SIRT2,SIRT3,SLC25A11,SLC25A4,SLC2A4,SLC8A1,SMTN,SP3,SPTBN1,SRSF2,STAB1,STAT3,STK11,STK3,SUCLG1,TG,THBS4,TLN1,TMEM43,TMPO,TNNC1,TNNI3,TNNI3K,TNNT2,TOR1AIP1,Tpm1,TRIM54,TTN,TWF1,TXN,UBE4B,XIRP1,ZMPSTE24
Cardiac Dilation	2.37E-16	ABCC9,ACSL1,ACTC1,ACTN2,ANKRD1,APOE,ATP6V1E1,BGN,BNIP3,CACNA1C,CACNB2,CAMK2D,CAPNS1,CDS2,CKMT2,COL3A1,COX7A1,CREB1,CRK,CRYAB,CTNNA3,CTSV,DES,DMD,DNAJC19,DNM1L,DSP,DTNA,EGLN1,EMD,FASN,FHL2,FHOD3,FLNC,FN1,GJA1,GLRX5,GPX1,Hnrnpa1,HSPB7,IGF2R,INSR,JPH2,JUP,LDB3,LIMS2,LMNA,MPC1,MPO,MYBPC2,MYBPC3,MYH6,MYH9,MYL2,MYL3,MYOM1,NCF1,NEXN,PDLIM5,PFKM,Pln,PRDX3,PRKAR1A,PTPN11,RAC1,RBM20,RTN4,RYR2,SCN5A,SCO2,SDHA,SERPINE1,SGCD,SLC25A11,SLC2A1,SLC2A4,SLC8A1,SRSF2,STAB1,SUCLG1,TLN1,TMEM43,TMPO,TNNC1,TNNI3,TNNT2,TOR1AIP1,TRIM54,TTN,ZMPSTE24
Cardiac Necrosis/Cell Death	1.03E-14	ABCC9,ACSL1,ACTC1,ADCY6,AKT1,BNIP3,CACNB2,CALR,CAMK2D,CAT,CCN1,CDKN1B,CREG1,CRYAB,CSK,CTNNB1,CTSG,CXADR,CYBB,DES,DSP,EGLN1,FASN,GSN,HADHA,HDAC2,HK2,HMOX1,HSPB1,HSPB6,HSPB8,IQGAP1,IVNS1ABP,KNG1,KRAS,LCN2,LRP1,MANF,MAP2K1,MAP2K3,MAPK1,MPO,MTPN,MYBPC3,MYH10,MYH6,MYLK3,NAMPT,NCL,NDUFA13,NPPA,NTN1,PARP1,PHB,PKN1,PRKAA1,PTPN11,RAC1,RPSA,RRAD,RTN4,S100A6,SGCA,SGCD,SLC8A1,STAT3,TFDP1,THBS4,TRIM54,UBE4B,XDH,ZYX

Cardiac Fibrosis	9.84E-14	ACSL1,ACTC1,APOE,BCS1L,BGN,CACNA1C,CAPNS1,CCN2,CNOT3,COQ9,CREB1,CTSV,CYBB,DES,DMD,DSP,DTNA,ENTPD1,FN1,GPX1,HMOX1,HSPB8,IRF3,ITGB1,KRT18,LCN2,LIMS2,LMNA,LPL,MB,MPO,MYBPC3,MYH6,MYLK3,NCF1,NDUFS6,NEXN,NPPA,PLG,Pln,PNKD,POSTN,PRDX3,PRKG1,PROC,PSMB8,SERPINE1,SGCA,SGCB,SGCD,SGCG,SIRT2,SIRT3,SLC2A4,SLC8A1,STAT3,STK11,STK3,TLN1,TNNI3,TNNT2,TRDN,XIRP1
Cardiac Dysfunction	1.51E-13	ACTC1,ACTN2,AKT1,ANKRD1,ANXA5,APOE,BGN,BNIP3,CACNA1C,CACNA2D1,CACNB2,CAPNS1,CCN2,CD36,CKMT2,CPT2,CRK,CRYAB,CTNNA3,CTNNB1,CTSV,CYBB,DES,DMD,DSP,DTNA,FHL2,GPX1,GRK2,HMOX1,HSPB2,IGF2R,ITGA5,JPH2,JUP,KCNJ11,LCN2,LDB3,LMNA,LPL,MAP2K1,MB,MYBPC3,MYDGF,MYH6,MYL3,MYLK3,NCF1,NEXN,NPPA,NT5E,PDLIM5,PFKM,PLG,PLIN5,Pln,POSTN,PRDX3,PRKG1,RNLS,ROCK2,RYR2,SCN5A,SERPINE1,SLC2A1,SLC8A1,STK11,TMEM43,TNNC1,TNNI3,TNNT2,Tpm1,TTN,XDH

Table 2.2*:* Top cardiovascular disease hits derived from the global proteome of Cdk5 deficient mice | Top 5 cardiovascular disease-based protein networks using Qiagen's Ingenuity Pathway Analysis software.

According to protein class, the majority of differentially expressed proteins belonged to the subcategories of metabolite interconversion enzyme and cytoskeletal proteins, whereas biological process analysis revealed the majority were involved in cellular and metabolic processes. Majority of protein hits were found to be localized to the cytoplasm and intracellular membrane-bound organelles. Lastly, molecular function analysis revealed top hits associated with molecular binding and catalytic activity (**Fig 2.10**). Further molecular functional annotation clustering revealed the top enriched cluster to be cell to cell adherens junction/cadherin binding (**Fig. 2.11**). Physical cell to cell adhesion is crucial for the maintenance of structure and function of the heart. Neighboring cardiomyocytes are connected by highly organized intracellular junction structures termed intercalated discs (IC).[108] These cardiac-specific structures are comprised of two cell adhesive junctions—adherens junction and desmosome, which are responsible for connecting adjacent cardiomyocytes to one another; this allows for synchronized contraction via electromechanical

coupling.[108-111] In several cardiac pathophysiological states, namely cardiomyopathies, there is a disturbance in both expression and distribution of IC's, specifically, lateralization of cell to cell adhesion.[112,113] In the literature, DCM has been reported to demonstrate a significant decrease in cadherin expression, namely N-cadherin. An N-cadherin conditional knockout mouse model was shown to display modest DCM with a loss of IC's. Consistent with this reporting, the Cdk5 deficient global proteomic dataset revealed a statistically significant decrease in N-cadherin expression (-0.2x fold change).

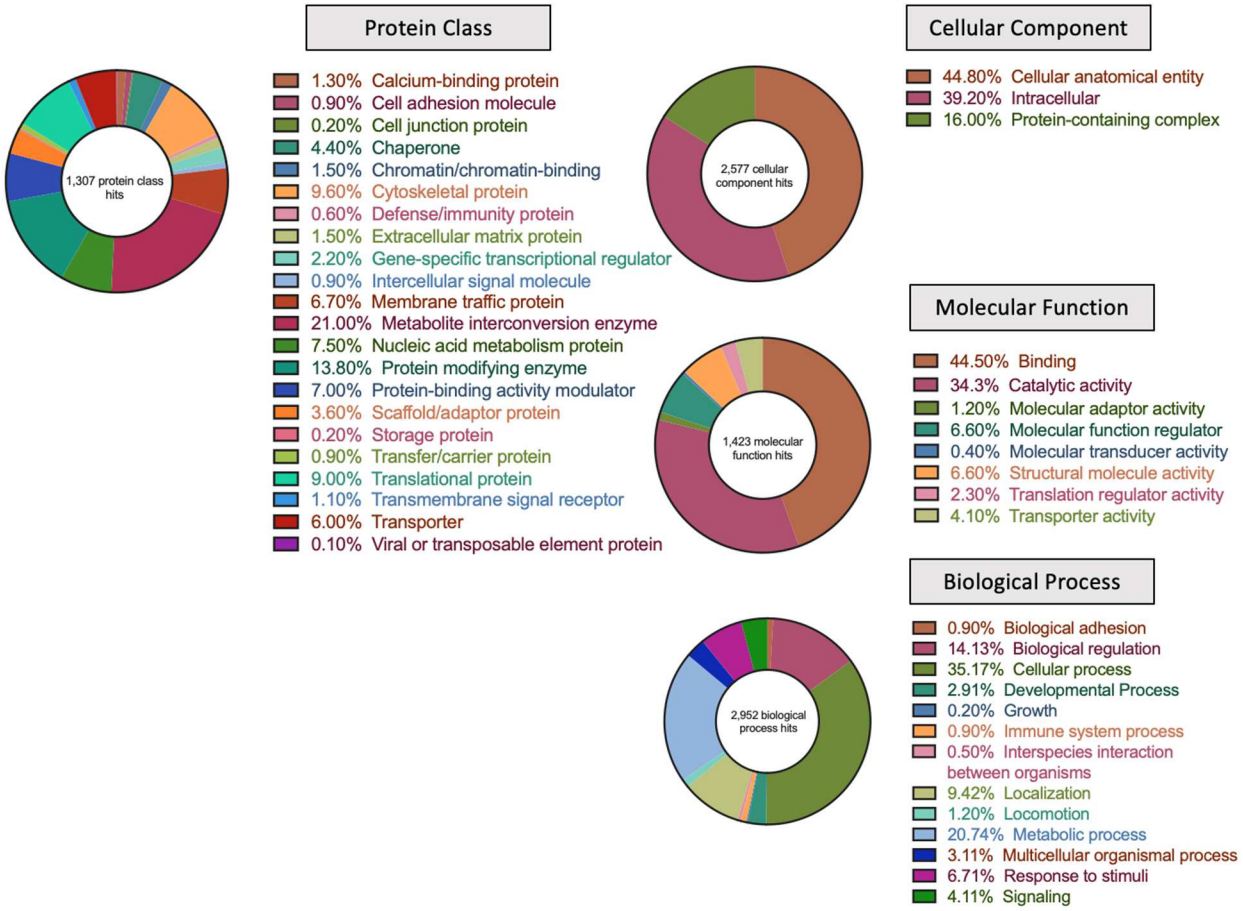

Figure 2.8: Functional classifications of differentially expressed proteins using gene ontology enrichment analysis| Gene ontology analysis of differentially expressed proteins in Cdk5 deficient mice were generated using PANTHER-GO slim.

*Percentages shown as percent protein/gene hit against total number of ontology category hit.

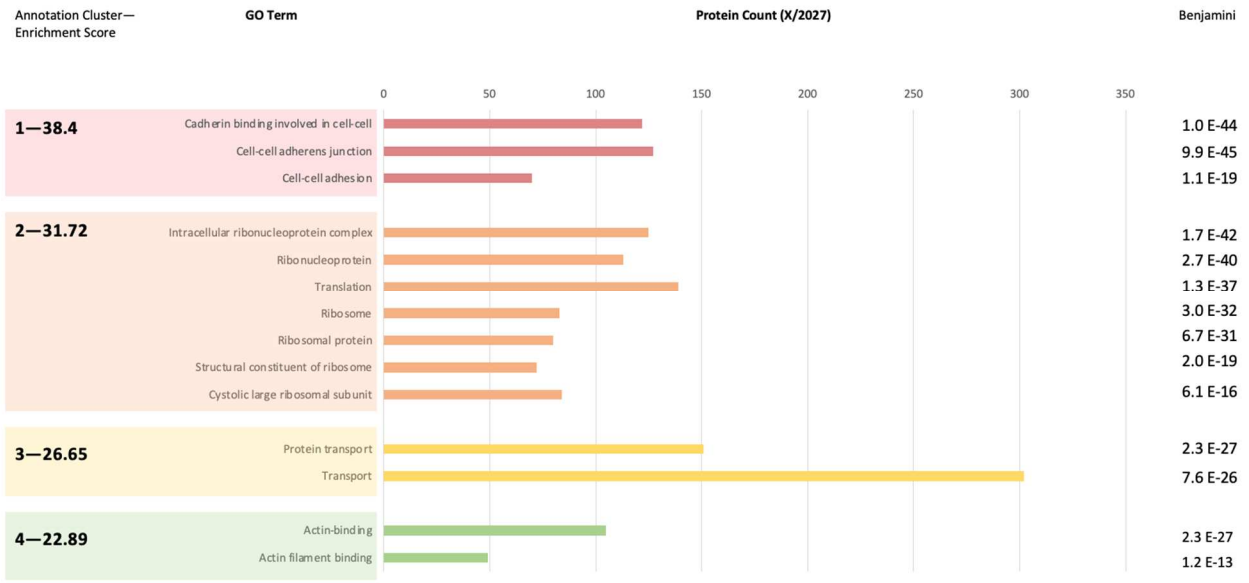

Figure 2.9*:* Functional annotation clustering in Cdk5 deficient mice | The Database for Annotation, Visualization, and Integrated Discovery (DAVID) v6.8 was used to generate molecular functional annotation clustering for global proteome changes in the Cdk5 deficient cohort. The 4 top enriched clusters with their corresponding molecular functions and enrichment scores are displayed above. Bars show the number of protein hits
*A "medium" classification stringency was used: similarity threshold = 0.5, linkage threshold = 0.5, similarity term overlap = 3, enrichment threshold = 1.0. A Benjamini correction is reported for significance.

2.4 Discussion

Prior to previously published findings from the Yazawa lab, a role for CDK5 in the heart had not been elucidated. The aim of this chapter was to determine whether Cdk5 was necessary for normal cardiac function in the adult heart. This was done by using a *in vivo* mouse model with a spatiotemporal knockout of Cdk5 in cardiomyocytes of C57B/6J mice at 3 months of age. Several measures were used to assess the cardiac phenotype in these mice including echocardiography, histological analysis as well as proteomic studies. Echocardiography revealed severe systolic dysfunction, with significant decreases in FS and EF. Additionally, significant LV dilation was observed with findings based on increased LVEDD, LVEDF as well as histological evidence showing morphology changes of LV enlargement along with LV wall thinning. Staining with H&E also revealed mononuclear cell infiltrate and evidence of collagen deposition. Lastly, global proteomic LC-MS/MS studies revealed changes in protein abundance indicative of activated cardiac pathophysiological pathways including cardiac enlargement, cardiac dilation, cardiac necrosis, cardiac fibrosis and overall cardiac dysfunction

Further analysis of global proteome changes in Cdk5 deficient mice including molecular functional annotation clustering and gene ontology enrichment analysis, revealed significant hits related to cell-to-cell adhesion. Evidence for the extensively studied role of CDK5 in the brain has demonstrated a critical role for CDK5 in the regulation of cell adhesion, specifically via N-cadherin, a Ca^{2+} dependent adhesion molecule.[114] Such studies have shown CDK5's necessity for neuronal positioning via cadherin and integrin activity regulation as well as integrity of the actin cytoskeleton and microtubules.[115-117] Another study looking at the role of CDK5 in human keratinocytes implicated CDK5 in cell-to-cell and cell-to-matrix adhesion via regulation of cadherins and integrins.[118] In the heart, the contractile ability of the cardiac muscle

is maintained by integrity and synchronicity of the cell-to-cell junctions.[119] In heart failure as well as cardiomyopathies, significant alterations in cell-to-cell junctions are observed. [120,121] Furthermore, haploinsufficiency is abundant in genes encoding proteins implicated in structural, regulatory as well as cell-signaling roles.[122] It is therefore plausible that CDK5 plays a significant role in cell-to-cell adhesion/IC disc function.

2.4 Methods

Mouse Study Approval

All reported murine experiments were conducted in accordance with the Columbia Institutional Animal Care and Use Committee (IACUC) approved animal protocol (Protocol #: AC-AABK3550). All Guidelines for Care and Use of Laboratory Animals established by Columbia University and as stated in the protocol were strictly adhered to.

Establishing Cardiac-specific Cdk5 Deficient Mouse Lines

Cdk5 flox mice (B6.129S4(Cg)-Cdk5tm1.1Lht/J) on a B6J background were obtained from Jackson Laboratory (JAX; catalog # 014156). These mutant mice contain LoxP sites flanking exons 1-5 of the 12 total exons in the *Cdk5* genomic sequence. *Cdk5* flox mice were subsequently crossed with an αMHC-MerCreMer line (B6.FVB(129)-*A1cf*$^{Tg(Myh6\text{-}cre/Esr1*)1Jmk}$/J) from Jackson Lab (JAX; catalog #005657). The αMHC-MerCreMer mice contain a MerCreMer transgene targeted to the cardiac specific promoter, *Myh6*. To induce cardiac-targeted recombination, Tamoxifen ≥99% (Millipore Sigma; catalog #: T5648-5G) was injected intraperitonially using a 25 gauge syringe at 12 weeks of age (diluted in 10% ethanol—90% sunflower seed oil—Millipore Sigma; catalog #: S5007-250mL). The dosing amount/schedule was dependent on gender of the mice. Female mice received 50 mg/kg over 3 consecutive days. Male mice received 37.5 mg/kg over 5 consecutive days. Additionally, 2 control lines were utilized for analysis—(1) *Cdk5* WT : αMHC-MerCreMer^{+} mice and (2) *Cdk5* $^{fl/fl\ or\ fl/+}$:α -MHC-MerCreMer WT mice.

Cdk5$^{fl/fl}$: αMHC-MerCreMer Mouse Genotyping:

DNA extracted from toe cuts were used for genotyping. Three sets of primers were used to confirm genotype of mice: (1) *Cdk5* forward: 5’ CAG TTT CTA GCA CCC AAC TGA TGT A

3’ and *Cdk5* reverse: 5’ GCT GTC CTG GAA CTC CAT CTA TAG 3’ (2) aMHC-MerCreMer WT forward: 5’ TCT ATT GCA CAC AGC AAT CCA 3’ and aMHC-MerCreMer WT reverse: 5’ CCA ACT CTT GTG AGA GGA GCA 3’ (3) aMHC-MerCreMer mutant forward: 5’ TCT ATT GCA CAC AGC AAT CCA 3’ and aMHC-MerCreMer mutant reverse: 5’ CCA GCA TTG TGA GAA CAA GG 3’. TaKaRa Ex Taq® DNA Polymerase (TaKaRa Bio USA; catalog #: RR001C) was used for all 3 PCR reactions.

Genotyping Use	**Primer F (5’→ 3’)**	**Primer R (5’→ 3’)**	**Band Length**	**Tm**
Cdk5	CAG TTT CTA GCA CCC AAC TGA TGT A	GCT GTC CTG GAA CTC CAT CTA TAG	Mutant: 460 Het: 460 + 660 WT: 660	60
aMHC-MerCreMer WT	TCT ATT GCA CAC AGC AAT CCA	CCA ACT CTT GTG AGA GGA GCA	295	50
aMHC-MerCreMer Mutant	TCT ATT GCA CAC AGC AAT CCA	CCA GCA TTG TGA GAA CAA GG	300	50

qRT-PCR

Total RNA was extracted from frozen mouse whole heart ventricular samples by utilizing the RNeasy mini kit (Qiagen; catalog #: 74004) and RNase-Free DNase kit (Qiagen; catalog #: 7254). cDNA was subsequently synthesized following Invitrogen’s SuperScript III First-Strand Synthesis System kit (ThermoFisher Scientific; catalog #: 18080051). The resulting 21 µl sample of cDNA was diluted with UltraPure DNase/RNase-Free Distilled Water (ThermoFisher Scientific; catalog #: 10977015) at a ratio of 1:4; 1 µl of each sample was used for qRT-PCR. qRT-PCR was ran using TB Green Advantage qPCR Premix (TaKaRa; catalog #: 639676) and StepOnePlus real time PCR systems (ThermoFisher Scientific; catalog #: 4376600) using a MicroAmp™ Fast Optical 96-Well Reaction Plate (ThermoFisher Scientific; catalog #: 4346907). Quantification was done by comparative CT using mouse *Gapdh* as a control

reference gene for normalization. qRT-PCR primer sets were as follows: (1) mouse *Cdk5* forward: 5' ACC TGG ACC CTG CTG AGA TTG TG 3' and mouse *Cdk5* reverse: 5' CCC CAT TCC TGT TTA TGA GC 3' (2). All oligo primers were synthesized by IDT.

Echocardiography Procedure

Echo's were performed one day post-final Tam injection in female/male cohorts. Prior to performing echo's, all mice were anesthetized using isoflurane (1-5% in oxygen via inhalation) using a knock-down anesthesia box for initial sedation, followed using a face mask for maintenance of sedation. The fur on the chest was subsequently shaved using an electric razor and mice were placed on a warming pad to maintain a constant body temperature of 37°C (±5°C). Once anesthetized/shaved, echo's were conducted using an iE33 ultrasound system (Philips Medical Systems, Andover, MA, USA) with a 15-7 L-io transducer (7-15 MHz) applied to the chest wall. Left-ventricular end-diastolic/end-systolic diameters (LVEDD/LVESD) and end-diastolic/end-systolic areas (LVEDA/LVESA) were measured using a two dimensional parasternal short-axis view at the midpapillary level. They were taken from three beats and averaged. LV end-diastolic/end-systolic volume (LVEDV/LVESV) were calculated with Teichholz method as follows: $LVEDV = 7.0/(2.4+LVEDD) \times LVEDD^3$; $LVESV = 7.0/(2.4+LVESD) \times LVESD^3$. Images taken in Motion-mode (M-mode) were used for determining heart rate. LV fractional shortening (FS), LV fractional area change (FAC), LV ejection fraction (EF), and cardiac output (CO) were calculated as follows: LVFS = (LVEDD-LVESD)/LVEDD × 100; LVFAC = (LVEDA-LVESA)/LVEDA × 100; LVEF = (LVEDV-LVESV)/LVEDV × 100; CO = (LVEDV-LVESV) × heart rate. After echocardiography procedure, mice were allowed to recover from anesthesia and

were subsequently placed on a warming pad in a separate container prior to returning to their cage. Mice were subsequently sacrificed post-echo for further cardiac-related analysis.

Mouse Cardiac Tissue Sampling

After echo, mice were sacrificed using CO_2 asphyxiation followed by cervical dislocation according to the Columbia University IACUC protocol, #AC-AABK3550. Whole hearts were excised, washed in glucose-free Tyrode's solution (1.8mM $CaCl_2$, 1mM $MgCl_2$, 140mM NaCl, 5.4mM KCl, 10mM glucose, and 10mM HEPES—pH7) and weighed. Heart weight was normalized by tibial length (average of left and right tibia). The atria were separated from the ventricles and chamber pairs were flash frozen in liquid nitrogen and stored at -80C. For RNA extraction, frozen tissue was homogenized and lysed using RNeasy Lysis Buffer (Qiagen; catalog #: 79216) supplemented with β-mercaptoethanol. Frozen tissue to be used for protein extraction was homogenized and lysed using cell lysis buffer (Abcam; catalog #: ab152163) supplemented with Protease Inhibitor Cocktail in DMSO (Sigma-Aldrich; catalog #: P8340), phosphatase inhibitor complex 2 (Sigma-Aldrich; catalog #: P5726) and phosphatase inhibitor complex 3 (Sigma-Aldrich; catalog #: P0044). Whole heart ventricular samples that were used for histology were fixed in 4% paraformaldehyde for 24 hours, followed by suspension in a 70% ethanol + 30% dH_2O solution. Fixed ventricles were subsequently sectioned at 5 μM thickness and paraffin embedded in coronal orientation on microscope slides (4 sections per slide). Slides were with H & E or MTS.

Global Quantitative Proteomics by Mass Spectroscopy

After echo, mice were sacrificed using CO_2 asphyxiation followed by cervical dislocation according to Columbia IACUC approved protocol # AC-AABK3550. Whole hearts were subsequently removed, washed in Tyrode's solution and the atria were separated from the

ventricles. After washing, whole heart ventricular samples were flash frozen in liquid nitrogen and stored at -80°C until further proteomic analysis.

For bottom-up global quantitative proteomics, TMT-based quantitative proteomics was used.[123] In summary frozen whole ventricular mouse tissues was lysed by bead-beating in 9M urea and 200mM EPPS (pH 8.5), supplemented with protease and phosphatase inhibitors. Samples were reduced with 5mM TCEP and alkylated with 10 mM iodoacetamide (IAA) that was quenched with 10 mM DTT. A total of 400 μg of protein was chloroform−methanol precipitated. Protein was reconstituted in 200 mM EPPS (pH 8.5) and digested by Lys-C overnight and trypsin for 6h, both at a 1:50 protease-to-peptide ratio. Digested peptides were quantified using a Nanodrop at 280nm and 350 μg of peptide from each sample were labeled with 800 μg TMT reagent using 16-plex TMT kit.[124] TMT labels were checked, 0.5 μg of each sample was pooled, desalted and analyzed by short SPS-MS3 method, and using normalization factor, samples were bulk mixed at 1:1 across all channels and 5.6 mg of bulk mixed sample was used for total proteome and phospho-proteome analysis. Mixed TMT-labeled sample was vacuum centrifuged and de-salted with C18 Sep-Pak (500mg) solid-phase extraction column.

De-salted sample was fractionated using BPRP chromatography. Peptides were subjected to a 50 min linear gradient from 5 to 42% acetonitrile in 10 mM ammonium bicarbonate pH 8 at a flow rate of 0.6 mL/min over Water X-bridge C18 column (3.5 μm particles, 4.6 mm ID and 250 mm in length). The peptide mixture was fractionated into a total of 96 fractions, which were consolidated into 31 fractions. Fractions were subsequently acidified with 1% formic acid, and 5% of each fraction were used for total proteome analysis. The remaining 95% of each fraction was further consolidated into 11 fractions for phospho-proteomics analysis (discussed in Chapter

4). All fractions were vacuum centrifuged to near dryness and desalted via StageTip, and 200 mg Sep-Pak solid-phase extraction column.

Thirty one desalted fractions were dissolved in 10 µl of 3% acetonitrile/0.1% formic acid injected using SPS-MS3. The UltiMate 3000 UHPLC system (ThermoFisher Scientific; catalog #: IQLAAAGABHFAPBMBFB) and EASY-Spray PepMap RSLC C18 50 cm x 75 µm ID column (ThermoFisher Scientific; catalog #: ES900) coupled with Orbitrap Fusion (ThermoFisher Scientific; catalog #: IQLAAEGAAPFADBMBCX) were used to separate fractioned peptides with a 5-30% acetonitrile gradient in 0.1% formic acid over 45 min at a flow rate of 250 nL/min. After each gradient, the column was washed with 90% buffer B for 10 min and re-equilibrated with 98% buffer A (0.1% formic acid, 100% HPLC-grade water) for 40 min. The full MS spectra were acquired in the Orbitrap Fusion™ Tribrid™ Mass Spectrometer (ThermoFisher Scientific; catalog #: IQLAAEGAAPFADBMBCX) at a resolution of 120,000. The 10 most intense MS1 ions were selected for MS2 analysis. The isolation width was set at 0.7 Da and isolated precursors were fragmented by CID at a normalized collision energy (NCE) of 35% and analyzed in the ion trap using "turbo" scan speed. Following acquisition of each MS2 spectrum, a synchronous precursor selection (SPS) MS3 scan was collected on the top 10 most intense ions in the MS2 spectrum. SPS-MS3 precursors were fragmented by higher energy collision-induced dissociation (HCD) at an NCE of 65% and analyzed using the Orbitrap.

Analysis of Raw Mass Spectrometric Data

Raw mass spectrometric data were analyzed using Proteome Discoverer 2.2 to perform database search and TMT reporter ions quantification. TMT tags on lysine residues and peptide N termini (+229.163 Da) and the carbamidomethylation of cysteine residues (+57.021 Da) were set

as static modifications, while the oxidation of methionine residues (+15.995 Da), deamidation (+0.984) on asparagine and glutamine and phosphorylation (+79.966) on serine, threonine, and tyrosine were set as a variable modification. Data was searched against a UniProt Mouse with peptide-spectrum match (PSMs) and protein-level FDR at 1% FDR. The signal-to-noise (S/N) measurements of each protein was be normalized so that the sum of the signal for all proteins in each channel was equivalent to account for equal protein loading.

Analysis of Global Proteomic Results

Peptide identification and quantification were imported into Perseus MaxQuant for statistical analysis (FDR<0.05) to identify proteins demonstrating statistically significant changes in abundance.[125] The following workflow was used: the generic matrix upload for the Cdk5 deficient global proteomic dataset was imported into Perseus. Next the "categorical annotation rows" function was used to assign common genotype/gender combination to each sample and rows were filtered based on a minimum number of valid values of 16 (i.e. only protein abundances with a quantifiable amount in every sample were included in the analysis). Next the filtered data was log transformed—log2(x). An unpaired two-sample t-test was conducted using 250 randomizations, FDR < 0.05 and s0=0.1. Data was reported using a volcano plots for two group comparison. For hierarchal clustering analysis, the log transformed data was normalized using a Z-score (without groupings). For differential expression analysis reflecting both gender and genotype differences, a multi-variate ANOVA with permutation-based FDR was ran. Statistical criteria was as follows: s0=0.1, FDR<0.05, 250 randomizations, no preservation of groupings in randomization.

Chapter 3: Effects of Cdk5 Activation on the Adult Mouse Myocardium

3.1 Introduction

Hyperactive CDK5 activity has been implicated in the underlying cardiac pathology of TS. Inhibition of CDK5 in TS-hiPSC-CM's using a range of genetic approaches and chemical inhibitors (i.e. PHA-793887) was shown to rescue the cellular LQTS phenotype.[44] The aim of the next set of experiments is to examine the cardiac-specific effects of increased Cdk5 activity in a "healthy" heart by utilizing an *in vivo* murine system. As show in Chapter 2, *in vivo* cardiac-specific Cdk5 deficiency in the adult mouse heart causes severe systolic dysfunction along with an acute DCM-like phenotype. Based on these findings, it is evident Cdk5 is necessary for cardiac function. While a role for Cdk*5* hyperactivity in TS was shown to be correlated with a LQTS/cardiac-arrhythmia phenotype, the impact of Cdk5 activation in healthy/steady state remains to be elucidated. The goal of this chapter is to examine the effect of Cdk5 activation via the overexpression of its activator, p35 to determine the effects on cardiac function.

Physiological activation of Cdk5 occurs after binding to its activator p35 (coded by the gene *Cdk5r1*).[126] This Cdk5-p35 complex is membrane associated and predominately localized to the cytoplasm due to myristoylation of p35.[25] In order to achieve increased Cdk5 activation, we had to overexpress p35. Overexpression of *Cdk5* on its own is insufficient to increase Cdk5 activity since Cdk5 proteins require p35 for kinase activity. The relationship between Cdk5 activation and p35 overexpression has been well established in the literature both *in vitro* and *in vivo*. p35 overexpression in neuroblastoma neuro-2a cells using a tetracycline trans-activator inducible system was shown to effectively increases Cdk5 activity. [127] A second group showed the effects

of *Cdk5r1* overexpression *in vivo* on Cdk5 activation for the promotion of primary rat β-cell proliferation and subsequent insulin secretion.[128]

To hyperactivate Cdk5 enzymatic activity in adult mouse hearts, an inducible human *CDK5R1/*p35 OE mouse line targeted to αMHC-MerCreMer was developed. The use of human *CDK5R1,* the mouse *Cdk5r1* homolog (93% cDNA sequence match), was to distinguish between endogenous vs synthetically overexpressed *Cdk5r1/CDK5R1* transcripts. This novel mouse line is the first to overexpress *CDK5R1*/p35 temporally and conditionally in the cardiac tissue of mice. *CDK5R1/*p35 OE mice were designed with a LoxP-Stop-LoxP (LSL) cassette under the strong/ubiquitously expressed CAG promoter to achieve Cre-mediated conditional activation of *CDK5R1* gene expression. *CDK5R1/*p35 OE mice were crossed with an αMHC-MerCreMer line (refer to Chapter 2) to establish the cardiac-tissue specific, temporally regulated *CDK5R1*/p35 OE mouse line. To characterize the phenotype of these cardiac-specific *CDK5R1/*p35 OE mice, echo and bottom-up TMT-based quantitative proteomic studies were conducted. Results from these studies demonstrated a modest decrease in systolic function, without any noticeable structural changes in the myocardium. Such findings are further discussed below.

3.2 Results

Conditional *CDK5R1*/p35 overexpression (OE), "*Rosa-Cag-LSL-Cdk5r1*", chimera mice were established from two mouse embryonic stem cells (mESC) #C4 and C14 clones. Once F1 mice reached 3 months of age, they were crossed with an αMHC-MerCreMer line (B6.FVB(129)-*A1cf*$^{Tg(Myh6\text{-}cre/Esr1*)1Jmk}$/J) from Jackson Lab (JAX; catalog #005657) (**Fig 3.1**). Once bred mice reached 3 months of age, they were injected with Tam to induce recombination and subsequent *CDK5R1*/p35 OE. In order to optimize breeding efficiency, WT^{MCM} served as the littermate control cohort. The Tam dosing schedule was the same as the one used for Cdk5 deficient mice as outlined in **Fig 2.3**. Confirmation of successful recombination was done via PCR and qRT-PCR (**Fig 3.2**).

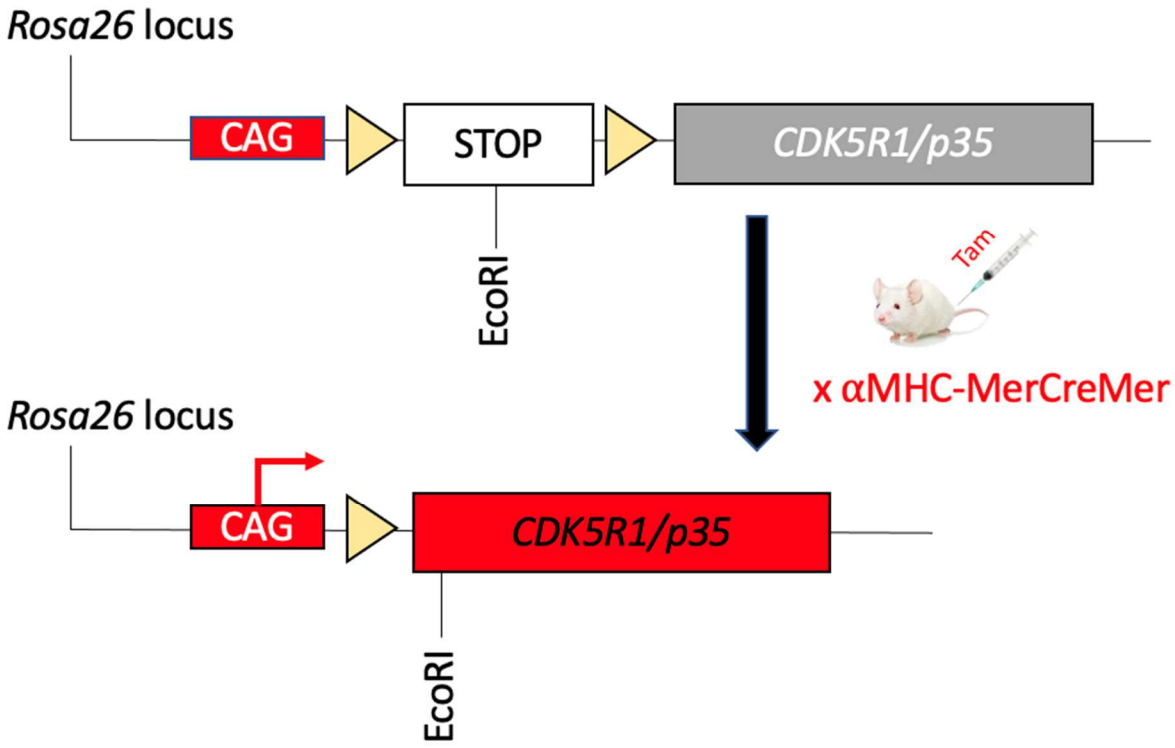

Figure 3.1: Generation of inducible cardiac-specific *CDK5R1*/p35 OE mouse model |*CDK5R1*/p35 OE mice were crossed with αMHC-MerCreMer (*Myh6-cre/Esr1**, JAX #5657) mice. Recombination was inducible upon administration of Tamoxifen.

A

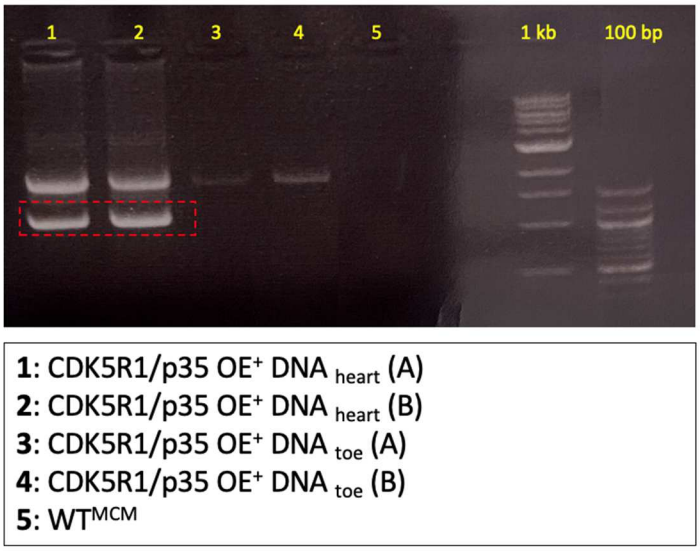

B

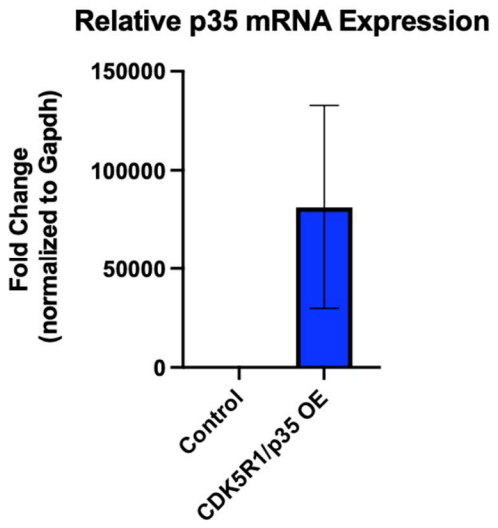

Figure 3.2: Confirmation of *CDK5R1*/p35 transgene Expression |A) PCR validation of recombination in cardiac tissue. B) q-RT-PCR confirmation of *CDK5R1*/p35 OE in cardiac tissue of *CDK5R1*/p35 OE mice post tamoxifen injection.

One day post final Tam injection, an assessment of cardiac function was performed via echo (**Fig 3.3**). Echo results showed a decline in systolic function with an EF of 35.32 ± 14.64 (vs. WT: 66.49 ± 2.625 and WT^{MCM}: 61.88 ± 7.207) and an FS 17.03 ± 7.696 in *CDK5R1*/p35 OE mice (vs WT: 35.92 ± 1.905 and WT^{MCM}: 32.72 ± 4.674 While the decline in systolic function was not as severe as the decline associated with Cdk5 deficiency, it was still rather significant. Minimal increase in LVEDD and LVEDV was observed, most likely due to recombination translocation artifact, as there was no statistically significant difference between the WT^{MCM} and *CDK5R1*/p35 OE cohorts (LVEDD = 3.906 ± 0.4478; LVEDV = 67.38 ± 18.46). Furthermore, histological assay of *CDK5R1*/p35 OE hearts did not reveal any changes in structure when comparing *CDK5R1*/p35 to their littermate control. Based on the discussed findings, it appeared

that Cdk5 activation in healthy adult male and female mice had a moderate effect on systolic function without any obvious structural phenotype.

A

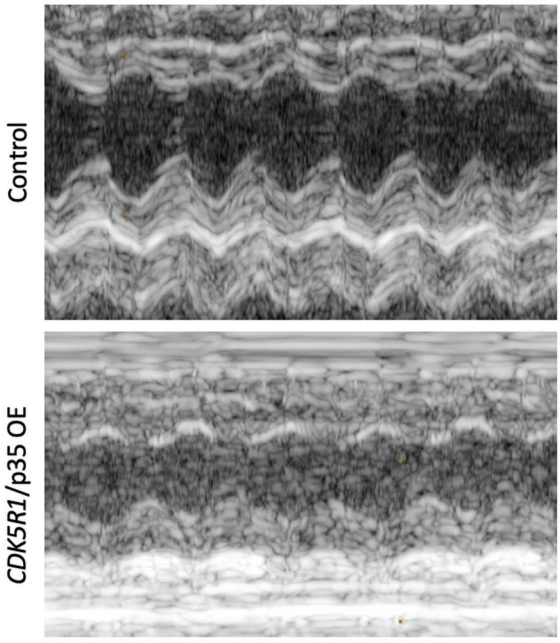

B

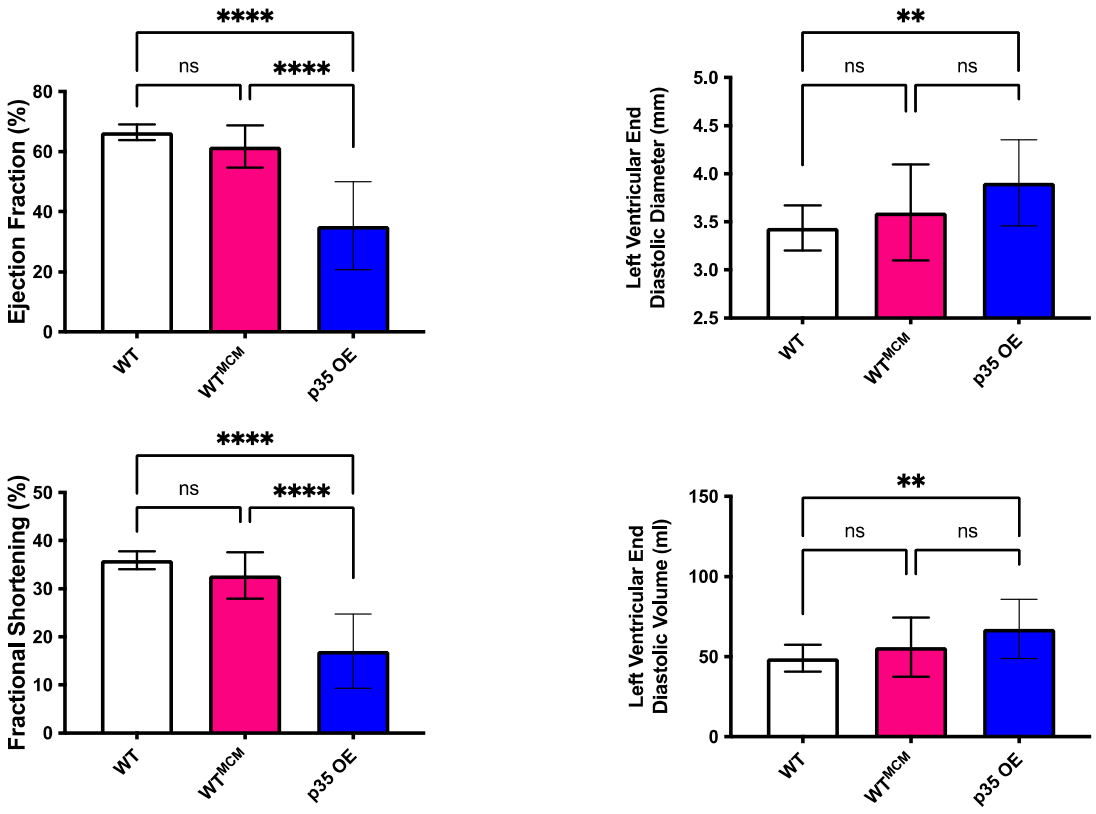

Figure 3.3*:* Assessment of cardiac function in *CDK5R1*/p35 OE mice |
A) Representative images of echo in M-mode from a control (example from male WT^{MCM} mouse) and *CDK5R1*/p35 OE deficient mouse (example from a female *CDK5R1*/p35 OE mouse).
B) Cardiac function was measured with echocardiography. Four measured values including ejection fraction (EF), fractional shortening (FS) , left ventricular end diastolic diameter (LVEDD) and left ventricular end diastolic volume (LVEDV) are shown. WT n=21 ; WT^{MCM} n=16 ; CDK5R1/p35 OE n=12. All error bars represent standard deviation. Statistical analysis done with on ordinary one-way ANOVA using Tukey's post-hoc multiple comparison using GraphPad Prism 8/9; P-values <0.05 were considered significant; *p<0.05, **p<0.01, ***p<0.001, ****p<0.0001; mean ± S.D.

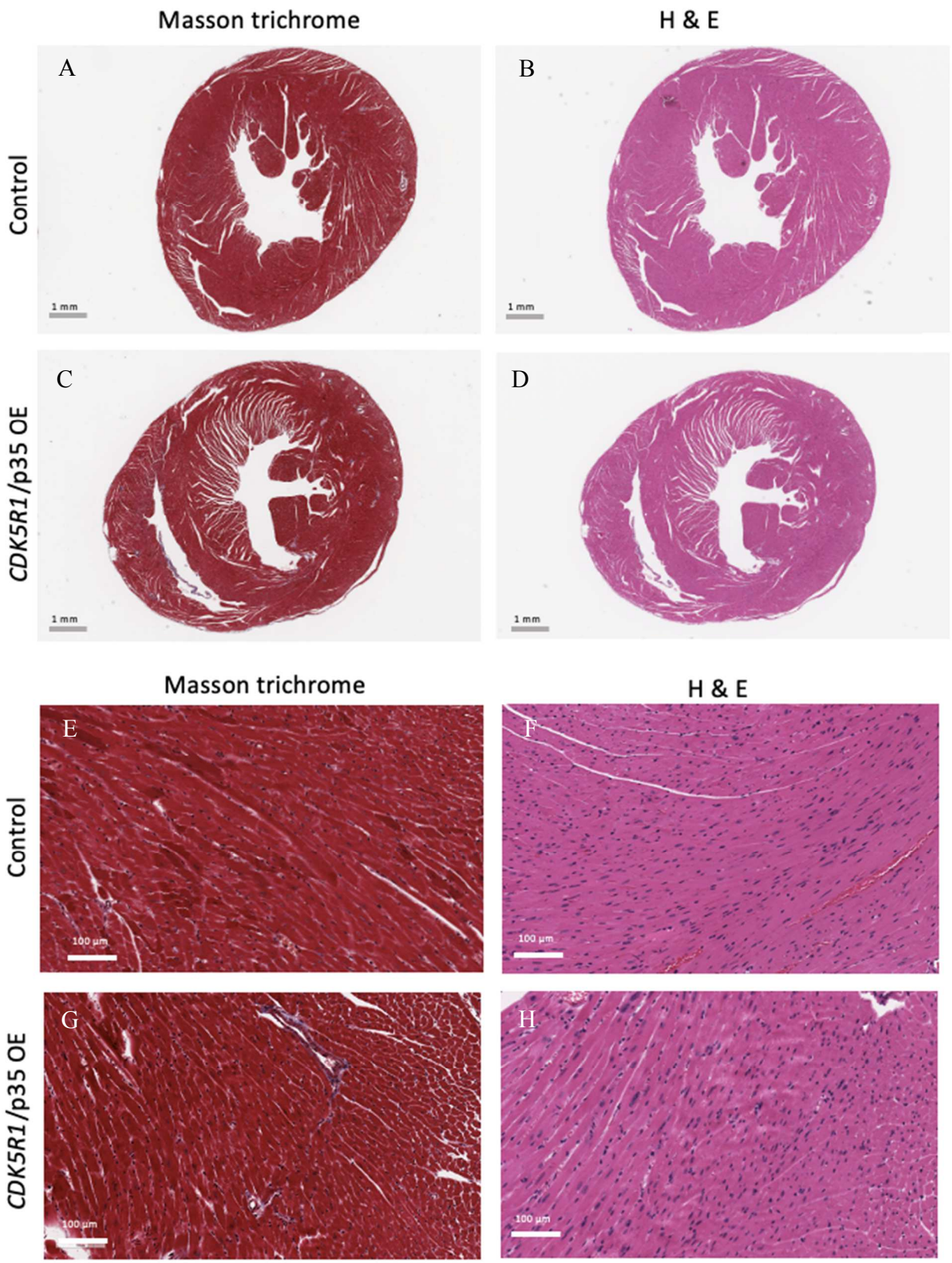
Masson trichrome
H & E
A
B
Control
1 mm
1 mm
C
D
CDK5R1/p35 OE
1 mm
1 mm
Masson trichrome
H & E
E
F
Control
100 µm
100 µm
G
H
CDK5R1/p35 OE
100 µm
100 µm

Figure 3.4: Histopathology of ventricular cardiac tissue from 12-week-old *CDK5R1*/p35 OE mice| Representative histological images from whole heart ventricular cross-sections of *CDK5R1*/p35 OE mice and control littermate (WT^{MCM}). Staining for morphology assessment is done with Mason's Trichome stain (MTS) and hematoxylin & eosin (H&E). In the MTS slides, nuclei and other basophilic structures are stained purple, while smooth muscle tissue stains bright red and collagen fibers appear in blue. In H&E stained slides, extracellular matrix and cytoplasm stain pink while nuclei appear in dark blue/purple.
A-D) Image of whole heart ventricular cross section with a scaling bar drawn to 1 mm
E-H) Zoomed in image from left ventricle muscle with scaling bar drawn to 100 µm

Lastly, TMT-based quantitative proteomics was performed to analyze the global and phospho-proteomes of *CDK5R1*/p35 OE mice. This chapter will only review global proteomic results; phosphoproteomic results will be discussed in Chapter 4. Four female and two male littermate control mice were used, along with 3 female and 3 male *CDK5R1*/p35 OE mice (**Fig 3.5**). Interestingly, there were no significant changes in the global proteome (**Fig 3.6**). The only global proteome change was a 1.5-fold increase in p35. What was observed, however, were significant changes to the phospho-proteome which will be addressed in Chapter 4.

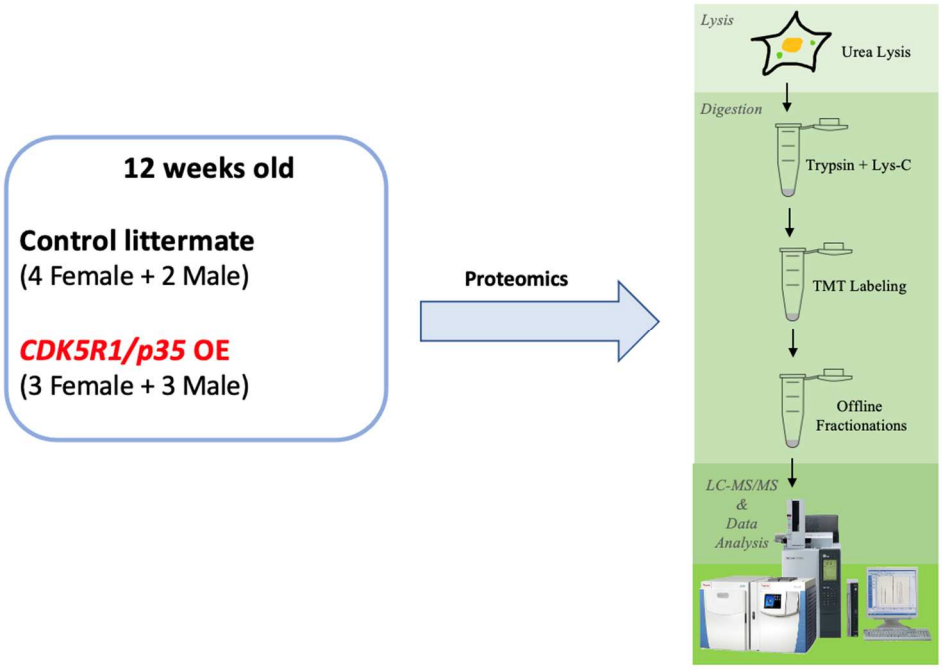

Figure 3.5: Experimental setup/ bottom-up proteomic workflow for *CDK5R1*/p35 OE mice

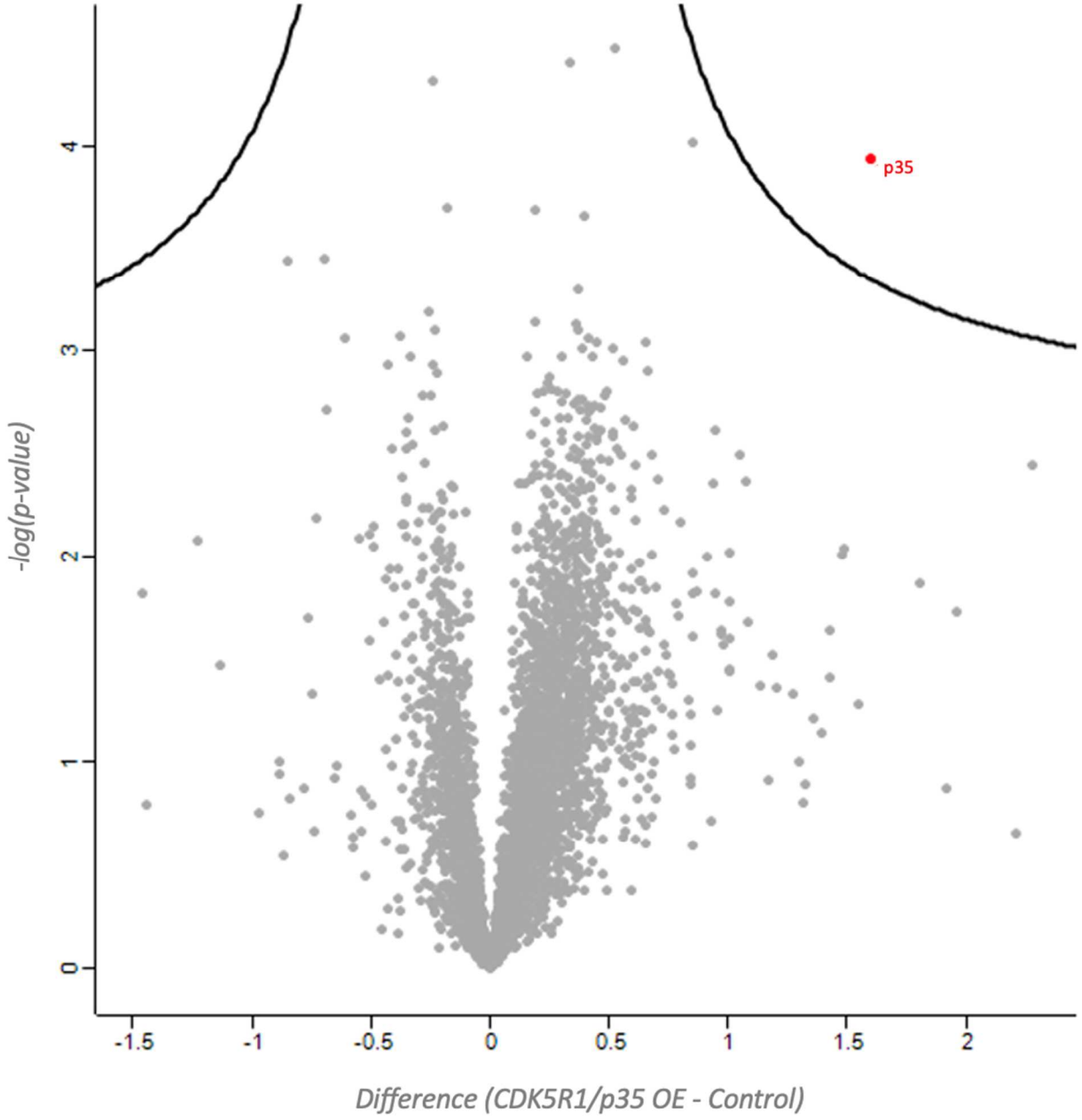

Figure 3.6*:* Global proteome changes in *CDK5R1*/p35 OE mice | Volcano plot depicting differential protein expression analysis between *CDK5R1*/p35 OE and littermate controls (WT^{MCM}). p35 was found to be the only significantly changed protein with a 1.5 fold increase in *CDK5R1*/p35 OE mice quantified.
* Unpaired student's t test: s0=0.1, FDR=0.05, 250 randomizations, no preservation of groupings in randomization.

3.3 Discussion

In Chapter 2, a cardiac-specific Cdk5 depletion mouse model was established. Conversely, to increase the kinase activity of Cdk5, a Cdk5 activation mouse model was discussed in this chapter. Cdk5 activation was achieved via overexpression of its activator, p35. As previously mentioned, the functional activity of Cdk5 is solely dependent on its association with p35, with Cdk5 OE alone shown insufficient for increasing kinase activity. [21,128-131] When assessing the cardiac function of *CDK5R1*/p35 OE mice, we saw systolic dysfunction without any cardiac structural abnormalities; this is contrary to what was observed in the Cdk5 deficient cohort in which systolic dysfunction was more severe, accompanied by LV dilation. Systolic dysfunction was modestly reduced based on LVEF and LVFS values, however, dysfunction was to a much lesser extent than that of the Cdk5 deficient cohort. Despite a modest decrease in systolic function, there were no morphological or significant histological changes observed in *CDK5R1*/p35 OE mouse hearts. Lastly, a review of the global proteome of Cdk5 activated mice revealed no changes in the differential expression of any other protein aside from p35.

Limitations of a cardiac-specific kinase activation model *in vivo* is extended to a lack of detection of kinase activity *in vivo*—this is due to a lack of *in vivo* kinase assay availability. The reason for establishing this mouse model was two-fold: (1) exploration of physiological effects of enhanced Cdk5 activation and (2) utilize a Cdk5 activation mouse model for the discovery of unknown cardiac-specific substrates. In theory, phosphorylation of Cdk5 targets should be increased in *CDK5R1*/p35 OE mice and subsequently decreased in Cdk5 deficient hearts. The elucidation of potential cardiac-specific substrates may provide insight into cardiac disease states as well as drug discovery for different cardiac disease.

3.4 Methods

Establishing Cardiac-specific *CDK5R1*/p35 OE Mouse Line

A novel transgenic mouse line was established in which mice with a C57B/6J background conditionally overexpressed *Cdk5* activator, *CDK5R1*/p35. Conditional human *CDK5R1*/p35 OE was targeted to the ubiquitous Rosa26 locus under the CAG promoter with a LoxP-STOP-LoxP cassette. Human CDK5R1 cDNA transcript was used to distinguish between endogenous and exogenous *Cdk5r1/CDK5R1*. "Rosa26-Cag-LSL-Cdk5r1" chimera mice were established from two mouse embryonic stem cells (mESC) #C4 and C14 clones. Once F1 mice reached adult age (3 months), they were crossed with an αMHC-MerCreMer Cre driver line (B6.FVB(129)-*A1cf*$^{Tg(Myh6\text{-}cre/Esr1*)1Jmk}$/J) from Jackson Lab (JAX; catalog #005657).

CDK5R1/p35 OE : αMHC-MerCreMer Mouse Genotyping:

DNA extracted from toe cuts were used for genotyping. Three sets of primers were used to confirm genotype of mice: (1) Rosa26 forward: 5' GGA CTA GGG CTG CGT GAG TCT CTG A 3' and Rosa26 reverse: 5' GGC GTT ACT ATG GGA ACA TAC GTC 3' (2) aMHC-MerCreMer WT forward: 5' TCT ATT GCA CAC AGC AAT CCA 3' and aMHC-MerCreMer WT reverse: 5' CCA ACT CTT GTG AGA GGA GCA 3' (3) aMHC-MerCreMer mutant forward: 5' TCT ATT GCA CAC AGC AAT CCA 3' and aMHC-MerCreMer mutant reverse: 5' CCA GCA TTG TGA GAA CAA GG 3'. To confirm targeted recombination and overexpression of *Cdk5r1*/p35, the following primer set was used: (4) *CDK5R1*/p35 recombination F: 5' CCG CGG GCC CTA AGA AGT TCC TAT TC 3' and p35 recombination R: 5' GTT GCG TCA GCA AAC ACA GT 3'. Vent® DNA Polymerase (New England BioLabs; catalog #: M0254L) was used for

Rosa26 PCR. TaKaRa Ex Taq® DNA Polymerase (TaKaRa Bio USA; catalog #: RR001C) was used for the latter 3 reactions—(2), (3) and (4).

Genotyping Use	Primer F (5'→ 3')	Primer R (5'→ 3')	Band Length	Tm
aMHC-MerCreMer WT	TCT ATT GCA CAC AGC AAT CCA	CCA ACT CTT GTG AGA GGA GCA	295	50
aMHC-MerCreMer Mutant	TCT ATT GCA CAC AGC AAT CCA	CCA GCA TTG TGA GAA CAA GG	300	50
Rosa26	GGA CTA GGG CTG CGT GAG TCT CTG A	GGC GTT ACT ATG GGA ACA TAC GTC	1500	60
CDK5R1/p35 recombination	CCG CGG GCC CTA AGA AGT TCC TAT TC	GTT GCG TCA GCA AAC ACA GT	Recomb: 1400 No recomb: 2300	60

qRT-PCR

Total RNA was extracted from frozen mouse whole heart ventricular samples from *CDK5R1*/p35 OE or WT^{MCM} cohorts by utilizing the RNeasy mini kit (Qiagen; catalog #: 74004) and RNase-Free DNase kit (Qiagen; catalog #: 7254). cDNA was subsequently synthesized following Invitrogen's SuperScript III First-Strand Synthesis System kit (ThermoFisher Scientific; catalog #: 18080051). The resulting sample of cDNA was diluted with UltraPure DNase/RNase-Free Distilled Water (ThermoFisher Scientific; catalog #: 10977015) at a ratio of 1:5. qRT-PCR was ran using TB Green Advantage qPCR Premix (TaKaRa; catalog #: 639676) and StepOnePlus real time PCR systems (ThermoFisher Scientific; catalog #: 4376600) using a MicroAmp™ Fast Optical 96-Well Reaction Plate (ThermoFisher Scientific; catalog #: 4346907). Quantification was done by comparative CT, using mouse Gapdh as a control reference gene for normalization. qRT-PCR primer sets were as follows: (1) human *CDK5R1* forward: 5' ATG CAT TGA ATC CTT CAC CC 3' and human *CDK5R1* reverse: CTT CTC CGA CCT GAA GAA GC' (2) mouse *Gapdh*

forward: 5’ AGG TCG GTG TGA ACG GAT TTG 3’ and mouse *Gapdh* reverse: 5’ GGG GTC GTT GAT GGC AAC A 3’. All oligo primers were synthesized by IDT.

Global Quantitative Proteomics by Mass Spectroscopy

After echo, mice were sacrificed using CO_2 asphyxiation followed by cervical dislocation according to Columbia IACUC approved protocol # AC-AABK3550. Whole hearts were subsequently removed, washed in Tyrode’s solution and the atria were separated from the ventricles. After washing, whole heart ventricular samples were flash frozen in liquid nitrogen and stored at -80 C until further proteomic experiments.

For bottom-up global quantitative proteomics, tandem mass tag (TMT)-based quantitative proteomics was used.[123] In summary, flash frozen mouse ventricular heart tissue was lysed by bead-beating in 9M urea and 200mM EPPS (pH 8.5), supplemented with protease and phosphatase inhibitors. Samples were reduced with 5mM TCEP and alkylated with 10 mM iodoacetamide (IAA) that was quenched with 10 mM DTT. A total of 400 μg of protein was chloroform−methanol precipitated. Protein was reconstituted in 200 mM EPPS (pH 8.5) and digested by Lys-C overnight and trypsin for 6h, both at a 1:50 protease-to-peptide ratio. Digested peptides were quantified using a Nanodrop at 280nm and 300 μg of peptide from each sample were labeled with 800 μg TMT reagent using 10-plex TMT kit.[124] TMT labels were checked, 0.5 μg of each sample was pooled, desalted and analyzed by short SPS-MS3 method, and using normalization factor, samples were bulk mixed at 1:1 across all channels and 100 μg of bulk mixed samples were used for total proteome and remaining for phospho-proteome analysis (phosphoproteomic analysis discussed in Chapter 4).

Mixed TMT-labeled samples were fractionated using the High pH Reversed-Phase Peptide

Fractionation Kit (ThermoFisher Scientific; catalog #: 84868) and each fraction was dried down in a speed-vac. Peptides were dissolved in 10 µl of 3% acetonitrile/0.1% formic acid injected using SPS-MS3. The UltiMate 3000 UHPLC system (ThermoFisher Scientific; catalog #: IQLAAAGABHFAPBMBFB) and EASY-Spray PepMap RSLC C18 50 cm x 75 µm ID column (ThermoFisher Scientific; catalog #: ES900) coupled with Orbitrap Fusion Tribrid Mass Spectrometer (ThermoFisher Scientific; catalog #: IQLAAEGAAPFADBMBCX) were used to separate fractioned peptides with a 5-30% acetonitrile gradient in 0.1% formic acid over 127min at a flow rate of 250 nL/min. After each gradient, the column was washed with 90% buffer B for 5 min and re-equilibrated with 98% buffer A (0.1% formic acid, 100% HPLC-grade water) for 40min. For High pH Reversed-Phase proteome fractions, the full MS spectra were acquired in the Orbitrap Fusion Tribrid Mass Spectrometer (ThermoFisher Scientific; catalog #: IQLAAEGAAPFADBMBCX) at a resolution of 120,000.

The 10 most intense MS1 ions were selected for MS2 analysis. The isolation width was set at 0.7 Da and isolated precursors were fragmented by CID at a normalized collision energy (NCE) of 35% and analyzed in the ion trap using "turbo" scan speed. Following acquisition of each MS2 spectrum, a synchronous precursor selection (SPS) MS3 scan was collected on the top 10 most intense ions in the MS2 spectrum. SPS-MS3 precursors were fragmented by higher energy collision-induced dissociation (HCD) at an NCE of 65% and analyzed using the Orbitrap.

Analysis of Global Raw Mass Spectrometric Data

Raw mass spectrometric data was analyzed using Proteome Discoverer 2.2 to perform database search and TMT reporter ions quantification. TMT tags on lysine residues and peptide N termini (+229.163 Da) and the carbamidomethylation of cysteine residues (+57.021 Da) was set

as static modifications, while the oxidation of methionine residues (+15.995 Da), deamidation (+0.984) on asparagine and glutamine and phosphorylation (+79.966) on serine, threonine, and tyrosine were set as a variable modification. Data was searched against a UniProt Mouse with peptide-spectrum match (PSMs) and protein-level FDR at 1% FDR. The signal-to-noise (S/N) measurements of each protein will be normalized so that the sum of the signal for all proteins in each channel was equivalent to account for equal protein loading.

Analysis of Global Proteomic Results

Peptide identification and quantification were imported into Perseus MaxQuant for statistical analysis (FDR<0.05) to identify proteins demonstrating statistically significant changes in abundance.[125] The following workflow was used: the generic matrix upload for *CDK5R1*/p35 OE global proteomic dataset was filtered based on a minimum number of valid values of 12 (i.e. only protein abundances with a quantifiable amount in every sample were included in the analysis). Next the "categorical annotation rows" function was used to assign common genotypes to each sample (either "*CDK5R1*/p35 OE" or "WT") and the data was subsequently log transformed—log2(x). For differential expression analysis, a two-sample student's T-test was ran using *CDK5R1*/p35 OE as "group 1" and "WT" as group 2. The following criteria was used for the T-test: s0=0.1, FDR=0.05, 250 randomizations, no preservation of groupings in randomization.

Chapter 4: Identifying Primary Substrates of Cdk5 in Adult Cardiac Tissue

4.1 Introduction

Protein phosphorylation is the most common and critical molecular regulator of protein function, localization, cell signaling and gene expression. Nearly 30% of all eukaryotic proteins are thought to be phosphorylated on at least one amino acid residue.[132] The phosphorylation state of proteins affect their activity, reactivity and ability to bind to other molecules.[133] Protein kinases selectively and reversibly modify other proteins by adding a hypervalent phosphate group (PO_4^{3-}) from ATP to a polar alkyl group of an amino acid residue. This phosphate addition transforms a once hydrophobic/apolar protein to a hydrophilic/polar protein. The protein is now able to adopt a variety of structural changes and alterations of protein confirmation necessary for a variety of biological changes including interaction with other molecules, substrate specificity and subcellular localization. Furthermore, adoption of structural changes can also affect regulation of protein function including assembly or detachment of protein complexes, as well as subcellular localization.[132-136]

Protein phosphorylation is an essential regulator of myocardial contraction and function. A balance between the phosphorylation/dephosphorylation state of proteins allows for maintenance of cardiac homeostasis.[137] Cardiac Ca^{2+} homeostasis, in particular, is controlled by kinase mediated protein phosphorylation via excitation contraction coupling mechanisms. For example, phosphorylation of regulatory proteins by protein kinase A (PKA) activates L-type voltage gated Ca^{2+} channels to increase Ca^{2+} influx and facilitates the subsequent release of Ca^{2+} stored in the sarcoplasmic reticulum. Furthermore, protein phosphorylation coordinates

mechanisms involved in the temporal regulation of contractility, relaxation, and subsequent myofilament Ca^{2+} affinity, all to sustain Ca^{2+} homeostasis.[119,138-140]

A known role for phosphorylation by CDK's in the heart has been limited to cardiac development and cardiomyocyte differentiation via cell cycle regulation. Cell-cycle relevant CDK expression is reportedly low after birth since cardiomyocytes are terminally differentiated and exit the cell cycle post-embryonic development.[141] For example, one group showed high cardiac-expression of CDK1, CDK2 and CDK4 throughout embryonic development and neonatal development, however, high levels of CDK expression subsided by the time rats reached adolescence. [142] Traditional cyclin-dependent CDK's have also been implicated in states of cardiac stress, including cardiac hypertrophy and heart failure. Postmitotic cardiomyocytes are known to proliferate during end stage heart failure, with one study reporting evidence of CDK6 expression during heart failure in humans.[141] While the aforementioned studies address the role of cell cycle relevant kinases, there is a lack of insight into cell cycle independent roles of CDK's such as CDK5. For this reason, non- cell-cycle substrates of cyclin-independent kinases, such as CDK5, remain to be explored.

Currently, the list of known cell-cycle independent, physiologically relevant substrates of CDK5 are limited to the brain (**Table 1.1)**. It is therefore the aim of this chapter to determine primary substrates of CDK5 in adult cardiac tissue. In this chapter, I discuss results from LC-MS/MS phosphoproteomic analysis to identify potential cardiac-specific Cdk5 substrates. Both Cdk5 deficient and *CDK5R1*/p35 OE cohorts (day 1 post final Tam injection) were subject to phosphoproteomic analysis. An acute time point was used for phosphoproteomic analysis in order to identify immediate/primary phosphorylation changes, rather than secondary changes that may occur resulting from downstream impact on physiological state. A comparison of proteins with a

significant decrease in phosphorylation immediately after Cdk5 depletion was induced vs proteins with a significant increase in phosphorylation immediately after Cdk5 activation was induced, allowed me to narrow down potential phospho-substrates. The identified proteins were further validated using a proximity ligation assay, looking at the co-localization of Cdk5 + target phosphoprotein in mouse cardiac tissue sections.

4.2 Results

Bottom-up phosphoproteomic analysis of the Cdk5 deficient cohort and *CDK5R1*/p35 OE cohort immediately following recombination (1 day post final Tam injection) was performed. The acute nature of the study serves a purpose of identifying the immediate phosphorylation changes due to Cdk5 deficiency/ Cdk5 activation.

Differential expression analysis of the phospho-proteome when comparing Cdk5 deficient vs control mice resulted in 538 differentially phosphorylated proteins (FDR = 0.05, S0=0.1) (**Fig 4.1**). The top 30 proteins with an overall increase and top 30 proteins with an overall decrease in phosphorylation are included in **Fig 4.1**. The top three proteins with an overall significant decrease in phosphorylation were beta-taxilin (Txlnb), Gap junction a1 (Gja1) and formin homology 2 domain containing 3 (Fhod3). Txlnb is a cardiac-enriched protein, with little known function.[143] Recently, decreased expression in *TXLNB* has been implicated in DCM.[144] Further discussion of Txlnb will be done later on in this chapter. GJA1 is a gap junction protein/connexin with a prominent role in cardiac cell-to-cell adhesion, migration and signaling. [145,146] In the heart, gap junctions function to ensure successful propagation of the cardiac impulse by providing pathways for intercellular current flow and communication [147,148]. Evidence of gap junction remodeling in which density as well as distribution of gap junctions are modified, have been implicated in nearly all cardiac arrhythmias. [149] In particular, dysregulation of GJA1 phosphorylation leads to gap junction remodeling and has been implicated in cardiac arrhythmias with GJA1 dephosphorylation occurring post-myocardial ischemia. The dephosphorylation event is thought to be a correlative mechanism with contractile failure and subsequent arrhythmia.[150] Furthermore, reports of patient specific familial mutations in GJA1 have resulted in DCM and subsequent heart failure [151,152] Lastly, FHOD3 is an established sarcomeric protein essential for sarcomeric organization;

increases in phosphorylation have been associated with cardiac hypertrophy, while pathophysiological effects on a decrease in phosphorylation have yet to be elucidated.[153]

The top three proteins with an overall significant increase in phosphorylation were chromosome 4 open reading frame 54 (C4orf54), plectin (Plec) and tenascin C (Tnc). Despite being highly expressed in cardiac tissue, little is known regarding the cardiac-specific function of C4orf54. PLEC is an intermediate filament binding protein, responsible for connecting cytoskeleton filaments to intracellular junction in the heart.[154] Phosphorylation of PLEC has been shown to be directly correlated with intermediate filament interaction.[155] Lastly TNC, an intracellular matrix protein, is known to play a crucial role in the regulation of cell adhesion as well as tissue remodeling in a number of cardiac disease states—a literature search did not reveal roles for changes in phosphorylation.[156]

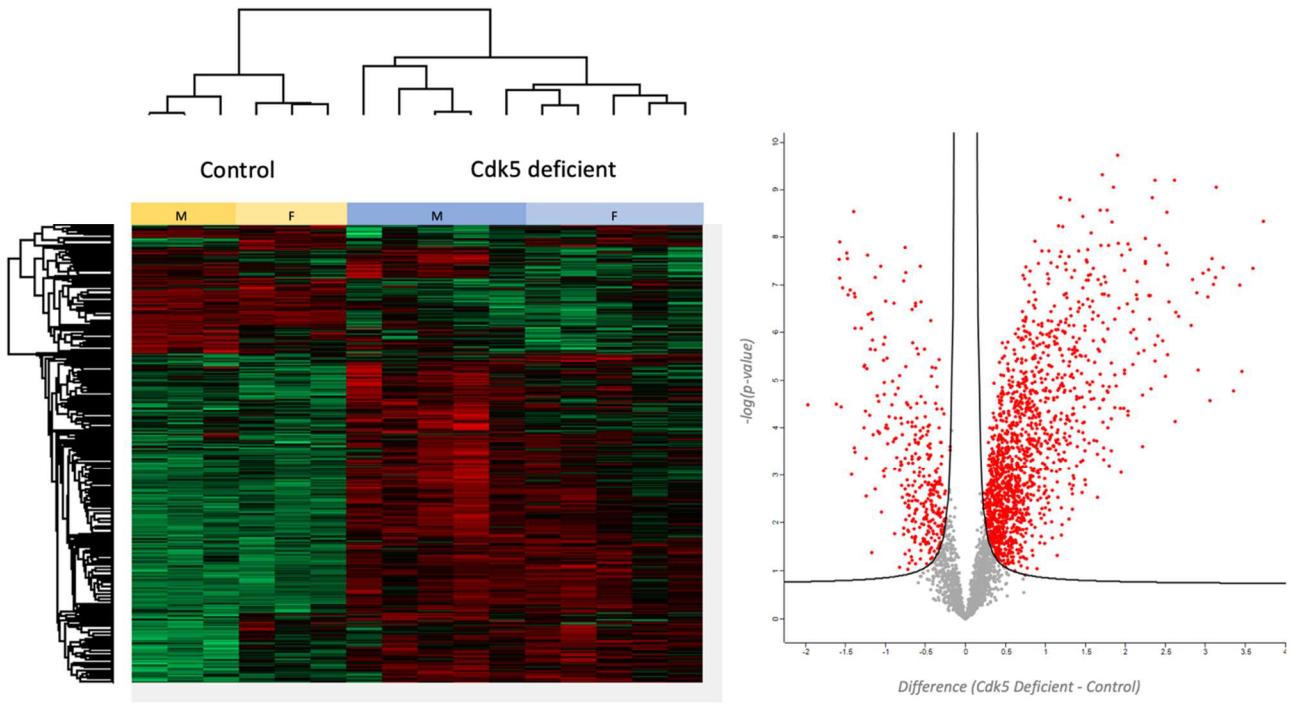

Figure 4.1*:* Comparative analysis of the Cdk5 deficient cardiac phospho-proteome

A) Unsupervised hierarchical clustering of differentially phosphorylated proteins between Cdk5 deficient vs littermate control mice (Cdk5 deficient n = 10; control WT n = 6).
B) Volcano plot representing proteins with significant differences in phosphorylated proteins when comparing Cdk5 deficient with control samples.
*For each protein, significance is expressed as FDR adjusted p-value as a function of difference between samples (log_2 fold change). FDR = 0.05, s0= 0.1. Significantly upregulated/downregulated proteins are shown with red circles.

Fold Change	Gene Symbol	Gene Name	-Log(p-value)
-1.972	*Txlnb*	taxilin beta	4.49
-1.577	*Gja1*	gap junction protein alpha 1	7.54
-1.57	*Fhod3*	formin homology 2 domain containing 3	7.89
-1.425	*Klhl31*	kelch like family member 31	3.01
-1.402	*Palld*	palladin, cytoskeletal associated protein	8.56
-1.392	*Fgf13*	fibroblast growth factor 13	3.58
-1.384	*Tacc2*	transforming acidic coiled-coil containing protein 2	6.75
-1.299	*Chchd2*	coiled-coil-helix-coiled-coil-helix domain containing 2	6.09
-1.264	*Celf2*	CUGBP Elav-like family member 2	5.29
-1.241	*Palmd*	palmdelphin	2.56
-1.24	*Ppp1r14c*	protein phosphatase 1 regulatory inhibitor subunit 14C	3.37
-1.233	*Mmachc*	metabolism of cobalamin associated C	5.25
-1.166	*Pde1c*	phosphodiesterase 1C	6.28
-1.13	*Nfib*	nuclear factor I B	2.71
-1.092	*Tbc1d4*	TBC1 domain family member 4	3.94
-1.076	*Efnb3*	ephrin B3	3.88
-1.046	*Denr*	density regulated re-initiation and release factor	2.23
-1.016	*Bckdha*	branched chain keto acid dehydrogenase E1 subunit alpha	2.96
-1.015	*Ppp1r3a*	protein phosphatase 1 regulatory subunit 3A	4.96
-1.008	*Sorbs1*	sorbin and SH3 domain containing 1	5.9
-0.998	*Myoz2*	myozenin 2	3.15
-0.945	*Tln2*	talin 2	2.15
-0.909	*Rnf207*	ring finger protein 207	4.98
-0.884	*Fyco1*	FYVE and coiled-coil domain autophagy adaptor 1	3.13
-0.874	*Ank3*	ankyrin 3	4.71
-0.827	*Pde4a*	phosphodiesterase 4A	5.1
-0.81	*Ndufs7*	NADH:ubiquinone oxidoreductase core subunit S7	3.29
-0.806	*Pde4dip*	phosphodiesterase 4D interacting protein	4.22
-0.798	*Sgca*	sarcoglycan alpha	2.78
-0.797	*Cnksr3*	CNKSR family member 3	3.23
3.728	*C4orf54*	chromosome 4 open reading frame 54	8.36
3.597	*Plec*	plectin	7.35

3.459	*Tnc*	tenascin C	5.19
3.433	*Krt80*	keratin 80	7
3.351	*Spp1*	secreted phosphoprotein 1	4.78
3.226	*Xirp2*	xin actin binding repeat containing 2	7.36
3.124	*Flnc*	filamin C	7.16
3.039	*Xirp1*	xin actin binding repeat containing 1	7.32
2.906	*Mybpc2*	myosin binding protein C2	5.21
2.821	*Ndufs3*	NADH:ubiquinone oxidoreductase core subunit S3	6.15
2.628	*Tpm2*	tropomyosin 2, beta	6.43
2.624	*Ttn*	titin	4.13
2.612	*Dsp*	desmoplakin	9.21
2.526	*Adprhl1*	ADP-ribosylhydrolase like 1	5.54
2.518	*Sptb*	spectrin beta, erythrocytic	8.54
2.403	*Cryab*	crystallin alpha B	5.93
2.373	*Jpt1*	Jupiter microtubule associated homolog 1	9.21
2.335	*Rtn4*	reticulon 4	8.84
2.266	*Dab2*	DAB adaptor protein 2	4.89
2.258	*Trim54*	tripartite motif containing 54	4.95
2.253	*Klhl9*	kelch like family member 9	7.44
2.249	*Psma5*	proteasome 20S subunit alpha 5	7.49
2.246	*Synpo2l*	synaptopodin 2 like	7.97
2.231	*Sec62*	SEC62 homolog, preprotein translocation factor	5.63
2.164	*Hax1*	HCLS1 associated protein X-1	5.56
2.15	*Sync*	syncoilin, intermediate filament protein	7.06
2.145	*Sqstm1*	sequestosome 1	6.7
2.138	*Hspbp1*	HSPA (Hsp70) binding protein 1	6.78
2.137	*Apobr*	apolipoprotein B receptor	5.87
2.064	*Obscn*	obscurin, cytoskeletal calmodulin and titin-interacting RhoGEF	6
2.034	*Tnni3*	troponin I3, cardiac type	4.35

Table 4.1*:* Graph and corresponding list of the top 30 proteins with a decrease/increase in phosphorylation based on fold change (log2 ratio) in Cdk5 deficient mouse cardiac tissue

Differential expression analysis of the phospho-proteome when comparing *CDK5R1*/p35 OE mice vs control mice resulted revealed clustering based on genotype in the twelve samples. A total of 3,074 differentially phosphorylated proteins/protein isoforms were found (FDR = 0.05, S0=0.1). The top 30 proteins with an overall increase and top 30 proteins with an overall decrease in phosphorylation are included in **Table 4.2**. The top three proteins with an overall significant decrease in phosphorylation were aspartate beta-hydroxylase (Asph), sorbin and SH3 domain containing 1 (Sorbs1) and HIV-1 Tat specific factor 1 (Htatsf1). Asph is a non-heme iron

containing protein that is located at the junctional sarcoplasmic reticulum in cardiac muscle; it has been implicated in cardiac remodeling and fibrosis.[157] Sorbs1 is an adaptor protein highly expressed in cardiac tissue, known to regulate cell-cell adhesion and cytoskeletal formation. It is also highly expressed in end stage heart failure patients.[158] Lastly, Htasf1 is a transcription factor that regulates transcriptional elongation. One published finding suggests Htasf1 functions as a $Na_V1.2$ associated protein—$Na_V1.2$ is a voltage-gated sodium channel expressed in aortic smooth muscle cells and cardiomyocytes, and plays a significant role in the generation propagation of cardiac action potentials.[159,160]

Conversely, the top three proteins with an overall significant increase in phosphorylation were cyclase associated actin cytoskeleton regulatory protein 2 (Cap2), talin 2 (Tln2) and caveolae associated protein 4 (Cavin4). All three proteins are crucial for maintaining cardiac cytoskeleton integrity. Cap2 is a cytoskeletal protein whose exact cardiac function is unknown. The protein is thought to regulate cell motility and muscle contraction—Cap2 loss-of-function and conditional knockout mouse models displayed a DCM/sudden heart failure, respectfully.[161,162] Tln2 is highly expressed in cardiac tissue and serves as a linkage between the extracellular matrix and cytoskeleton, playing a large roll in cell adhesion.[163,164] The role of increased phosphorylation of these proteins is currently unknown.

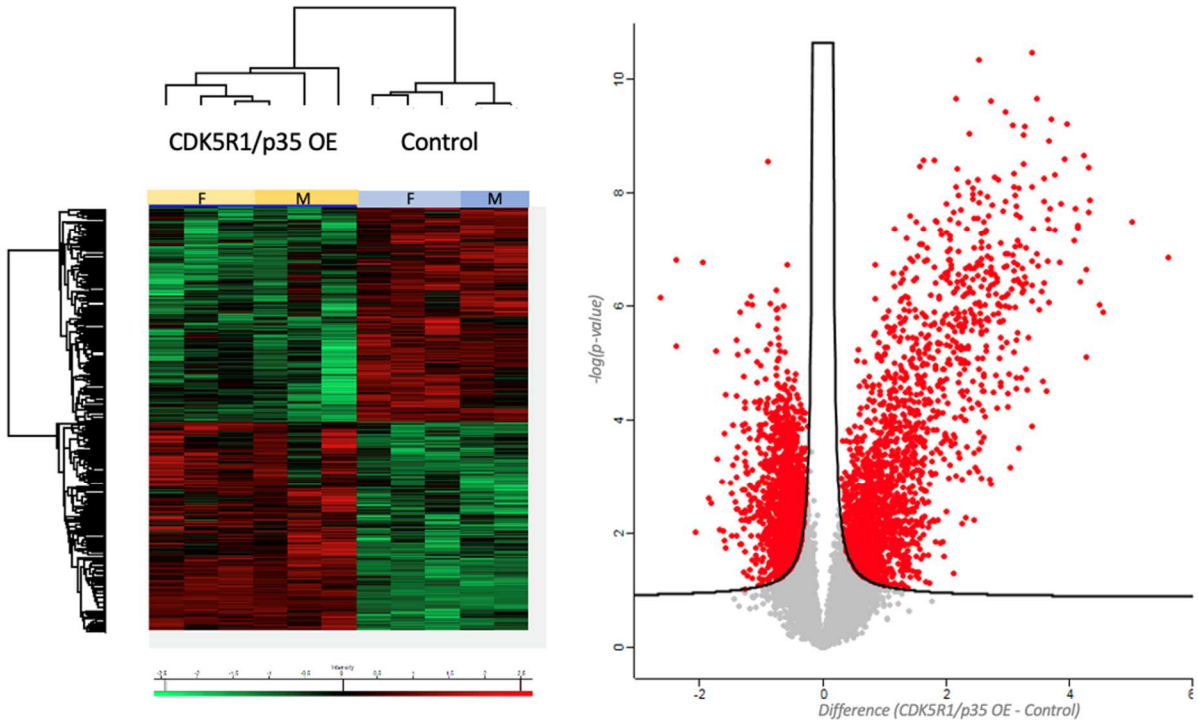

Figure 4.2: Comparative analysis of the CDK5R1/p35 OE cardiac phospho-proteome
A) Unsupervised hierarchical clustering of significantly phosphorylated proteins between *CDK5R1/p35* OE and control littermate mice (CDK5R1/p35 OE n = 6; control WT n = 5).
B) Volcano plot representing proteins with significant differences in phosphorylated proteins when comparing CDK5R1/p35 OE cardiac tissue with control samples.
*For each protein, significance is expressed as FDR adjusted p-value as a function of difference between samples (log_2 fold change). FDR = 0.05, s0= 0.1. Significantly upregulated/downregulated proteins are shown with red circles.

Fold Change	Gene Symbol	Gene Name	-Log (p-value)
-2.067	*Asph*	aspartate beta-hydroxylase	2.02
-1.951	*Sorbs1*	sorbin and SH3 domain containing 1	6.77
-1.85	*Htatsf1*	HIV-1 Tat specific factor 1	2.63
-1.808	*Gja1*	gap junction protein alpha 1	2.55
-1.598	*Palm*	paralemmin	3.78
-1.501	*Tbc1d4*	TBC1 domain family member 4	2.9
-1.454	*Rap1gap2*	RAP1 GTPase activating protein 2	3.92
-1.452	*Il10rb*	interleukin 10 receptor subunit beta	3.21
-1.45	*Plin1*	perilipin 1	0.85
-1.411	*Leo1*	LEO1 homolog, Paf1/RNA polymerase II complex component	2.43

-1.41	*Ythdc1*	YTH domain containing 1	3
-1.404	*Cycs*	cytochrome c, somatic	5.41
-1.341	*Pi4k2a*	phosphatidylinositol 4-kinase type 2 alpha	5.91
-1.314	*Prkab1*	protein kinase AMP-activated non-catalytic subunit beta 1	1.82
-1.314	*Ctnna3*	catenin alpha 3	2.23
-1.295	*Cdk13*	cyclin dependent kinase 13	3.92
-1.287	*Pspc1*	paraspeckle component 1	1.33
-1.273	*Cdc42ep1*	CDC42 effector protein 1	1.03
-1.273	*Tnni3k*	TNNI3 interacting kinase	1.68
-1.272	*Ttc7b*	tetratricopeptide repeat domain 7B	4.22
-1.271	*Acot7*	acyl-CoA thioesterase 7	4.32
-1.268	*Frmd5*	FERM domain containing 5	2.38
-1.263	*Tcea3*	transcription elongation factor A3	2.78
-1.263	*Cic*	capicua transcriptional repressor	3.94
-1.239	*Fxr1*	FMR1 autosomal homolog 1	3.08
-1.236	*Tcp11l2*	t-complex 11 like 2	3.19
-1.235	*Gtf2f1*	general transcription factor IIF subunit 1	2.27
-1.234	*Ank1*	ankyrin 1	5.21
-1.227	*Ncl*	nucleolin	1.26
-1.219	*Tbc1d17*	TBC1 domain family member 17	3.09
5.611	*Cap2*	cyclase associated actin cytoskeleton regulatory protein 2	6.85
5.022	*Tln2*	talin 2	7.49
4.557	*Cavin4*	caveolae associated protein 4	5.89
4.503	*Usp10*	ubiquitin specific peptidase 10	6.03
4.32	*Bcas3*	BCAS3 microtubule associated cell migration factor	8.44
4.31	*Ephx2*	epoxide hydrolase 2	7.65
4.282	*Ttn*	titin	5.1
4.274	*Plec*	plectin	6.64
4.25	*Ilrun*	inflammation and lipid regulator with UBA-like and NBR1-like domains	8.66
4.178	*Speg*	striated muscle enriched protein kinase	6.42
4.152	*Slc16a1*	solute carrier family 16 member 1	7.43
4.134	*Dennd4c*	DENN domain containing 4C	7.39
4.104	*Tbc1d13*	TBC1 domain family member 13	7.72
4.088	*Vps13c*	vacuolar protein sorting 13 homolog C	7.15
3.958	*Dtna*	dystrobrevin alpha	9.22
3.92	*Pex19*	peroxisomal biogenesis factor 19	8.59
3.873	*Usp14*	ubiquitin specific peptidase 14	7.8
3.855	*Tmem185a*	transmembrane protein 185A	6.76
3.78	*Ehd4*	EH domain containing 4	7.34
3.77	*Ccdc93*	coiled-coil domain containing 93	8.32
3.685	*Coro6*	coronin 6	7.71
3.677	*Perm1*	PPARGC1 and ESRR induced regulator, muscle 1	7.36
3.67	*Naca*	nascent polypeptide associated complex subunit alpha	6.07
3.624	*Ccdc8*	coiled-coil domain containing 8	4.52
3.589	*Ociad1*	OCIA domain containing 1	7.84

3.57	*Flnc*	filamin C	4.69
3.549	*Sgpp1*	sphingosine-1-phosphate phosphatase 1	6.26
3.517	*Synpo*	synaptopodin	5.93
3.491	*Dmac1*	distal membrane arm assembly complex 1	6.7
3.486	*Dact3*	dishevelled binding antagonist of beta catenin 3	6.91

Table 4.2*:* Graph and corresponding list of the top 30 proteins with a decrease/increase in phosphorylation based on fold change (log2 ratio) in *CDK5R1*/p35 OE mouse cardiac tissue

Proteins with a significant decrease in phosphorylation in the Cdk5 deficient cohort, and opposing increase in phosphorylation in the *CDK5R1*/p35 OE cohort were considered potential candidates for cardiac-related Cdk5 substrates. For further narrowing of substrate candidates, specific phospho-sites of proteins with significant phosphorylation changes that were decreased in Cdk5 deficient mice and subsequently increased in *CDK5R1*/p35 OE mice were analyzed. A total of 18 common proteins with an overall opposing changes in phosphorylation (decreased phosphorylation in Cdk5 deficient mice and increased phosphorylation in *CDK5R1*/p35 OE mice) were identified. The list of identified substrate candidates can be found in **Figure 4.3**. One of the identified substrates was $Ca_V1.2$—the Cdk5 substrate candidate that our lab had identified based on prior Timothy Syndrome studies led by LouJin Song.

A

Protein	Cdk5 Deficient Phospho Log Ratio	*CDK5R1*/p35 OE Phospho Log Ratio
Palld	-1.264	3.006
Ppp1r14c	-1.24	1.259
Denr	-1.046	1.434
Ppp1r3a	-1.015	0.948
Txlnb	-0.841	0.707
Pde4dip	-0.806	0.138
Sgca	-0.798	0.922
Prune2	-0.788	1.39
Atp2b1	-0.756	0.645
C10orf71	-0.719	1.094
Cavin2	-0.704	3.397
Svil	-0.604	2.566
Slc9a1	-0.585	0.671
Kiaa1191	-0.517	0.088
Cav1.2	-0.501	1.34
Gab1	-0.479	1.398
Tacc2	-0.434	1.862
Atp1a1	-0.432	2.439

B

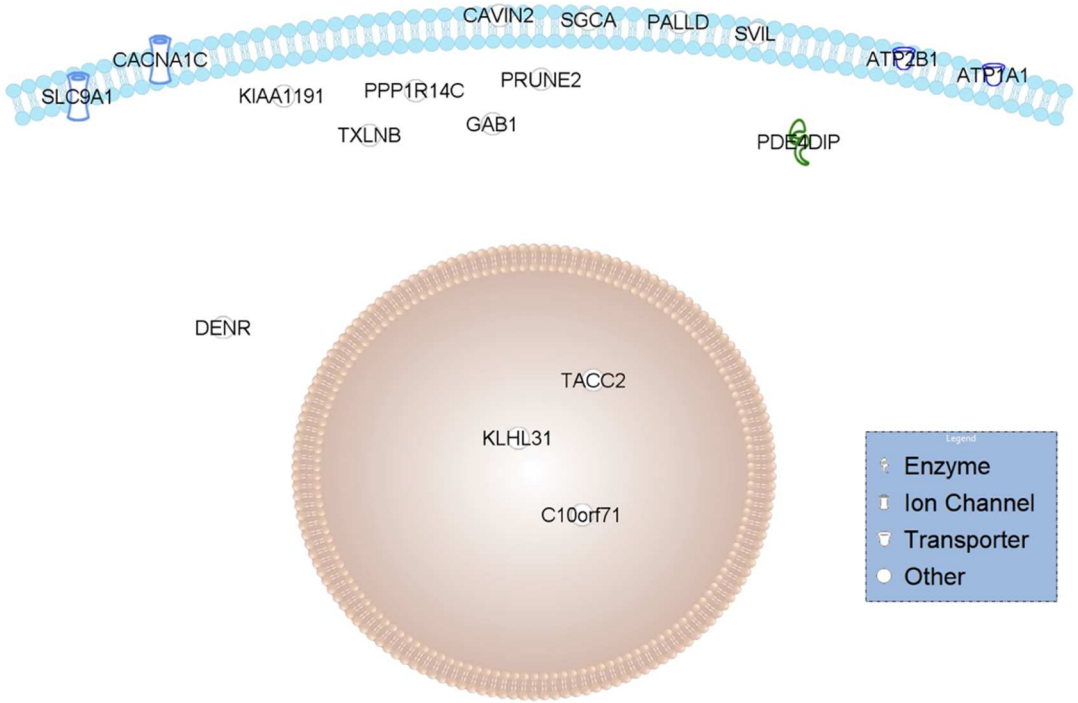

Figure 4.3*:* |Potential Cdk5 substrates
A) List of proteins with a significant decrease in phosphorylation in Cdk5 deficient mice, and subsequent increase in phosphorylation in *CDK5R1*/p35 OE mice.
B) Sub-cellular location of each potential protein substrate.

Pathway analysis of the potential substrate list of Cdk5 as outlined in **Figure 4.3** revealed hits associated with microtubule dynamics, transport of molecules, muscle contraction/function and cardiac contractility (**Table 4.3**). These proteins play an essential role in cell-to-cell adhesion, which is also a major function of Cdk5 in the brain. Cdk5 is known to phosphorylate cytoskeletal proteins, signaling molecules, ion channels and regulatory proteins involved in microtubule and actin dynamics, cell-cell/cell-ECM adhesion and cytoskeletal regulation. [114-117]

Pathway Hits	Potential Cdk5 substrates
Microtubule Dynamics	Atp2b1, Gab1, Palld, Pde4dip, Prune2, Slc9a1, Tacc2
Transport of Molecules	Atp1a1, Atp2b1, Cav1.2, Gab1, Ppp1r3a, Slc9a1
Muscle Contraction	Atp1a1, Atp2b1, Cav1.2, Sgca
Function of Muscle	Atp1a1, C10orf71, Gab1, Sgca
Cardiac Contractility	Atpa1, Gab1, Slc9a1

Table 4.3*: |*IPA pathway analysis of 18 identified potential phospho-targets of Cdk5.

Lastly, potential phospho-sites in proteins of interest were further narrowed down dependent on whether they followed the known Cdk5 consensus motif "(S/T)PX(K/H/R)." The two proteins/phospho-sites that met these criteria were (1) Txlnb on Serine 78 and (2) density regulated re-initiation and release protein on Serine 73 (Denr). As previously mentioned, Txlnb is a cardiac- and skeletal-muscle enriched protein with high cell-type expression in cardiomyocytes (**Fig 4.4**) Currently, little is known about Txlnb's physiological function. One group published an abstract hypothesizing a role for Txlnb in cardiac protein proteostasis via regulation of protein synthesis, autophagy, proteosome degradation and ubiquitination. Txlnb knockout mice display increased protein ubiquitination and decreased proteasome activity—an increase in protein

ubiquitination has also been associated with the pathophysiology of DCM.[143,165] Another group recently published a paper identifying *TXLNB* in humans as a novel DCM-associated gene.[144] Lastly, in a mouse model of myotonic dystrophy, *Txlnb* expression was found to be significantly downregulated.[166] Myotonic dystrophy is an autosomal dominant disorder of the skeletal and smooth muscle caused by an expansion of "CUG" repeats.[167] Individuals with myotonic dystrophy experience progressive muscle wasting and weakness, along with prolonged muscle contractions. Myotonic dystrophy also has cardiac-manifestations that include conduction disturbances, arrhythmias and cardiomyopathies.[168]

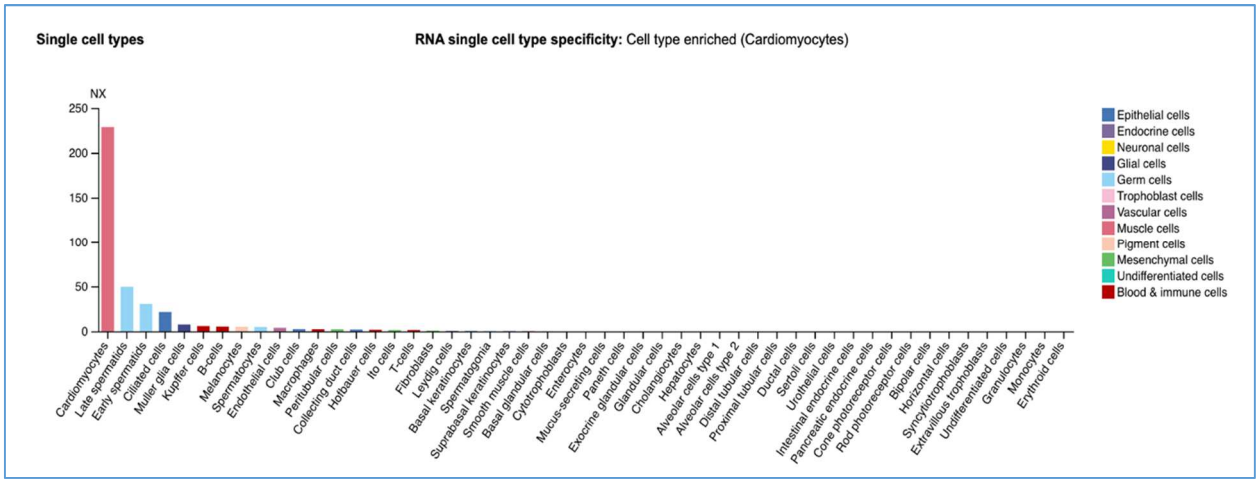

Figure 4.4: Cardiomyocytes exhibit highest cell type expression of TXLNB |RNA single cell type specificity demonstrates highest cell-type specific expression of TXLNB in cardiomyocytes. (*Figure taken from proteinatlas.org*)

The second potential substrate identified based on proteomic data is Denr. DENR is an mRNA translation factor whose expression has been postulated to be regulated by direct cell to cell contact.[169] There is very little known about the physiological and functional roles DENR aside from its expression in various tissue types. While DENR is found to be expressed in cardiac tissue (**Fig 4.5**), its cardiac-specific role remains unknown.

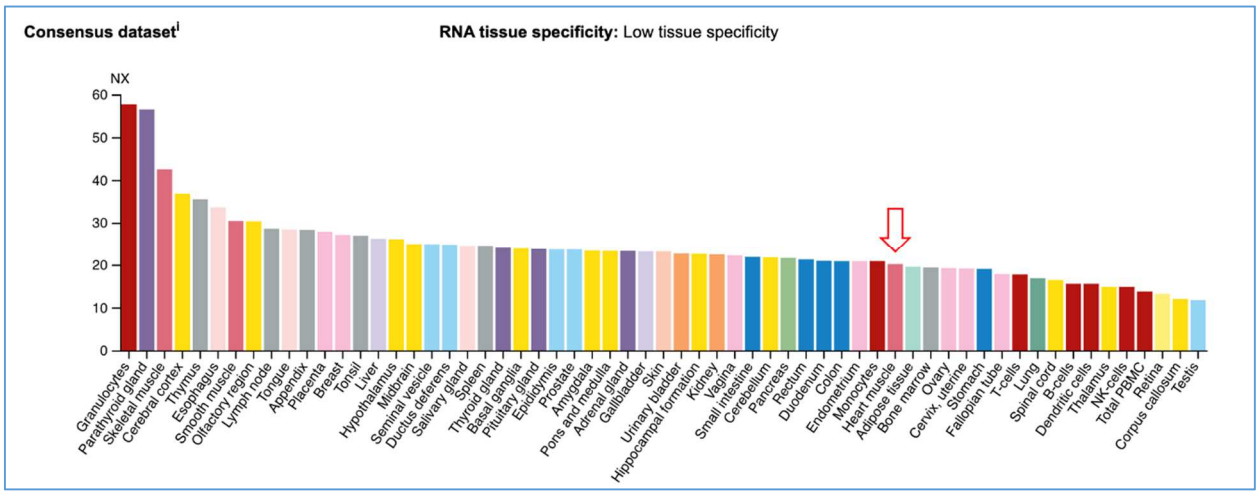

Figure 4.5: Tissue-specific expression of DENR |RNA tissue-specific expression of DENR. Medium expression is found in heart muscle. (*Figure taken from proteinatlas.org*)

To further explore Txlnb and Denr as potential Cdk5 substrates, a proximity ligation assay (PLA) was performed. *In situ* proximity ligation assay's combine oligo-labeled antibodies with ligation and PCR amplification to allow for detection of protein-protein interactions. Such detection can be used for epitope-epitope interaction on one protein, or protein-protein interaction between two co-localized proteins. In summary, two primary antibodies (from different species origins) are each bound by a positive or negative PLA probe—PLA probes are secondary antibodies covalently bound to a short oligonucleotide. Upon addition of ligase (and if epitopes/proteins are within a <40 nm proximity), the positive and negative PLA probes can hybridize and form a rolling circle DNA template for amplification with the addition of DNA polymerase. Lastly, fluorescent probes are added to the amplified DNA, allowing for detection with fluorescent microscopy. An illustrated schematic of this assay is shown in **Figure 4.6**.

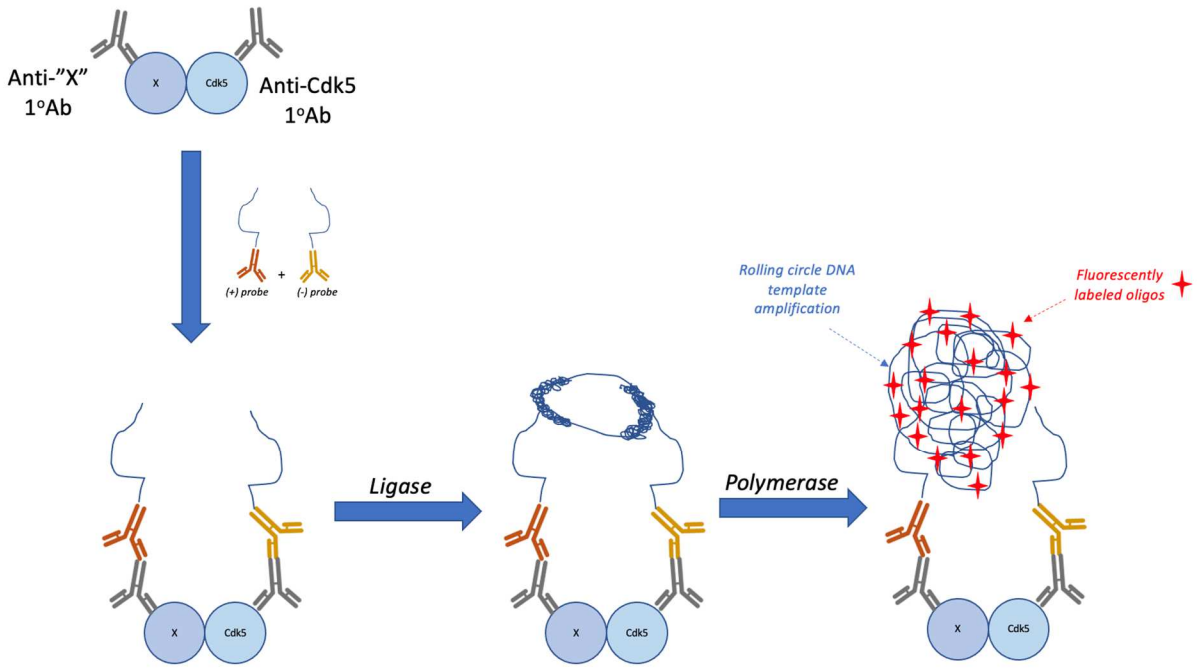

Figure 4.6: Proximity ligation assay schematic

In situ PLA was used to determine co-localization between Cdk5-Txlnb and Cdk5-Denr. Whole heart ventricular tissue sections from WT mice and Cdk5 deficient mice were deparaffinized and a proximity ligation assay was performed using the Duolink in Situ Proximity Ligation Assay Fluorescence kit for mouse/rabbit antibodies. Cdk5 deficient mouse ventricle embedded tissue sections were used as a negative control. Results from the PLA of Cdk5-Txlnb revealed co-localization of the two proteins in WT mice (**Fig 4.7**), while Cdk5-Denr did not give a detectible signal (image not included). While it is possible that Denr may not be a potential cardiac-specific Cdk5 substrate, technical issues could explain why the PLA did not give a result with Cdk5-Denr. If there was a lack of antibody-epitope compatibility for the Denr protein, one would not get a detectible fluorescent signal. It is also possible that the Cdk5-Denr complex is masked by other molecules in the cardiac tissue sample, or the epitope used for antibody production is not exposed in the cardiac tissue sample.

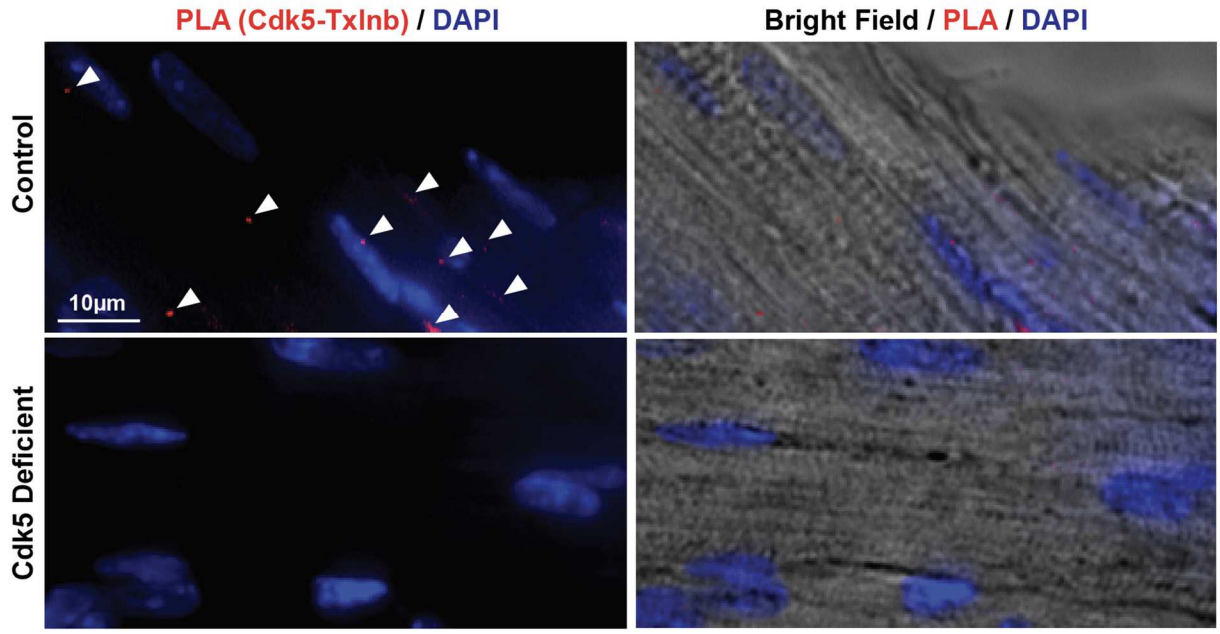

Figure 4.7: Protein-protein interaction between Cdk5 & Txlnb |Representative confocal fluorescent and bright field images of control (example from female WT) and Cdk5 deficient (example from female *Cdk5*$^{fl/lf}$) mouse used with proximity ligation assay (PLA, SIGMAR1-hERG red) and DAPI (blue) staining; scale bar, 10 μm. White triangles indicate location of co-localization with fluorescent signal.

4.3 Discussion

Protein phosphorylation is the most common post-translational modification necessary for the regulation of protein function, cell signaling and biological pathways.[170] The goal of this chapter is to identify potential novel cardiac-specific substrates of Cdk5. Cdk5 is a proline directed serine/threonine kinase that phosphorylates its substrate targets by adding a phosphate group from ATP to a targeted amino acid residue. The role of Cdk5 has been extensively studied in the brain, and as a result, 19 different neuronal-specific substrates have been identified.[21,29] Prior findings from the Yazawa lab as well as findings reported in this thesis have demonstrated a critical role for Cdk5 in cardiac function and cardiac disease pathophysiology. Exactly how Cdk5 modulates cardiac function and impacts cardiac pathophysiological conditions remains to be understood. By identifying cardiac-specific Cdk5 substrates, we may be able to uncover novel mechanisms underlying cardiac function and cardiovascular disease states.

To identify phospho-substrate targets, phosphoproteomic LC-MS/MS was performed on both Cdk5 deficient and *CDK5R1*/p35 OE mouse cardiac tissue. Differential expression analysis of the Cdk5 deficient and *CDK5R1*/p35 OE phospho-proteome revealed significant phosphorylation changes in proteins associated with cell-cell adhesion and cardiac contractility. Phosphoproteomic analysis confirmed a lack in difference between the $Cdk5^{fl/+}$ and $Cdk5^{fl/fl}$ cohorts, once again, consistent with what was observed in echo and histological results.

Interestingly, while *CDK5R1*/p35 OE hearts did not have any significant global proteome changes (FDR = 0.05, S0=0.1), there were significant changes observed in the phospho-proteome, with over 3,000 significantly differentially phosphorylated proteins/protein isoforms identified. By activating Cdk5, it seems a downstream phosphorylation cascade may have been activated. When certain kinases are continuously activated, it can subsequently activate downstream

signaling molecules, in turn, causing this phosphorylation cascade. To confirm the top two candidate Cdk5 substrates, a PLA was performed to look for co-localization of Cdk5 and Txlnb/Denr. Co-localization was observed between Cdk5 and Txlnb only in WT mouse cardiac tissue. This co-localization was no longer evident in Cdk5 deficient mouse cardiac tissue. The investigation of protein phosphorylation in vivo is limited, with analysis beyond phospho-proteomics reduced to in vitro biochemical assays; kinases removed from their physiological environment don't always behave the same way in vitro. Limitations associated with such analysis include experiment-specific reagents/conditions that alter availability of phospho-substrates and the phosphorylation state of the substrate in the cell potentially preventing it being utilized as a substrate in non-physiological assay.[171] It is also possible that the site can only be phosphorylated when in a given complex. The next step in adequate confirmation of the identified phospho-site on Txlnb (Serine 78) and Denr (Serine 73) involves phosphoantibody production. While this is a technically challenging and time-consuming endeavor, our lab has prior expertise in antibody production—this is included as part of future directions for this project.

4.4 Methods

Phospho-Proteomics by Mass Spectroscopy for Cdk5 Deficient Cohort

For phospho-proteome analysis, 11 desalted fractions were enriched for phosphopeptides using a mixture of MagReSyn Ti-IMAC and Zr-IMAC resins according Resyn Bioscience instructions. In briefly, 200 µg of labeled peptide were dissolved in 0.2 ml of binding buffer (80% Acetonitrile, 1M glycolic acid and 5% TFA) and incubated with equilibrated (10 µl of each Ti-IMAC and Zr-IMAC) resins at room temperature for 30 min, and the resin was washed 3 three times to remove the unbound, non-phosphorylated peptides. Phospho-peptides were eluted using 1% ammonium hydroxide. The enriched phospho-peptides were further de-salted with SDB-SCX stageTip and each fraction dried down in a speed-vac. Dried phospho-peptides were in dissolved in 10 µl of (3% acetonitrile/ 0.1% formic acid) injected using MSA-SPS-MS3 and NL-SPS-MS3 methods (ref. M2). The UltiMate 3000 UHPLC system and EASY-Spray PepMap RSLC C18 50 cm x 75 µm ID column coupled with Orbitrap Fusion were used to separate fractioned peptides with a 5-30% acetonitrile gradient in 0.1% formic acid over 45 min at a flow rate of 250 nL/min. After each gradient, the column was washed with 90% buffer B for 10 min and re-equilibrated with 98% buffer A (0.1% formic acid, 100% HPLC-grade water) for 40 min. Phosphopeptide analysis, two methods were used for each fraction. For both methods, the full MS spectra were acquired in the Orbitrap at a resolution of 120,000. The 10 most intense MS1 ions were selected for MS2 analysis. Following the acquisition of each MS2 spectrum, a synchronous-precursor-selection (SPS)-MS3 scan was collected on the Top 10 most intense ions in the MS2 spectrum. The isolation width was set at 0.7 Da, and isolated precursors were fragmented using two methods. In the first method, we used collision-induced dissociation (CID) at normalized collision energy (NCE) of 35% with MultiStage Activation (MSA), and in the second method with NL-triggered

MS3 using higher energy collision-induced dissociation (HCD) at normalized collision energy (NCE) of 35%. SPS-MS3 precursors were fragmented by higher energy collision-induced dissociation (HCD) at NCE of 65% and analyzed using the Orbitrap.

Raw mass spectrometric data were analyzed using Proteome Discoverer 2.4 to perform database search and TMT reporter ions quantification. TMT tags on lysine residues and peptide N termini (+229.163 Da) and the carbamidomethylation of cysteine residues (+57.021 Da) was set as static modifications, while the oxidation of methionine residues (+15.995 Da), deamidation (+0.984) on asparagine and glutamine and phosphorylation (+79.966) on serine, threonine, and tyrosine were set as a variable modification. Data were searched against a UniProt Mouse with peptide-spectrum match (PSMs) and protein-level FDR at 1% FDR. The signal-to-noise (S/N) measurements of each protein will be normalized so that the sum of the signal for all proteins in each channel was equivalent to account for equal protein loading.

Phospho-Proteomics by Mass Spectroscopy for *CDK5R1/*p35 OE Cohort

For phospho-proteome analysis, ~3mg bulk mixed TMT-labeled samples were dried and desalted using a 200 mg Sep-Pak solid-phase extraction column. Desalted peptides were enriched for phospho-peptides using a mixture of MagReSyn Ti-IMAC and Zr-IMAC resins according Resyn Bioscience instructions. In briefly, 3 mg of labeled peptide were dissolved in 1 ml of binding buffer (80% Acetonitrile, 1M glycolic acid and 5% TFA) and incubated with equilibrated 300 µl (150 µl of each Ti-IMAC and Zr-IMAC) resins at room temperature for 30 min, and the resin was washed 3 three times to remove the unbound, non-phosphorylated peptides. Phospho-peptides were eluted using 1% ammonium hydroxide. The enriched phospho-peptides were further

fractionated in eight fractions using the High pH Reversed-Phase Peptide Fractionation Kit (ThermoFisher Scientific; catalog #: 84868) and each fraction dried down in a speed-vac.

Dried phospho-peptides were in dissolved in 10 µl of (3% acetonitrile/ 0.1% formic acid) injected using MSA-SPS-MS3 and NL-SPS-MS3 methods.[172] The UltiMate 3000 UHPLC system and EASY-Spray PepMap RSLC C18 50 cm x 75 µm ID column coupled with Orbitrap Fusion were used to separate fractioned peptides with a 5-30% acetonitrile gradient in 0.1% formic acid over 45 min at a flow rate of 250 nL/min. After each gradient, the column was washed with 90% buffer B for 10 min and re-equilibrated with 98% buffer A (0.1% formic acid, 100% HPLC-grade water) for 40min. Phospho-peptide analysis, two methods were used for each fraction. For both methods, the full MS spectra were acquired in the Orbitrap at a resolution of 120,000. The 10 most intense MS1 ions were selected for MS2 analysis.

Following the acquisition of each MS2 spectrum, a synchronous-precursor-selection (SPS)-MS3 scan was collected on the Top 10 most intense ions in the MS2 spectrum. The isolation width was set at 0.7 Da, and isolated precursors were fragmented using two methods. In the first method, we used collision-induced dissociation CID at normalized collision energy (NCE) of 35% with MSA, and in the second method with NL-triggered MS3 using higher energy collision-induced dissociation HCD at NCE of 35%. SPS-MS3 precursors were fragmented by HCD at NCE of 65% and analyzed using the Orbitrap.

Analysis of Raw Phosphoproteomic Mass Spectrometric Data for both Cdk5 deficient and *CDK5R1/*p35 OE Cohorts

Raw phospho-proteome mass spectrometric data were analyzed using Proteome Discoverer 2.2 to perform database search and TMT reporter ions quantification. TMT tags on

lysine residues and peptide N termini (+229.163 Da) and the carbamidomethylation of cysteine residues (+57.021 Da) was set as static modifications, while the oxidation of methionine residues (+15.995 Da), deamidation (+0.984) on asparagine and glutamine and phosphorylation (+79.966) on serine, threonine, and tyrosine were set as a variable modification. Data were searched against a UniProt Mouse with peptide-spectrum match (PSMs) and protein-level FDR at 1% FDR. The signal-to-noise (S/N) measurements of each protein will be normalized so that the sum of the signal for all proteins in each channel was equivalent to account for equal protein loading.

Analysis of Phosphoproteomic Results for both Cdk5 deficient and *CDK5R1/*p35 OE Cohorts

Phospho-peptide identification and quantification were imported into Perseus MaxQuant for statistical analysis (FDR<0.05) to identify proteins demonstrating statistically significant changes in abundance.[125] The workflow used for phosphoproteomic comparison is comparable to the workflow previously outlined in **Sections 2.4/3.4,** respectfully.

Identifying Cardiac-Specific Cdk5 Substrates

To narrow down potential phosphorylation targets of Cdk5, the list of all significantly phosphorylated proteins (FDR<0.05) from the Cdk5 deficient phosphoproteomic dataset and *CDK5R1*/p35 OE dataset were pasted into an excel sheet. Next, a "=VLOOKUP" function was utilized to identify the associated phospho-log ratio from each of the two cohorts. Significantly changed proteins that did not appear in both cohorts were filtered out of the merged dataset. Then, leveraging excels "IF" function to create a "0" or "1" dummy variable that indicates an inverse relationship ("0" being no inverse relationship observed and "1" being the presence of an inverse relationship), the dataset was filtered to include proteins that had an increase in phosphorylation

in the *CDK5R1*/p35 OE cohort and corresponding decrease in phosphorylation in the Cdk5 deficient cohort. The final list consisted of 23 proteins.

As the significant changes in protein phosphorylation were cumulatively derived and not based on specific phospho-site (limitations of mass-spec output format and subsequent analysis), significantly changed phosphorylation sites were manually compared between the Cdk5 deficient and *CDK5R1*/p35 OE cohorts. Sites that were overlapping between both proteins and that followed the known CDK5 consensus sequence were utilized for further analysis.

Proximity Ligation Assay

A proximity ligation assay was performed using the Duolink in Situ Proximity Ligation Assay Fluorescence kit for mouse/rabbit antibodies (Sigma-Aldrich, catalog #: DUO92101). Standard PLA for tissue *in situ* were adhered to.[173,174] In summary, 5μM-thick sections of paraffin embedded whole heart ventricular tissue (see protocol in "Mouse Cardiac Tissue Sampling" method section) were deparaffinized and rehydrated by immersing in xylene, ethanol and distilled water. Using a hydrophobic barrier pen, a circle was draw on the slide surrounding each tissue section. Slides were washed three times with PBS, permeabilized for 30 minutes at room temperature with 0.2% Triton X-100 in PBS and then washed another three times with PBS. Permeabilized samples were blocked with blocking solution from the Duolink kit for 1 hour at 37C in a humidity chamber followed by three more washes with PBS.

Next, sections on slides were co-incubated with a 1:500 dilution of mouse anti-CDK5 antibody (Santa Cruz Technology; catalog #: sc-6247) and either: (1) IHC-plus Polyclonal Rabbit anti-human TXLNB Antibody (LSBio; catalog #: LS-A8163) at 1:1000 dilution or (2) Rabbit anti-human Polyclonal DENR Antibody (Novus Biological; catalog #: NBP2-13913) at a 1:1000

dilution with Duolink Antibody Diluent for 24 hours. After incubation, slides were washed and subsequently incubated with the PLUS and MINUS probes in a 1:5 dilution with Duolink Antibody Diluent for 1 hour at 37 C in a preheated humidity chamber. After washing, Ligase from the kit was added to the slides in a 1:5 dilution with Ligation Buffer and Ultrapure water. The slides were incubated for 30 minutes in a pre-heated humidity chamber at 37 C.

Imaging of PLA Fluorescence Signals

The PLA fluorescence signals were imaged using an inverted Nikon Eclipse Ti-U Inverted Fluorescence microscope with a Nikon 40x objective lens (CFI S Flour, Bright Field; NA, 0.90; W.D. 0.30mm; cover glass thickness, 0.17), standard DAPI and RFP filter sets (Chroma), Lambda DG-4 Plus (Sutter Instrument), Spectra-X LED (Lumencor) and MetaMorph software (Molecular Devices).

Conclusion

5.1 Translational Relevance of CDK5

One of the hallmark indicators of cardiac dysfunction is an alteration in cardiac protein phosphorylation. Protein phosphorylation is a key regulator of cardiac contractility, structural integrity and metabolism.[139,171,175] Protein phosphorylation by a number of kinases including Ca^{2+}-calmodulin protein kinase (CAM-PK), protein kinase C (PKC), ERK's and mitogen-activated protein kinases (MAPK's) has been studied in a number of cardiac pathophysiological conditions.[171] What remains to be elucidated, however, is how phosphorylation triggers modulation in protein activity and subsequent downstream pathophysiological effects.

One such cardiovascular disease state in which a dysregulation of phosphorylation has been implicated is heart failure. Heart failure is a life-threatening condition in which the heart's ability to fill up with or to eject blood is impaired. This insufficient cardiac output prohibits a sufficient amount of blood from being delivered to tissue throughout the body.[176] Disturbance in cardiac protein phosphorylation is associated with mechanisms involved in cardiac dysfunction and subsequent heart failure.[172] For example, altered Ca^{2+} handling and impaired myofilament contraction have been linked to defects in phosphorylation of cardiac troponin I via PKA. Altered phosphorylation of such contractile proteins are associated with end stage heart failure.[177]

In collaboration with the Junco Warren lab and Dr. Stavros Drakos at the University of Utah, our lab obtained myocardial tissue from human donors who passed away due to either heart failure or non-cardiac related causes. A total of 4 control tissue samples and 5 heart failure samples were obtained (**Table 5.1**). I decided to look at protein expression levels of CDK5 and p35 in each cardiac tissue sample in order to: (1) detect expression of CDK5 in human cardiac tissue, (2)

determine whether there is a correlation between heart failure and CDK5/p35 expression and (3) determine potential correlation between severity of cardiac dysfunction as indicated by EF and CDK5/p35 expression.

Condition	Gender	Age	Race	Body Weight	Height	Cause of Death	Cardiac/ Respiratory Arrest	Ischemia (CAD)	Ejection Fraction	Heart Failure Etiology
Control	F	42	White	70.4	5'1"	Anoxia/Drug intoxication	yes	no	60	n/a
Control	F	69	White	64.7	5'5"	CVA-Stroke/ICH	no	no	56	n/a
Control	F	51	White	69	5'3"	Anoxia/Drug intoxication	no	no	60	n/a
Control	F	61	White	75	5'6"	CVA-Stroke/ICH	no	no	80	n/a
Heart Failure	M	45	White	50.4	5'9.6"	Heart Failure	n/a	yes	24	ischemic
Heart Failure	F	27	Asian	77	5'4"	Heart Failure	n/a	yes	15	mixed (ischemic and non-ischemic)
Heart Failure	M	62	White	105.5	6'1"	Heart Failure	n/a	yes	14	non ischemic, idiopathic
Heart Failure	M	45	White	109.2	5'10"	Heart Failure	n/a	yes	25	ischemic
Heart Failure	M	39	White	94.8	5'10"	Heart Failure	n/a	no	32	non ischemic, idiopathic

Table 5.1*:* Information on human heart donors| Information concerning heart donors' gender, age, race, body weight, height, cause of death, cardiac/respiratory arrest status, ischemia/coronary artery disease status, ejection fraction, and heart failure etiology are listed above. Samples and corresponding information was obtained from collaborators in the Junco Warren lab at the University of Utah.

Analysis of CDK5 and p35 expression via western blot assay revealed a significant correlation between heart failure status and an increase in CDK5 and p35 expression, with both CDK5 and p35 being significantly higher in heart failure samples (**Fig. 2—A,B**). This data was really interesting, as we had initially hypothesized that there would be a decrease in CDK5 expression associated with heart failure. During heart failure, the goal of the myocardium is to compensate for cardiac output. One potential explanation for this observed increase in CDK5/p35 expression pattern could be a result of a compensatory mechanism (i.e. cardiac remodeling, increased heart rate) associated with heart failure and overall cardiac dysfunction.[178] As part of future directions, a double overexpression mouse model of both Cdk5 and p35 will be established.

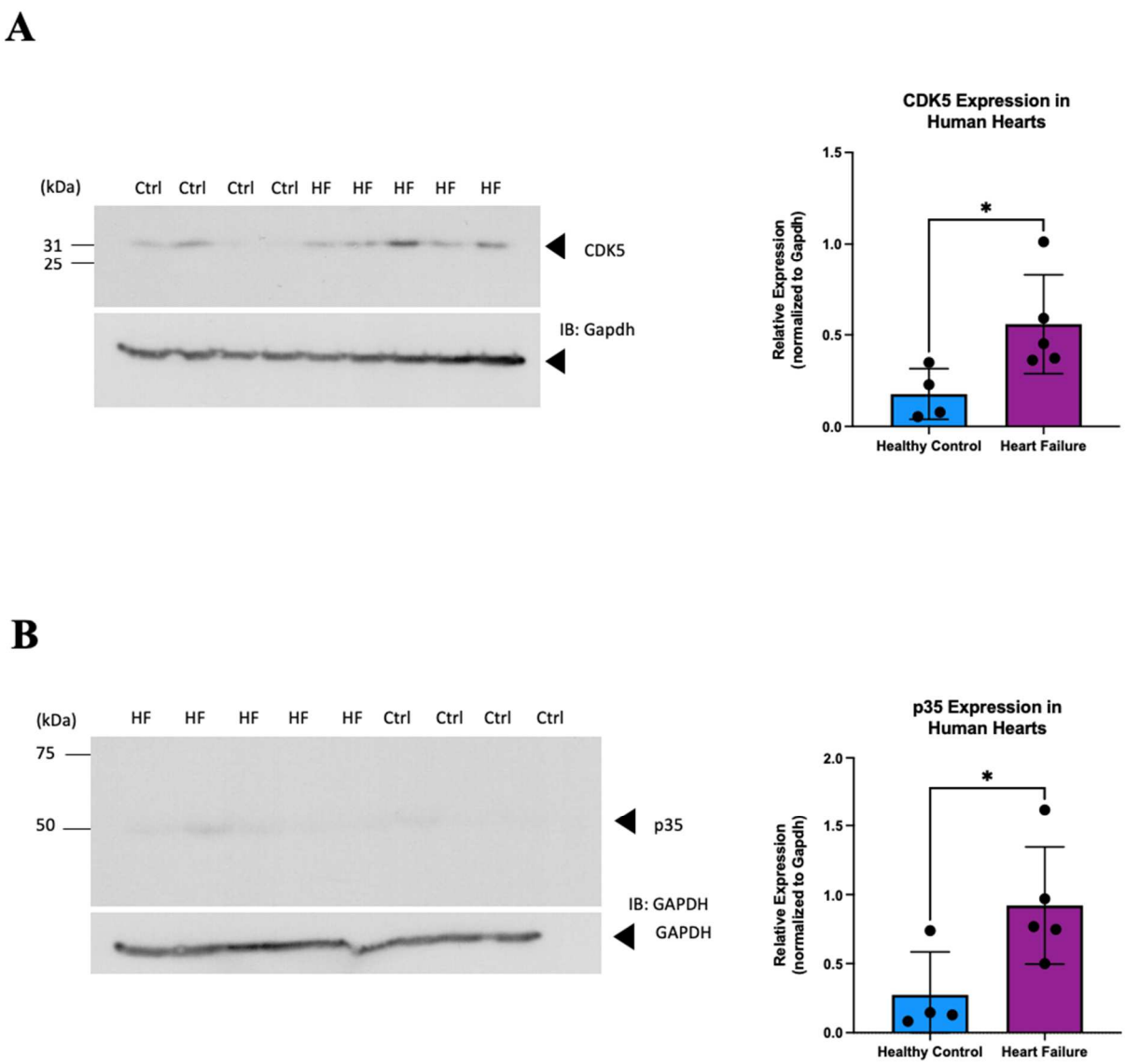

Figure 5.1: Expression of CDK5 and p35 in human heart failure and control samples |
A,B) Western blot analysis of CDK5 and p35 from human myocardial tissue collected from the left ventricle apex of individuals who passed away due to heart failure or non-cardiac related causes. A total of 4 control tissue samples and 5 heart failure samples were used. Band intensities were quantified using ImageJ. All samples were normalized to GAPDH.

5.2 Final Thoughts & Future Directions

Previously, a role for CDK5 in cardiac function and cardiovascular disease states had not been explored. CDK5 has been established in the literature as a unique CDK, having cell-cycle independent functions in a number of biological systems/processes including insulin secretion, metabolism, myogenesis, the immune system, the lymphatic system, cell motility and cell migration. [26] Furthermore, the majority of CDK5's well-known functions have been in the brain. As a result of such neuro-focused studies, the majority of elucidated human CDK5 substrates are neuronal-tissue specific.

In this study, two novel mouse models were established in order to determine Cdk5's impact on cardiac function: (1) an inducible Cdk5 deficient mouse model and (2) an inducible Cdk5 activation mouse model. Tam inducible cardiac-specific Cdk5 deficiency in adult mice resulted in severe systolic dysfunction, with significant decreases in FS, EF, LVEDD and LVEDF. Histological analysis showing significant enlargement of the LV along with LV wall thinning. Additionally, mononuclear cell infiltrate and modest evidence of collagen deposition were observed based on H&E and MT stains of paraffin embedded cardiac tissue sections. Lastly, global proteomic LC-MS/MS studies revealed changes in protein abundance indicative of a cardiac enlargement/DCM-like phenotype. Analysis of biological and functional pathways associated with proteome changes revealed a majority of differentially expressed proteins implicated in cell-adhesion. In the heart, the contractile ability of the cardiac muscle is maintained by integrity and synchronicity of the cell-to-cell junctions.[119] In heart failure as well as cardiomyopathies, significant alterations in cell-to-cell junctions are observed. [120,121] It is therefore plausible that CDK5 plays a significant role in the regulation of cell-to-cell adhesion in cardiac tissue.

Interestingly, when analyzing a model of Cdk5 activation (via OE of its activator p35), a striking cardiac phenotype was not observed. Echo recordings revealed a moderate reduction in systolic function as defined by reduced LVEF and LVFS. Again, such reductions were not nearly as significant/severe in comparison with the Cdk5 deficient mouse model. Furthermore, a lack of significant morphological and histological changes were noted along with a lack of changes to the global proteome. The only significant protein change detected by global proteomic analysis was a ~1.5 fold increase in Cdk5's activator, p35, which we exogenously overexpressed to establish the Cdk5 activation model. It is evident that alterations in baseline/homeostatic levels of Cdk5 results in cardiac impairment.

In addition to differences in control vs Cdk5 deficient/Cdk5 activation phenotypes, further phenotypical differences were observed based on gender of mice. Male mice experienced more severe systolic effects from Cdk5 deficiency than did female mice. Furthermore, the global proteome changes in Cdk5 deficient male mice were more significant than were female mice. While a minimal number of gender-specific differences were noted in the global proteome of control mice, a significant number of gender-related changes in the phospho-proteome were observed (**Fig. 5.2**). Phospho-proteome differences could be a potential explanation for gender bias towards males in predisposition as well as manifestation of cardiovascular disease. Notedly, DCM along with heart failure and a number of additional cardiac disease states have an increased incidence rate in men vs women.[179] Gender difference studies are currently being pursued as part of future directions for this project. A deeper understanding of molecular mechanisms underlying gender difference and response to cardiovascular disease states will be useful for precision medicine initiatives and drug discovery.

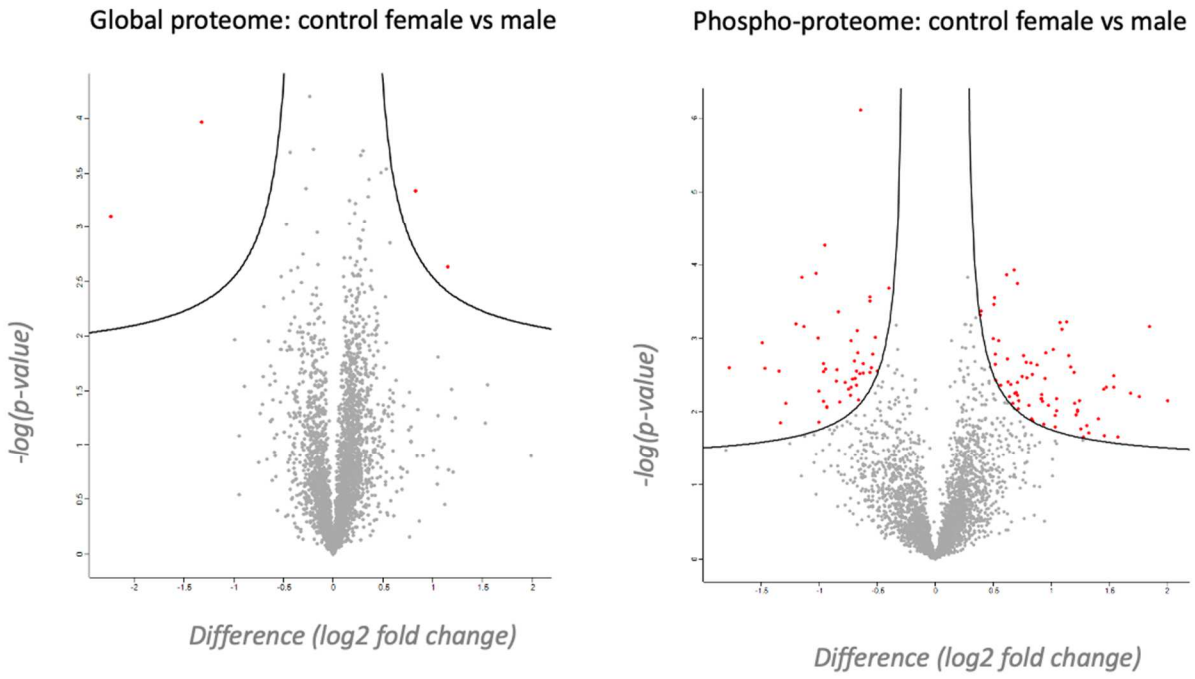

Figure 5.2*:* Differences in the global vs phospho-proteome of control mice

Limitations of spatiotemporal Cre-recombinase mediated mouse models targeted to cardiac tissue are present. Both Tam as well as Cre-recombination are known to have baseline levels of transient cardiotoxic effects. These effects can be minimized and accounted for with adequate Tam dosing optimization as well as utilization of appropriate experimental controls. In this study, we demonstrate minimal observed toxicity with optimized Tam dosing in both WT and WT^{MCM} cohorts.

A comparison of the phospho-proteome of Cdk5 deficient and Cdk5 activation mice allowed for identification of potential phospho-substrates in the heart. Phosphoproteomic and PLA studies revealed Txlnb, an understudied but highly expressed cardiac protein recently implicated in DCM, as a potential cardiac-specific substrate. As part of future directions, a phosphoprotein antibody for Txlnb—Serine78 is being produced. Furthermore, we plan to conduct knock-in experiments utilizing CRSIPR/Cas9 to generate mutant mice with an Ala-substitution on Txlnb-

Serine78. Validation of Cdk5 phosphorylation of Txlnb on the suspected phospho-site will provide further validation of the accuracy of our findings. Identification of Cdk5-cardiac specific phospho-targets may help us elucidate a mechanism by which Cdk5 regulates cardiac pathophysiological function.

Notedly, a role for Cdk5 in cardiac development was not discussed in this thesis. Preliminary findings from our lab have suggested that cardiac-specific depletion of Cdk5 caused embryonic lethality (~E14.5) due to cardiac dysfunction in the mouse (not shown). As part of future efforts by the lab, analysis of embryonic heart phenotypes in Cdk5 cardiac conditional knockout mice are currently being analyzed—this includes heart contraction assays, cardiac Ca^{2+} imaging, gene expression profiling and histology. Preliminary results using Cdk5 conditional knockout embryos indicate that Cdk5 is essential for heart development.

Lastly, as part of a follow-up to this project, potential therapeutic applications of p35 OE for cardiomyopathies are being explored. An adeno-associated virus (AAV) vector system has already been constructed to overexpress *CDK5R1*/p35. The AAV was constructed using a pAAV9 backbone, driven by the cardiomyocyte specific gene expression promoter, cardiac troponin T (cTNT) (**Fig 5.3**). Additionally, this construct will allow for YFP fluorescent intensity readout as it is correlated to p35 expression due to the self-cleaving peptide P2A system used in the construct. Successful infection using the aforementioned construct has already been confirmed using iPSC-CM's in the lab. The established AAV is also appropriate for use in *in vivo* mouse models, while multiplicity of infection has yet to be validated. We are also establishing both a CDK5 and p35 shRNA for translational application in heart failure models. Additionally, the effects of p35 OE in doxorubicin-induced DCM as well as Duchenne Muscular Dystrophy related DCM are being explored by our lab. Outcomes of this study as well as future directions provide new insight into

cardiac function, novel players in cardiovascular disease states, as well as the potential to be translational for development of new therapeutic targets for heart disease.

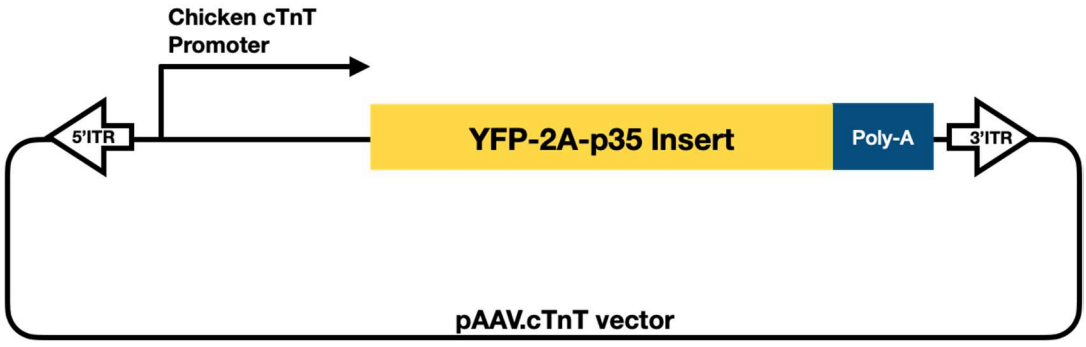

Figure 5.3*:* pAAV9-cTNT::hCDK5R1/p35 construct map | pAAV-YFP-2A-p35 viral construct. p35/YFP expression is driven by the cTnT promoter. Addgene #69915 vector is used as the backbone for this pAAV construct.

5.3 Methods

Human Heart Myocardial Samples

Flash frozen samples of human myocardial tissue were received from the Junco Warren lab at the University of Utah. Myocardial tissue was collected from the left ventricle apex of donor hearts that did not meet transplant requirements for non-cardiac related reasons (control samples). Left ventricular apex myocardial tissue was also collected from individuals who had passed away due heart failure (heart failure samples). A total of 4 control tissue samples and 5 heart failure samples were used for western blot analysis. The samples used for this study had been used for published studies from the Junco Warren lab.[180]

Western Blot of Human Myocardial Samples

Each human myocardial tissue sample was homogenized and subsequently lysed using lysis buffer containing 1% Triton X-100, 150 mM NaCl, 50 mM Tris-HCl (pH 7.4) and 1x protease inhibitor cocktail (Sigma-Aldrich; catalog #: P8340). Following lysis, protein concentrations were measured for each sample using a Pierce Bicinchoninic Acid assay kit (ThermoFisher Scientific; catalog #: 23225). Samples were prepared to a final amount of 20 μg of protein per well from each of the nine samples. Samples were denatured in 2× sodium dodecyl sulfate (SDS) sample buffer containing 8M Urea, 40 mM Tris-HCl, 2% (SDS), 10% beta-mercaptoethanol and 0.01% bromophenol blue. Each sample was then boiled on a heat block at 95 C for 5 minutes. SDS-polyacrylamide gel electrophoresis was run by loading samples onto a Tris-HCl SDS page gel (containing 10% Acrylamide-Bis) with a 5% stacking gel and 10% separation gel along with the ladder. All samples were subsequently to electro-transferred to Polyvinylidene difluoride (PVDF)

membranes using XCell SureLock Mini-Cell and XCell Blot Module system (Life Technologies; catalog #: EI0002) for approximately 14 hours/overnight.

The second/following day, membranes were blocked using 5% non-fat dry milk in Tris-based saline solution with Tween, 50 mM Tris-HCl, 150 mM NaCl, and 0.1% Tween (TBS-T) for 90 minutes at room temperature and subsequently stained with primary antibody diluted in blocking buffer overnight. The following two antibodies were used for Western blot: (1) anti-Cdk5 rabbit monoclonal Ab, (abcam; catalog #: ab40773) at a dilution of 1:1000 (2) anti-p35/p25 rabbit monoclonal antibody (Cell Signaling; catalog #:C64B10) at a dilution of 1:1000.

On the third/last day, PVDF membranes were incubated with a secondary goat anti-rabbit antibody (ThermoFisher Scientific; catalog #: 31460) at a 1:10,000 dilution in 5% nonfat dry milk + TBS-T blocking solution for one hour at room temperature. After secondary antibody stain, membranes were incubated with the Pierce ECL Western blotting substrate (ThermoFisher Scientific; catalog #: 32209) for chemiluminescence followed by exposure to X-ray films in a dark room. Following CDK5/p35 staining, membranes were stripped with buffer containing 62.5mM Tris-HCl, 2% SDS, 114mM beta-mercaptoethanol at 42oC for 15-20 minutes, followed by washing six times with PBS. A second round of immunoblotting was done for GAPDH in order to normalize band intensities. Band intensities for CDK5 & p35 antibodies were optimal at 1 hour exposure, and GAPDH was optimal after touch exposure. Protein band intensities of CDK5/p35 were quantified using ImageJ and were normalized to their corresponding GAPDH values. Statical significance was conducted in GraphPad Prism using an unpaired two-tailed t-test, with 7 degrees of freedom.

Statistical Analysis

For western blot protein expression quantification, protein band intensities of CDK5 and p35 were quantified using ImageJ and were normalized to their corresponding GAPDH values. Statical significance was conducted in GraphPad Prism using an unpaired two-tailed t-test, with 7 degrees of freedom. For analysis of the correlation between EF and CDK5/p35 protein expression, a Pearson's correlation test was ran using GraphPad Prism.

References

1 Malumbres, M. & Barbacid, M. Mammalian cyclin-dependent kinases. *Trends Biochem Sci* **30**, 630-641, doi:10.1016/j.tibs.2005.09.005 (2005).

2 Morgan, D. O. *The Cell Cycle: Principles of Control*. (New Science Press Ltd, 2007).

3 Bansal, A. K., Singh, L. R. & Kamli, M. R. *Posttranslational Modifications Associated With Cancer and Their Therapeutic Implications*. (Academic Press, 2019).

4 Abdel-Magid, A. F. Potential of Cyclin-Dependent Kinase Inhibitors as Cancer Therapy. *ACS Med Chem Lett* **12**, 182-184, doi:10.1021/acsmedchemlett.1c00017 (2021).

5 Wood, D. J. & Endicott, J. A. Structural insights into the functional diversity of the CDK-cyclin family. *Open Biol* **8**, doi:10.1098/rsob.180112 (2018).

6 Borquez, D. A. *et al.* Bioinformatic survey for new physiological substrates of Cyclin-dependent kinase 5. *Genomics* **101**, 221-228, doi:10.1016/j.ygeno.2013.01.003 (2013).

7 Swaffer, M. P., Jones, A. W., Flynn, H. R., Snijders, A. P. & Nurse, P. CDK Substrate Phosphorylation and Ordering the Cell Cycle. *Cell* **167**, 1750-1761 e1716, doi:10.1016/j.cell.2016.11.034 (2016).

8 Mapelli, M. & Musacchio, A. The structural perspective on CDK5. *Neurosignals* **12**, 164-172, doi:10.1159/000074617 (2003).

9 Ip, N. Y. & Tsai, L.-H. *Cyclin Dependent Kinase 5 (Cdk5)*. (Springer, 2008).

10 Tarricone, C. *et al.* Structure and Regulation of the CDK5-p25nck5a Complex. *Molecular Cell* **8**, 657-669 (2001).

11 Dhariwala, F. A. & Rajadhyaksha, M. S. An unusual member of the Cdk family: Cdk5. *Cell Mol Neurobiol* **28**, 351-369, doi:10.1007/s10571-007-9242-1 (2008).

12 Sharma, S. & Sicinski, P. A kinase of many talents: non-neuronal functions of CDK5 in development and disease. *Open Biol* **10**, 190287, doi:10.1098/rsob.190287 (2020).

13 Malumbres, M. Cyclin-dependent kinases. *Genome Biology* **15** (2014).

14 Juric, V. & Murphy, B. Cyclin-dependent kinase inhibitors in brain cancer: current state and future directions. *Cancer Drug Resist*, doi:10.20517/cdr.2019.105 (2020).

15 Nurse, P., Masui, Y. & Hartwell, L. Understanding the cell cycle. *Nature Medicine* **4**, 1103-1106 (1998).

16 Nikolov, D. B. & Burley, S. K. RNA polymerase II transcription initiation- A structural view. *Proc Natl Acad Sci U S A* **94**, 15-22 (1997).

17 Sharma, P. *et al.* Identification of substrate binding site of cyclin-dependent kinase 5. *J Biol Chem* **274**, 9600-9606, doi:10.1074/jbc.274.14.9600 (1999).

18 Huang, H. *et al.* Cdk5-dependent phosphorylation of liprinalpha1 mediates neuronal activity-dependent synapse development. *Proc Natl Acad Sci U S A* **114**, E6992-E7001, doi:10.1073/pnas.1708240114 (2017).

19 Lew, J. CDK5: A new lead to survival. *Cell Cycle* **12**, 1981-1982, doi:10.4161/cc.25304 (2013).

20 Khair, N. Z. *et al.* Discovery of CDK5 Inhibitors through Structure-Guided Approach. *ACS Med Chem Lett* **10**, 786-791, doi:10.1021/acsmedchemlett.9b00029 (2019).

21 Dhavan, R. & Tsai, L.-H. A Decade of CDK5. *Nature Reviews: Molecular Cellular Biology* **2**, 749-759 (2001).

22 Kimura, T., Ishiguro, K. & Hisanaga, S. Physiological and pathological phosphorylation of tau by Cdk5. *Front Mol Neurosci* **7**, 65, doi:10.3389/fnmol.2014.00065 (2014).

23 Chow, H. M. *et al.* CDK5 activator protein p25 preferentially binds and activates GSK3beta. *Proc Natl Acad Sci U S A* **111**, E4887-4895, doi:10.1073/pnas.1402627111 (2014).

24 Pant, N. D. A. W. A. H. C. Cyclin-dependent kinase 5 (cdk5) activation requires interaction with three domains of p35. *Journal of Neuroscience Research* (2002).

25 Asada, A. *et al.* Myristoylation of p39 and p35 is a determinant of cytoplasmic or nuclear localization of active cyclin-dependent kinase 5 complexes. *J Neurochem* **106**, 1325-1336, doi:10.1111/j.1471-4159.2008.05500.x (2008).

26 Alison Shupp, M. C. C., Richard G. Pestell. Biological functions of CDK5 and potential CDK5 targeted clinical treatments. *Oncotarget* **8**, 17373-17382 (2017).

27 Chae, T. *et al.* Mice Lacking p35, a Neuronal Specific Activator of Cdk5, Display Cortical Lamination Defects, Seizures, and Adult Lethality. *Neuron* **18**, 29-42 (1997).

28 Hisanaga, S. & Saito, T. The regulation of cyclin-dependent kinase 5 activity through the metabolism of p35 or p39 Cdk5 activator. *Neurosignals* **12**, 221-229, doi:10.1159/000074624 (2003).

29 Dhavan, R., Greer, P. L., Morabito, M. A., Orlando, L. R. & Tsai, L.-H. The Cyclin-Dependent Kinase 5 Activators p35 and p39 Interact with the α-Subunit of Ca2+:Calmodulin-Dependent Protein Kinase II and α-Actinin-1 in a Calcium-Dependent Manner. *The Journal of Neuroscience* **22**, 7879-7891 (2002).

30 Patrick, G. N., Zhou, P., Kwon, Y. T., Howley, P. M. & Tsai, L. H. p35, the neuronal-specific activator of cyclin-dependent kinase 5 (Cdk5) is degraded by the ubiquitin-proteasome pathway. *J Biol Chem* **273**, 24057-24064, doi:10.1074/jbc.273.37.24057 (1998).

31 Takasugi, T. *et al.* Two Degradation Pathways of the p35 Cdk5 (Cyclin-dependent Kinase) Activation Subunit, Dependent and Independent of Ubiquitination. *J Biol Chem* **291**, 4649-4657, doi:10.1074/jbc.M115.692871 (2016).

32 Shah, K. & Rossie, S. Tale of the Good and the Bad Cdk5: Remodeling of the Actin Cytoskeleton in the Brain. *Mol Neurobiol* **55**, 3426-3438, doi:10.1007/s12035-017-0525-3 (2018).

33 Roufayel, R. & Murshid, N. CDK5: Key Regulator of Apoptosis and Cell Survival. *Biomedicines* **7**, doi:10.3390/biomedicines7040088 (2019).

34 Gilmore, E. C., Oshima, T., Goffinet, A. M., Kulkarni, A. B. & Herrup, K. Cyclin-Dependent Kinase 5-Deficient Mice Demonstrate Novel Developmental Arrest in Cerebral Cortex. *The Journal of Neuroscience* **18**, 6370-6377 (1998).

35 Gaztañaga, L., Marchlinski, F. E. & Betensky, B. P. Mechanisms of Cardiac Arrhythmias. *Revista Española de Cardiología (English Edition)* **65**, 174-185, doi:10.1016/j.rec.2011.09.020 (2012).

36 Fukuyama, M. *et al.* Long QT syndrome type 8: novel CACNA1C mutations causing QT prolongation and variant phenotypes. *Europace* **16**, 1828-1837, doi:10.1093/europace/euu063 (2014).

37 Han, D., Xue, X., Yan, Y. & Li, G. Dysfunctional Cav1.2 channel in Timothy syndrome, from cell to bedside. *Exp Biol Med (Maywood)* **244**, 960-971, doi:10.1177/1535370219863149 (2019).

38 Schwartz, P. J. *et al.* Prevalence of the congenital long-QT syndrome. *Circulation* **120**, 1761-1767, doi:10.1161/CIRCULATIONAHA.109.863209 (2009).

39 Schwartz, P. J., Crotti, L. & Insolia, R. Long-QT syndrome: from genetics to management. *Circ Arrhythm Electrophysiol* **5**, 868-877, doi:10.1161/CIRCEP.111.962019 (2012).

40 Wallace, E. *et al.* Long QT Syndrome: Genetics and Future Perspective. *Pediatr Cardiol* **40**, 1419-1430, doi:10.1007/s00246-019-02151-x (2019).

41 Flucher, B. E. & Franzini-Armstrong, C. Formation of junctions involved in excitation-contraction coupling in skeletal and cardiac muscle. *Proc Natl Acad Sci U S A* **93**, 8101-8106 (1996).

42 Song, L. *et al.* Dual optical recordings for action potentials and calcium handling in induced pluripotent stem cell models of cardiac arrhythmias using genetically encoded fluorescent indicators. *Stem cells translational medicine* **4**, 468-475, doi:10.5966/sctm.2014-0245 (2015).

43 Yazawa, M. *et al.* Using induced pluripotent stem cells to investigate cardiac phenotypes in Timothy syndrome. *Nature* **471**, 230-234, doi:10.1038/nature09855 (2011).

44 Song, L., Park, S. E., Isseroff, Y., Morikawa, K. & Yazawa, M. Inhibition of CDK5 Alleviates the Cardiac Phenotypes in Timothy Syndrome. *Stem Cell Reports* **9**, 50-57, doi:10.1016/j.stemcr.2017.05.028 (2017).

45 Lin, Z. P., Zhu, Y. L. & Ratner, E. S. Targeting Cyclin-Dependent Kinases for Treatment of Gynecologic Cancers. *Front Oncol* **8**, 303, doi:10.3389/fonc.2018.00303 (2018).

46 Anda, S., Rothe, C., Boye, E. & Grallert, B. Consequences of abnormal CDK activity in S phase. *Cell Cycle* **15**, 963-973, doi:10.1080/15384101.2016.1152423 (2016).

47 Law, M. E., Corsino, P. E., Narayan, S. & Law, B. K. Cyclin-Dependent Kinase Inhibitors as Anticancer Therapeutics. *Mol Pharmacol* **88**, 846-852, doi:10.1124/mol.115.099325 (2015).

48 Reddy, H. K. *et al.* Cyclin-dependent kinase 4 expression is essential for neu-induced breast tumorigenesis. *Cancer Res* **65**, 10174-10178, doi:10.1158/0008-5472.CAN-05-2639 (2005).

49 Feng, Y. *et al.* Transcriptional activation of CBFbeta by CDK11(p110) is necessary to promote osteosarcoma cell proliferation. *Cell Commun Signal* **17**, 125, doi:10.1186/s12964-019-0440-5 (2019).

50 Firestein, R. *et al.* CDK8 expression in 470 colorectal cancers in relation to beta-catenin activation, other molecular alterations and patient survival. *Int J Cancer* **126**, 2863-2873, doi:10.1002/ijc.24908 (2010).

51 Wells, C. I. *et al.* Quantifying CDK inhibitor selectivity in live cells. *Nat Commun* **11**, 2743, doi:10.1038/s41467-020-16559-0 (2020).

52 Pozo, K. & Bibb, J. A. The Emerging Role of Cdk5 in Cancer. *Trends Cancer* **2**, 606-618, doi:10.1016/j.trecan.2016.09.001 (2016).

53 Bhandari, D. *et al.* Cyclin-dependent kinase 5 activates guanine nucleotide exchange factor GIV/Girdin to orchestrate migration-proliferation dichotomy. *Proc Natl Acad Sci U S A* **112**, E4874-4883, doi:10.1073/pnas.1514157112 (2015).

54 Hanahan, D. & Weinberg, R. A. Hallmarks of cancer: the next generation. *Cell* **144**, 646-674, doi:10.1016/j.cell.2011.02.013 (2011).

55 Liang, Q. *et al.* CDK5 is essential for TGF-beta1-induced epithelial-mesenchymal transition and breast cancer progression. *Sci Rep* **3**, 2932, doi:10.1038/srep02932 (2013).

56 Ardelt, M. A. *et al.* Inhibition of Cyclin-Dependent Kinase 5: A Strategy to Improve Sorafenib Response in Hepatocellular Carcinoma Therapy. *Hepatology* **69**, 376-393, doi:10.1002/hep.30190 (2019).

57 Whittaker, S. R., Mallinger, A., Workman, P. & Clarke, P. A. Inhibitors of cyclin-dependent kinases as cancer therapeutics. *Pharmacol Ther* **173**, 83-105, doi:10.1016/j.pharmthera.2017.02.008 (2017).

58 Ahn, J. S. *et al.* Defining Cdk5 ligand chemical space with small molecule inhibitors of tau phosphorylation. *Chem Biol* **12**, 811-823, doi:10.1016/j.chembiol.2005.05.011 (2005).

59 Klein, M. E., Kovatcheva, M., Davis, L. E., Tap, W. D. & Koff, A. CDK4/6 Inhibitors: The Mechanism of Action May Not Be as Simple as Once Thought. *Cancer Cell* **34**, 9-20, doi:10.1016/j.ccell.2018.03.023 (2018).

60 Sekine, C. *et al.* Successful treatment of animal models of rheumatoid arthritis with small-molecule cyclin-dependent kinase inhibitors. *J Immunol* **180**, 1954-1961, doi:10.4049/jimmunol.180.3.1954 (2008).

61 Rostam, M. A. *et al.* Flavopiridol Inhibits TGF-beta-Stimulated Biglycan Synthesis by Blocking Linker Region Phosphorylation and Nuclear Translocation of Smad2. *J Pharmacol Exp Ther* **365**, 156-164, doi:10.1124/jpet.117.244483 (2018).

62 Chen, E. X. *et al.* A Phase I study of cyclin-dependent kinase inhibitor, AT7519, in patients with advanced cancer: NCIC Clinical Trials Group IND 177. *Br J Cancer* **111**, 2262-2267, doi:10.1038/bjc.2014.565 (2014).

63 Gojo, I. *et al.* Clinical and laboratory studies of the novel cyclin-dependent kinase inhibitor dinaciclib (SCH 727965) in acute leukemias. *Cancer Chemother Pharmacol* **72**, 897-908, doi:10.1007/s00280-013-2249-z (2013).

64 Nemunaitis, J. J. *et al.* A first-in-human, phase 1, dose-escalation study of dinaciclib, a novel cyclin-dependent kinase inhibitor, administered weekly in subjects with advanced malignancies. *Journal of Translational Medicine* **11** (2013).

65 Padula, S. L., Velayutham, N. & Yutzey, K. E. Transcriptional Regulation of Postnatal Cardiomyocyte Maturation and Regeneration. *Int J Mol Sci* **22**, doi:10.3390/ijms22063288 (2021).

66 Harkins, S. & Whitton, J. L. Chromosomal mapping of the alphaMHC-MerCreMer transgene in mice reveals a large genomic deletion. *Transgenic Res* **25**, 639-648, doi:10.1007/s11248-016-9960-6 (2016).

67 Hsieh, P. C. *et al.* Evidence from a genetic fate-mapping study that stem cells refresh adult mammalian cardiomyocytes after injury. *Nat Med* **13**, 970-974, doi:10.1038/nm1618 (2007).

68 James, J. & Robbins, J. Healing a Heart Through Genetic Intervention. *Circ Res* **118**, 920-922, doi:10.1161/CIRCRESAHA.116.308468 (2016).

69 Stuart, C. A. *et al.* Myosin content of individual human muscle fibers isolated by laser capture microdissection. *Am J Physiol Cell Physiol* **310**, C381-389, doi:10.1152/ajpcell.00317.2015 (2016).

70 Barany, M. ATPase Activity of Myosin Correlated with Speed of Muscle Shortening. *The Journal of General Phsyiology* **50**, 197-218, doi:10.1085/jgp.50.6.197 (1967).

71 Kam, M. K., Lee, K. Y., Tam, P. K. & Lui, V. C. Generation of NSE-MerCreMer transgenic mice with tamoxifen inducible Cre activity in neurons. *PLoS One* **7**, e35799, doi:10.1371/journal.pone.0035799 (2012).

72 Temporally Regulated and Tissue-Specific Gene Manipulations in the Adult and Embryonic Heart Using a Tamoxifen-Inducible Cre Protein.

73 Neven, P. & Vergote, I. Tamoxifen, screening and new oestrogen receptor modulators. *Best Pract Res Clin Obstet Gynaecol* **15**, 365-380, doi:10.1053/beog.2001.0182 (2001).

74 Nakamura, E., Nguyen, M. T. & Mackem, S. Kinetics of tamoxifen-regulated Cre activity in mice using a cartilage-specific CreER(T) to assay temporal activity windows along the proximodistal limb skeleton. *Dev Dyn* **235**, 2603-2612, doi:10.1002/dvdy.20892 (2006).

75 Smedley, D., Salimova, E. & Rosenthal, N. Cre recombinase resources for conditional mouse mutagenesis. *Methods* **53**, 411-416, doi:10.1016/j.ymeth.2010.12.027 (2011).

76 Nagy, A. Cre Recombinase- The Universal Reagent for Genome Tailoring. *Genesis* **26**, 99-109 (1999).

77 Zhang, Y. *et al.* Inducible site-directed recombination in mouse embryonic stem cells. *Nucleic Acids Research* **24**, 543-548 (1995).

78 McLellan, M. A. Cre-loxP Mediated Recombination:General Principles and Experimental Considerations. *Current protocols in mouse biology* **7**, 1-12, doi:10.1002/cpmo.22 (2017).

79 Bersell, K. *et al.* Moderate and high amounts of tamoxifen in alphaMHC-MerCreMer mice induce a DNA damage response, leading to heart failure and death. *Dis Model Mech* **6**, 1459-1469, doi:10.1242/dmm.010447 (2013).

80 Oh, J. K. Echocardiography in heart failure: beyond diagnosis. *Eur J Echocardiogr* **8**, 4-14, doi:10.1016/j.euje.2006.09.002 (2007).

81 Tissot, C., Muehlethaler, V. & Sekarski, N. Basics of Functional Echocardiography in Children and Neonates. *Front Pediatr* **5**, 235, doi:10.3389/fped.2017.00235 (2017).

82 Tissot, C. & Singh, Y. Neonatal functional echocardiography. *Curr Opin Pediatr* **32**, 235-244, doi:10.1097/MOP.0000000000000887 (2020).

83 Lindsey, M. L., Kassiri, Z., Virag, J. A. I., de Castro Bras, L. E. & Scherrer-Crosbie, M. Guidelines for measuring cardiac physiology in mice. *Am J Physiol Heart Circ Physiol* **314**, H733-H752, doi:10.1152/ajpheart.00339.2017 (2018).

84 Wang, Z. *et al.* DBA/1 mice display equivalent cardiac function to C57BL/6J mice. *Exp Physiol* **106**, 868-881, doi:10.1113/EP089228 (2021).

85 Pinamonti, B., Abate, E., De Luca, A., Finocchiaro, G. & Korcova, R. in *Dilated Cardiomyopathy: From Genetics to Clinical Management* (eds G. Sinagra, M. Merlo, & B. Pinamonti) 83-111 (2019).

86 Kathiriya, I. S. *et al.* Modeling Human TBX5 Haploinsufficiency Predicts Regulatory Networks for Congenital Heart Disease. *Dev Cell* **56**, 292-309 e299, doi:10.1016/j.devcel.2020.11.020 (2021).

87 Nishina, S. *et al.* Biallelic CDK9 variants as a cause of a new multiple-malformation syndrome with retinal dystrophy mimicking the CHARGE syndrome. *J Hum Genet*, doi:10.1038/s10038-021-00909-x (2021).

88 Colas, P. Cyclin-dependent kinases and rare developmental disorders. *Orphanet J Rare Dis* **15**, 203, doi:10.1186/s13023-020-01472-y (2020).

89 Morton, J. P. *et al.* LKB1 Haploinsufficiency Cooperates With Kras to Promote Pancreatic Cancer Through Suppression of p21-Dependent Growth Arrest. *Gastroenterology* **139**, 586-597 (2010).

90 Zhou, J. *et al.* Loss of Adult Cardiac Myocyte GSK-3 Leads to Mitotic Catastrophe Resulting in Fatal Dilated Cardiomyopathy. *Circ Res* **118**, 1208-1222, doi:10.1161/CIRCRESAHA.116.308544 (2016).

91 Tannous, C. *et al.* NMRK2 Gene Is Upregulated in Dilated Cardiomyopathy and Required for Cardiac Function and NAD Levels during Aging. *Int J Mol Sci* **22**, doi:10.3390/ijms22073534 (2021).

92 Ahmad, F. *et al.* Nicotinamide riboside kinase-2 alleviates ischemia-induced heart failure through P38 signaling. *Biochim Biophys Acta Mol Basis Dis* **1866**, 165609, doi:10.1016/j.bbadis.2019.165609 (2020).

93 Tang, W. H. *et al.* Plasma myeloperoxidase levels in patients with chronic heart failure. *Am J Cardiol* **98**, 796-799, doi:10.1016/j.amjcard.2006.04.018 (2006).

94 Ali, M. *et al.* Myeloperoxidase Inhibition Improves Ventricular Function and Remodeling After Experimental Myocardial Infarction. *JACC Basic Transl Sci* **1**, 633-643, doi:10.1016/j.jacbts.2016.09.004 (2016).

95 Gedikli, O., Kiris, A., Hosoglu, Y., Karahan, C. & Kaplan, S. Serum myeloperoxidase level is associated with heart-type fatty acid-binding protein but not troponin T in patients with chronic heart failure. *Med Princ Pract* **24**, 42-46, doi:10.1159/000368717 (2015).

96 Nicholls, S. J. & Hazen, S. L. Myeloperoxidase and cardiovascular disease. *Arterioscler Thromb Vasc Biol* **25**, 1102-1111, doi:10.1161/01.ATV.0000163262.83456.6d (2005).

97 Taylor, A. M. The Resurrection of Myeloperoxidase as a Therapeutic Target: Is it Lazarus or Just an Apparition? *JACC Basic Transl Sci* **1**, 644-646, doi:10.1016/j.jacbts.2016.10.003 (2016).

98 Mathiasen, A. B., Henningsen, K. M. A., Jurjevna, M., Mygind, H. N. D. & Kastrup, J. YKL-40: a new biomarker in cardiovascular disease? *Biomarkers Medicine* **4**, 591-600 (2010).

99 Ridker, P. M., Chasman, D. I., Rose, L., Loscalzo, J. & Elias, J. A. Plasma levels of the proinflammatory chitin-binding glycoprotein YKL-40, variation in the chitinase 3-like 1 gene (CHI3L1), and incident cardiovascular events. *J Am Heart Assoc* **3**, e000897, doi:10.1161/JAHA.114.000897 (2014).

100 Miller, C. L. *et al.* Role of Ca2+/calmodulin-stimulated cyclic nucleotide phosphodiesterase 1 in mediating cardiomyocyte hypertrophy. *Circ Res* **105**, 956-964, doi:10.1161/CIRCRESAHA.109.198515 (2009).

101 Vandeput, F. *et al.* Cyclic nucleotide phosphodiesterase PDE1C1 in human cardiac myocytes. *J Biol Chem* **282**, 32749-32757, doi:10.1074/jbc.M703173200 (2007).

102 Shete, V. *et al.* Mouse Cardiac Pde1C Is a Direct Transcriptional Target of Pparalpha. *Int J Mol Sci* **19**, doi:10.3390/ijms19123704 (2018).

103 Knight, W. E. *et al.* PDE1C deficiency antagonizes pathological cardiac remodeling and dysfunction. *Proc Natl Acad Sci U S A* **113**, E7116-E7125, doi:10.1073/pnas.1607728113 (2016).

104 Shi, J., Luo, L., Eash, J., Ibebunjo, C. & Glass, D. J. The SCF-Fbxo40 complex induces IRS1 ubiquitination in skeletal muscle, limiting IGF1 signaling. *Dev Cell* **21**, 835-847, doi:10.1016/j.devcel.2011.09.011 (2011).

105 Sandri, M. & Robbins, J. Proteotoxicity: an underappreciated pathology in cardiac disease. *J Mol Cell Cardiol* **71**, 3-10, doi:10.1016/j.yjmcc.2013.12.015 (2014).

106 Iskratsch, T. *et al.* Formin follows function: a muscle-specific isoform of FHOD3 is regulated by CK2 phosphorylation and promotes myofibril maintenance. *J Cell Biol* **191**, 1159-1172, doi:10.1083/jcb.201005060 (2010).

107 Iskratsch, T. *et al.* Two distinct phosphorylation events govern the function of muscle FHOD3. *Cell Mol Life Sci* **70**, 893-908, doi:10.1007/s00018-012-1154-7 (2013).

108 Li, J. Alterations in cell adhesion proteins and cardiomyopathy. *World J Cardiol* **6**, 304-313, doi:10.4330/wjc.v6.i5.304 (2014).

109 Sheikh, F., Ross, R. S. & Chen, J. Cell-cell connection to cardiac disease. *Trends Cardiovasc Med* **19**, 182-190, doi:10.1016/j.tcm.2009.12.001 (2009).

110 Chopra, A., Tabdanov, E., Patel, H., Janmey, P. A. & Kresh, J. Y. Cardiac myocyte remodeling mediated by N-cadherin-dependent mechanosensing. *Am J Physiol Heart Circ Physiol* **300**, H1252-1266, doi:10.1152/ajpheart.00515.2010 (2011).

111 Pruna, M. & Ehler, E. The intercalated disc: a mechanosensing signalling node in cardiomyopathy. *Biophys Rev* **12**, 931-946, doi:10.1007/s12551-020-00737-x (2020).

112 McCain, M. L., Lee, H., Aratyn-Schaus, Y., Kleber, A. G. & Parker, K. K. Cooperative coupling of cell-matrix and cell-cell adhesions in cardiac muscle. *Proc Natl Acad Sci U S A* **109**, 9881-9886, doi:10.1073/pnas.1203007109 (2012).

113 Rampazzo, A., Calore, M., van Hengel, J. & van Roy, F. Intercalated discs and arrhythmogenic cardiomyopathy. *Circ Cardiovasc Genet* **7**, 930-940, doi:10.1161/CIRCGENETICS.114.000645 (2014).

114 Homayouni, R. & Curran, T. Cortical development- Cdk5 gets into sticky situations. *Current Biology* **10**, R331-R334 (2000).

115 Ohshima, T. *et al.* Migration Defects of cdk52:2 Neurons in the Developing Cerebellum is Cell Autonomous. *The Journal of Neuroscience* **19**, 6017-6026 (1999).

116 Nikolac, M., Dudek, H., Kwon, Y. T., Ramos, Y. F. M. & Tsai, L.-H. The cdk5:p35 kinase is essential for neurite outgrowth during neuronal differentiation. *Genes and Development* **10**, 816-825 (1996).

117 Ohshima, T. *et al.* Targeted disruption of the cyclin-dependent kinase 5 gene results in abnormal corticogenesis, neuronal pathology and perinatal death. *Proc Natl Acad Sci U S A* **93**, 11173-11178 (1996).

118 Nakano, N. *et al.* CDK5 regulates cell-cell and cell-matrix adhesion in human keratinocytes. *Br J Dermatol* **153**, 37-45, doi:10.1111/j.1365-2133.2005.06583.x (2005).

119 Solaro, J. R. *Regulation of cardiac contractility* (Morgan & Claypool Life Sciences, 2011).

120 Ackermann, M. A. *et al.* TGF-beta1 affects cell-cell adhesion in the heart in an NCAM1-dependent mechanism. *J Mol Cell Cardiol* **112**, 49-57, doi:10.1016/j.yjmcc.2017.08.015 (2017).

121 Sequeira, V., Nijenkamp, L. L., Regan, J. A. & van der Velden, J. The physiological role of cardiac cytoskeleton and its alterations in heart failure. *Biochim Biophys Acta* **1838**, 700-722, doi:10.1016/j.bbamem.2013.07.011 (2014).

122 Morrill, S. A. & Amon, A. Why haploinsufficiency persists. *Proc Natl Acad Sci U S A* **116**, 11866-11871, doi:10.1073/pnas.1900437116 (2019).

123 Pappireddi, N., Martin, L. & Wuhr, M. A Review on Quantitative Multiplexed Proteomics. *Chembiochem* **20**, 1210-1224, doi:10.1002/cbic.201800650 (2019).

124 Navarrete-Perea, J., Yu, Q., Gygi, S. P. & Paulo, J. A. Streamlined Tandem Mass Tag (SL-TMT) Protocol: An Efficient Strategy for Quantitative (Phospho)proteome Profiling Using Tandem Mass Tag-Synchronous Precursor Selection-MS3. *J Proteome Res* **17**, 2226-2236, doi:10.1021/acs.jproteome.8b00217 (2018).

125 Tyanova, S. *et al.* The Perseus computational platform for comprehensive analysis of (prote)omics data. *Nat Methods* **13**, 731-740, doi:10.1038/nmeth.3901 (2016).

126 Arif, A. Extraneuronal activities and regulatory mechanisms of the atypical cyclin-dependent kinase Cdk5. *Biochem Pharmacol* **84**, 985-993, doi:10.1016/j.bcp.2012.06.027 (2012).

127 Utreras, E., Maccioni, R. & Gonzalez-Billault, C. Cyclin-dependent kinase 5 activator p35 over-expression and amyloid beta synergism increase apoptosis in cultured neuronal cells. *Neuroscience* **161**, 978-987, doi:10.1016/j.neuroscience.2009.04.002 (2009).

128 Carrie Draney, A. E. H., Samuel G. Grover, Benjamin O. Jack, and Jeffery S. Tessem. Cdk5r1 Overexpression Induces Primary Beta-Cell Proliferation. *Journal of Diabetes Research* **2016**, doi:10.1155/2016/6375804 (2016).

129 Feldmann, G. *et al.* Inhibiting the cyclin-dependent kinase CDK5 blocks pancreatic cancer formation and progression through the suppression of Ras-Ral signaling. *Cancer Res* **70**, 4460-4469, doi:10.1158/0008-5472.CAN-09-1107 (2010).

130 Tsai, L.-H., Delalle, I., Jr., V. S. C., Chae, T. & Harlow, E. p35 is a neural-specific regulatory subunit of cyclin-dependent kinase 5. *Nature* **371**, 419-423 (1994).

131 Mao, D. & Hinds, P. W. p35 is required for CDK5 activation in cellular senescence. *J Biol Chem* **285**, 14671-14680, doi:10.1074/jbc.M109.066118 (2010).

132 Ubersax, J. A. & Ferrell, J. E., Jr. Mechanisms of specificity in protein phosphorylation. *Nat Rev Mol Cell Biol* **8**, 530-541, doi:10.1038/nrm2203 (2007).

133 Ardito, F., Giuliani, M., Perrone, D., Troiano, G. & Lo Muzio, L. The crucial role of protein phosphorylation in cell signaling and its use as targeted therapy (Review). *Int J Mol Med* **40**, 271-280, doi:10.3892/ijmm.2017.3036 (2017).

134 Garcia-Garcia, T. *et al.* Role of Protein Phosphorylation in the Regulation of Cell Cycle and DNA-Related Processes in Bacteria. *Front Microbiol* **7**, 184, doi:10.3389/fmicb.2016.00184 (2016).

135 Via, A. & Zanzoni, A. *Protein phosphorylation in health and disease*. (Frontiers Research Topics, 2016).

136 Allnutt, A. B., Waters, A. K., Kesari, S. & Yenugonda, V. M. Physiological and Pathological Roles of Cdk5: Potential Directions for Therapeutic Targeting in Neurodegenerative Disease. *ACS Chem Neurosci* **11**, 1218-1230, doi:10.1021/acschemneuro.0c00096 (2020).

137 Rapundalo, S. T. Cardiac protein phosphorylation- functional and pathophysiological correlates. *Cardiovascular Research* **38**, 559-588 (1998).

138 Catterall, W. A. Voltage-gated calcium channels. *Cold Spring Harb Perspect Biol* **3**, a003947, doi:10.1101/cshperspect.a003947 (2011).

139 Luo, M. & Anderson, M. E. Mechanisms of altered Ca(2)(+) handling in heart failure. *Circ Res* **113**, 690-708, doi:10.1161/CIRCRESAHA.113.301651 (2013).

140 Sequeira, V. & Maack, C. Rebalancing protein phosphorylation in heart failure to prevent arrhythmias. *Eur J Heart Fail* **20**, 1686-1689, doi:10.1002/ejhf.1315 (2018).

141 Burton, P. J., Yacoub, M. H. & Barton, P. J. R. Cyclin-dependent kinase inhibitor expression in human heart failure. *European Heart Journal* **20**, 604-611 (1999).

142 Kang, M. J., Kim, J.-S., Chae, S.-W., Koh, K. N. & Koh, G. Y. Cyclins and Cyclin Dependent Kinases during Cardiac Development. *Molecular Cell* **7**, 360-366 (1997).

143 McLendon, J. M., Zhang, X., Stein, C. S. & Boudreau, R. L. TXLNB Signaling may not Intersect with Cardiac Proteotoxicity by CRYAB-R120G. *The FASEB Journal* **34**, 1-1 (2020).

144 Verdonschot, J. A. J. *et al.* Mutations in PDLIM5 are rare in dilated cardiomyopathy but are emerging as potential disease modifiers. *Mol Genet Genomic Med* **8**, e1049, doi:10.1002/mgg3.1049 (2020).

145 Agullo-Pascual, E. & Delmar, M. The noncanonical functions of Cx43 in the heart. *J Membr Biol* **245**, 477-482, doi:10.1007/s00232-012-9466-y (2012).

146 Rodriguez-Sinovas, A., Sanchez, J. A., Valls-Lacalle, L., Consegal, M. & Ferreira-Gonzalez, I. Connexins in the Heart: Regulation, Function and Involvement in Cardiac Disease. *Int J Mol Sci* **22**, doi:10.3390/ijms22094413 (2021).

147 Nielsen, M. S. *et al.* Gap Juctions. *Compr Physiol* **2**, 1981-2035, doi:10.1002/cphy.c110051 (2012).

148 Zhang, S. S. & Shaw, R. M. Multilayered regulation of cardiac ion channels. *Biochim Biophys Acta* **1833**, 876-885, doi:10.1016/j.bbamcr.2012.10.020 (2013).

149 Habo J. Jongsma, R. W. Gap Junctions in Cardiovascular Disease. *Circulation Research* **86**, 1193-1197 (2000).

150 Lampe, P. D. & Lau, A. F. The effects of connexin phosphorylation on gap junctional communication. *The International Journal of Biochemistry & Cell Biology* **36**, 1171-1186, doi:10.1016/s1357-2725(03)00264-4 (2004).

151 Wittlieb-Weber, C. A., Haude, K. M., Fong, C. T. & Vinocur, J. M. A novel GJA1 mutation causing familial oculodentodigital dysplasia with dilated cardiomyopathy and arrhythmia. *HeartRhythm Case Rep* **2**, 32-35, doi:10.1016/j.hrcr.2015.08.013 (2016).

152 Rosello-Lleti, E. *et al.* Cardiac protein changes in ischaemic and dilated cardiomyopathy: a proteomic study of human left ventricular tissue. *J Cell Mol Med* **16**, 2471-2486, doi:10.1111/j.1582-4934.2012.01565.x (2012).

153 Zhou, Q. *et al.* Crucial Role of ROCK2-Mediated Phosphorylation and Upregulation of FHOD3 in the Pathogenesis of Angiotensin II-Induced Cardiac Hypertrophy. *Hypertension* **69**, 1070-1083, doi:10.1161/HYPERTENSIONAHA.116.08662 (2017).

154 Hoorntje, E. T. *et al.* No major role for rare plectin variants in arrhythmogenic right ventricular cardiomyopathy. *PLoS One* **13**, e0203078, doi:10.1371/journal.pone.0203078 (2018).

155 Castanon, M. J., Walko, G., Winter, L. & Wiche, G. Plectin-intermediate filament partnership in skin, skeletal muscle, and peripheral nerve. *Histochem Cell Biol* **140**, 33-53, doi:10.1007/s00418-013-1102-0 (2013).

156 Franz, M., Jung, C., Lauten, A., Figulla, H. R. & Berndt, A. Tenascin-C in cardiovascular remodeling: potential impact for diagnosis, prognosis estimation and targeted therapy. *Cell Adh Migr* **9**, 90-95, doi:10.1080/19336918.2014.1000075 (2015).

157 Hong, C.-S. *et al.* Cardiac remodeling and atrial fibrillation in transgenic miceoverexpressing junctin. *The FASEB Journal*, doi:10.1096/fj.01-0908fje (2002).

158 Gehmlich, K. *et al.* Paxillin and ponsin interact in nascent costameres of muscle cells. *J Mol Biol* **369**, 665-682, doi:10.1016/j.jmb.2007.03.050 (2007).

159 Meguro, K. *et al.* Function and role of voltage-gated sodium channel NaV1.7 expressed in aortic smooth muscle cells. *Am J Physiol Heart Circ Physiol* **296**, H211-219, doi:10.1152/ajpheart.00960.2008 (2009).

160 Kanellopoulos, A. H. *et al.* Mapping protein interactions of sodium channel NaV1.7 using epitope-tagged gene-targeted mice. *EMBO J* **37**, 427-445, doi:10.15252/embj.201796692 (2018).

161 Peche, V. S. *et al.* Ablation of cyclase-associated protein 2 (CAP2) leads to cardiomyopathy. *Cell Mol Life Sci* **70**, 527-543, doi:10.1007/s00018-012-1142-y (2013).

162 Field, J. *et al.* CAP2 in cardiac conduction, sudden cardiac death and eye development. *Sci Rep* **5**, 17256, doi:10.1038/srep17256 (2015).

163 Monkley, S. J., Pritchard, C. A. & Critchley, D. R. Analysis of the mammalian talin2 gene TLN2. *Biochem Biophys Res Commun* **286**, 880-885, doi:10.1006/bbrc.2001.5497 (2001).

164 Senetar, M. A., Moncman, C. L. & McCann, R. O. Talin2 is induced during striated muscle differentiation and is targeted to stable adhesion complexes in mature muscle. *Cell Motil Cytoskeleton* **64**, 157-173, doi:10.1002/cm.20173 (2007).

165 Weekes, J. *et al.* Hyperubiquitination of proteins in dilatedcardiomyopathy. *Proteomics* **3**, 208-216 (2003).

166 Sobczak, K., Wheeler, T. M., Wang, W. & Thornton, C. A. RNA interference targeting CUG repeats in a mouse model of myotonic dystrophy. *Mol Ther* **21**, 380-387, doi:10.1038/mt.2012.222 (2013).

167 Bird, T. D. *Myotonic Dystrophy Type 1*. 1-27 (1999).

168 Lau, J. K., Sy, R. W., Corbett, A. & Kritharides, L. Myotonic dystrophy and the heart: A systematic review of evaluation and management. *Int J Cardiol* **184**, 600-608, doi:10.1016/j.ijcard.2015.03.069 (2015).

169 Bohlen, J. *et al.* DENR promotes translation reinitiation via ribosome recycling to drive expression of oncogenes including ATF4. *Nat Commun* **11**, 4676, doi:10.1038/s41467-020-18452-2 (2020).

170 Manning, G., Whyte, D. B., Martinez, R., Hunter, T. & Sudarsanam, S. The Protein Kinase Complement of the Human Genome. *Science* **298**, 1912-1916 (2002).

171 Rapunaldo, S. T. Cardiac protein phosphorylation- functional and pathophysiological correlates. *Cardiovascular Research* **38**, 559-588 (1998).

172 Jiang, X. *et al.* Sensitive and Accurate Quantitation of Phosphopeptides Using TMT Isobaric Labeling Technique. *J Proteome Res* **16**, 4244-4252, doi:10.1021/acs.jproteome.7b00610 (2017).

173 Hegazy, M. *et al.* Proximity Ligation Assay for Detecting Protein-Protein Interactions and Protein Modifications in Cells and Tissues in Situ. *Curr Protoc Cell Biol* **89**, e115, doi:10.1002/cpcb.115 (2020).

174 Sable, R. *et al.* Proximity ligation assay to study protein–protein interactions of proteins on two different cells. *BioTechniques* **65**, 149-157 (2018).

175 Weber, S., Meyer-Roxlau, S., Wagner, M., Dobrev, D. & El-Armouche, A. Counteracting Protein Kinase Activity in the Heart: The Multiple Roles of Protein Phosphatases. *Front Pharmacol* **6**, 270, doi:10.3389/fphar.2015.00270 (2015).

176 Houser, S. R. *et al.* Animal models of heart failure: a scientific statement from the American Heart Association. *Circ Res* **111**, 131-150, doi:10.1161/RES.0b013e3182582523 (2012).

177 Velden, J. v. d. *et al.* Increased Ca2+-sensitivity of the contractile apparatus in end-stage human heart failure results from altered phosphorylation of contractile proteins. *Cardiovascular Research* **57**, 37-47 (2002).

178 Azevedo, P. S., Polegato, B. F., Minicucci, M. F., Paiva, S. A. & Zornoff, L. A. Cardiac Remodeling: Concepts, Clinical Impact, Pathophysiological Mechanisms and Pharmacologic Treatment. *Arq Bras Cardiol* **106**, 62-69, doi:10.5935/abc.20160005 (2016).

179 Fairweather, D., Cooper, L. T., Jr. & Blauwet, L. A. Sex and gender differences in myocarditis and dilated cardiomyopathy. *Curr Probl Cardiol* **38**, 7-46, doi:10.1016/j.cpcardiol.2012.07.003 (2013).

180 Oka, S. I. *et al.* Perm1 regulates cardiac energetics as a downstream target of the histone methyltransferase Smyd1. *PLoS One* **15**, e0234913, doi:10.1371/journal.pone.0234913 (2020).